SMARTPHONE ENABLED BIOSENSOR SYSTEMS FOR NUTRITION DIAGNOSTICS AND PREVENTIVE CARE AT THE POINT-OF-NEED

A Dissertation

Presented to the Faculty of the Graduate School

of Cornell University

In Partial Fulfillment of the Requirements for the Degree of

Doctor of Philosophy

by

Seoho Lee

May 2016

SMARTPHONE ENABLED BIOSENSOR SYSTEMS FOR NUTRITION DIAGNOSTICS AND PREVENTIVE CARE AT THE POINT-OF-NEED

Seoho Lee, Ph. D.

Cornell University 2016

Micronutrient deficiencies and infectious diseases represent major global health burdens and their early diagnostics at the point-of-need (PON) has the potential to improve the current predicament by allowing more rapid and effective patient treatment/management. In this work we show how such diagnostics can be enabled by coupling the two powerful technologies: (1) lab-on-a-chip biosensor systems with capabilities to perform complex biochemical measurements at the PON, and (2) smartphone technology with powerful imaging, computing and communication capabilities which can be exploited to obtain and analyze results from these biosensor systems.

In the first and main part of the dissertation, we discuss the development of NutriPhone, a smartphone-enabled biosensor system for micronutrient deficiency diagnosis at the PON. As our initial prototype, a system for quantification of vitamin D levels on a smartphone is demonstrated. The system consists of a smartphone accessory, an app, and an immunoreaction-based biosensor that allows the colorimetric detection of 25-hydroxyvitamin D. For personalized diagnosis of vitamin B_{12} deficiency, we present an advanced version of NutriPhone which improves upon the limitations of the previous prototype by incorporating a custom lateral flow assay for vitamin B_{12} capable of processing and analyzing whole blood samples on-chip in 15 min. We validate the effectiveness of the NutriPhone system in a domestic human trial in which it was used to correctly diagnose the B_{12} status of human participants. We envision this as the first step toward the development of a comprehensive system for the analysis of multiple vitamins/micronutrients from a drop of finger prick blood.

In the second part of the dissertation, we discuss other applications of lab-on-a-chip biosensor systems in preventive care, namely: infectious disease diagnostics and traumatic injury prevention. First, we discuss

the need for rapid differential diagnosis of causative agents behind acute febrile illnesses, and present a novel assay scheme which enables the 4-plex detection of IgG/IgM antibodies to dengue and chikungunya viruses on a single biosensing platform. Second, we discuss the development of an autonomous integrated device using an aptamer-based affinity biosensor for the prevention of hemorrhagic shock, the leading cause of death for people with traumatic injuries.

BIOGRAPHICAL SKETCH

Seoho Lee was born April 30, 1988 in Seoul, Korea. He received his Bachelors of Science (B.S.) with High Distinction in Mechanical Engineering from the University of Toronto in May of 2011. In August of 2011, he joined the Ph.D. program in the Sibley School of Mechanical and Aerospace Engineering at Cornell University. He obtained his Master of Science (M.S.) in Mechanical Engineering from Cornell University in December of 2014.

As an undergraduate researcher, Seoho worked with diverse research groups with expertise in microfluidics (Advisor: Prof. Axel Guenther; U. of Toronto), ultrasonics (Advisor: Prof. Anthony Sinclair; U. of Toronto), microcellular plastics (Advisor: Prof. Chul B. Park; U. of Toronto) and fuel cells (Advisor: Prof. Suk W. Cha; Seoul National U.). He was the recipient of the Undergraduate Research Student Award (URSA) from Natural Sciences and Engineering Research Council (NSERC) for the two consecutive summers of 2009 and 2010.

At Cornell University, his interest in nanotechnology and microfluidics led him to join the Erickson Lab under the advisory of Prof. David Erickson, where he led and contributed in various research projects including the development of smartphone based biosensor systems for nutrition and infectious disease diagnostics, autonomous systems for traumatic injury prevention, and implantable biosensor systems for biophysical monitoring of flying birds. He was awarded the Postgraduate Scholarship - Doctoral (PGS-D) from NSERC in 2014–‘16.

Outside his academic life, Seoho enjoyed travelling, working out, and playing soccer. He participated in Cornell’s Intramural League for outdoor and indoor soccer each year. In addition, he was the captain of the Cornell Korean Student Association (KSA) soccer team from ’13-’15, during which the team placed 1st at the Eastcoast Binghamton Tournament for the first time since the team’s establishment in the early 2000s.

사랑하는 가족들에게,

그리고 너무나 보고싶은 친구 김상윤에게 바칩니다.

ACKNOWLEDGMENTS

I would like express my sincere gratitude to my adviser Professor David Erickson for his guidance, support and expertise throughout my years at Cornell. He has played a crucial role in shaping my abilities to conduct high-quality research independently, lead and manage multiple projects, and communicate effectively in publications/presentations. I also would like to thank him for keeping me motivated to aim higher and achieve more, while allowing me the freedom to pursue my research interests in and out of the lab. He has been a great example to me of a successful researcher and entrepreneur, and I am confident that what I have learned from him will help me find success in my own career.

I gratefully acknowledge my committee members – Professor Saurabh Mehta and Professor Alex Travis for their insightful feedback and advice that have led to the successful completion of this dissertation. My work in the field of nutrition and infectious diseases would not have been possible without the expertise and knowledge from Professor Mehta, and I am very grateful. I am also very thankful to my former advisors from my undergraduate years – Professor Anthony Sinclair, Professor Chul B. Park, Professor Axel Guenther and Professor Suk W. Cha for their mentorship and teachings.

During my time at Cornell, I have had the privilege to interact and collaborate with numerous people. I would first like to thank my former and current lab members Vlad Oncescu, Dakota O'Dell, Jess Hohenstein, Matthew Mancuso and Abdurrahman Gumus for the collaboration that have led to much of the work presented in this thesis. I also would like to acknowledge other lab members who have kept me company during the long hours at the lab, and provided useful suggestions/comments throughout, namely Li Jiang, Perry Schein, Elizabeth Rey, Aadhar Jain, Pilgyu Kang, Erica Jung, Ryan Snodgrass, Sasank Vemulapati and Ruisheng Wang. For my work in nutritional sciences, I acknowledge the help from Susannah Colt, Balaji Srinivasan, Vicky Simon and Erica Bender.

I owe a great debt of gratitude to the administrative staff in our department, namely Patti Wojcik, Laura Houghton and Marcia Sawyer; I would not have been able to focus on my daily research activities and meet

tight deadlines time after time if it had not been for their help on the administrative side. Completion of my thesis depended on the financial support from multiple funding agencies: National Science and Engineering Research Council of Canada (NSERC) through a Postgraduate scholarship, National Science Foundation (NSF) and Office of Naval Research (ONR).

My time in Ithaca has been enriched by my Cornellian friends who have become a big part of my life; I greatly value all the memories we now share. I feel truly fortunate to have known my best friends from Toronto throughout all these years, since before my journey at Cornell had even begun. Namely, I would like to thank Hansuk Kim, Hyun-Chul Chai, Sanghyun Park and Haesung Yoon for their friendship and the countless memories together. I acknowledge that this thesis could not have been completed without the support from my best friend-since-childhood, Sangyun Kim, who I know is watching over me from up above; at the times of hardship, I relied heavily on him for good advices and encouragements, and words cannot express how much I miss him.

Finally I would like to thank my family for their love and support. As a foreigner in the US, I have been comforted by the presence of my uncle and aunt in Staten Island who have provided a welcoming home that I could visit in just hours of driving. I am also grateful for my big brother Joonho for all his caring and sacrifices. Most of all, I express my love and sincere gratitude to my parents and grandmother who have supported me in all my pursuits and always put me first in their prayers.

TABLE OF CONTENTS

LIST OF FIGURES

LIST OF TABLES

Chapter 1:

Opportunities in point-of-need nutrition diagnostics and the role of smartphone technology†

1.1 Abstract

Micronutrient deficiency is widespread and negatively impacts morbidity, mortality, and quality of life globally. On-going advancements in nutritional biomarker discovery are enabling objective and accurate assessment of an individual's micronutrient and broader nutritional status. The vast majority of such assessment however still needs to be conducted in traditional centralized laboratory facilities which are not readily accessible in terms of cost and time in both the developed and developing countries. Point-of-need (PON) nutrition diagnostic technologies can significantly improve the situation by allowing rapid evaluation of one's nutritional status and providing an easy feedback mechanism for tracking changes in diet or supplementation. We believe that nutrition diagnostics represents a particularly appealing opportunity over other PON applications for two reasons: (1) healthy ranges for many micronutrients are well defined which allows for a unbiased diagnosis, and (2) many deficiencies can be reversed through changes in diet or supplementation before they become severe. In this chapter, we provide background on nutritional biomarkers used in nutrition diagnostics and review the emerging technologies that exploit them at the point-of-need. Furthermore, we discuss how the smartphone technology can be transformative to the deployment of these diagnostic devices.

---

† This chapter was reproduced from:

- **Lee, S.,** Srinivasan, B., Vemulapati, S., Mehta, S., Erickson, D. (2016) Personalized Nutrition Diagnostics at the Point of Need. (Under Review in Lab on a Chip)
- Erickson, D., O'Dell, D., Jiang, L., Oncescu, V., Gumus, A., **Lee, S.**, Mancuso, M., Mehta, S. (2014) Smartphone technology can be transformative to the deployment of lab-on-chip diagnostics. **Lab on a Chip**. 14: 3159-3164

1.2 Introduction

Micronutrient deficiency is prevalent worldwide and is associated with an increased risk of developing numerous health complications.[1-3] Iron deficiency for example is responsible for many of the 2 billion cases of anaemia, which in turn contributes to 20% of all maternal deaths.[4] Vitamin B_{12} deficiency is the leading cause of cognitive decline in the elderly, and affects a high percentage of the vegetarian and vegan populations whose dietary constraints prevent them from a sufficient B_{12} intake.[5-7] Vitamin A deficiency is also widespread and is the primary cause of blindness globally[4]. It is estimated that 77% of the US adults are considered to be vitamin D insufficient[8], and face increased risks of developing bone diseases[9], cardiovascular diseases[10] and infections[11-13].

Tackling micronutrient deficiencies has been identified by the Copenhagen Consensus as one of the most cost-effective intervention to further global development and progress.[14] Furthermore, numerous international agencies have identified the development of tools to efficiently measure micronutrient deficiencies as a priority (e.g. Gates Foundation[15]). Despite these, effective intervention for micronutrient deficiency has been a challenge as this often requires information about the micronutrient status of the population at the individual level. Unfortunately, most people around the globe have limited knowledge about their micronutrient status which is largely due to the difficulty in obtaining nutritional status measurements. The current standard methods of nutritional analysis need to be performed in centralized lab facilities, and thus are time consuming, labour intensive and can be even more challenging in resource-limited settings where the risks of micronutrient deficiencies are typically higher.[16] The problem is further complicated by the fact that deficiencies are often asymptomatic, resulting in patients who are unaware of the severity of their deficiencies until complications develop.

We believe that recent advancements in point-of-need (PON) devices can be applied to nutritional diagnostics and help tackle the micronutrient deficiency problem by making deficiency and tracking tests more accessible. In addition to being globally prevalent and having significant health consequences, micronutrient deficiency has two unique traits that make their PON diagnosis particularly appealing. First,

unlike many other biomarkers found in bodily fluids, the healthy ranges for nutritional biomarkers have been well studied and well defined, which enables one to often make more explicit and unbiased nutritional diagnosis. Second, many cases of micronutrient deficiencies can be reversed through simple changes in diet (e.g. supplementation, food fortification and food diversification) and/or behaviour modification before the condition becomes severe. This means that the effect of deploying a simple PON tool that can inform people of their micronutrient deficiencies can also make relatively simple therapeutic recommendations and the outcomes can be tracked with far fewer confounders.

In the following sections, we outline the role of nutritional biomarkers in nutritional analysis and the factors that may complicate their detection, and the lap-on-chip (LOC) technologies that have emerged to help address the world's micronutrient deficiency problem. We then discuss the challenges and opportunities facing the PON nutrition diagnosis at the consumer level. Lastly, we discuss the role of smartphone technologies in the deployment of the LOC diagnostic devices.

1.3 Nutritional biomarker considerations for diagnostic device design

Nutritional biomarkers are biochemical indicators found in bodily fluids that provide objective and specific means to assess one's micronutrient status.[17] They play a particularly important role in the diagnosis of micronutrient deficiencies for which patients are often asymptomatic and therefore not observable using common screening approaches based on anthropometric indicators (i.e. body measurements and clinical symptoms).[18] Since the concept of nutritional biomarkers was first introduced more than 30 years ago by Solomon *et al.*[19], the importance of nutritional biomarkers in assessing one's nutritional status has been well recognized and investigated. Prior to reviewing the technological state of the art, we first present a selection of standard biomarkers that can be used as detection targets of common micronutrient deficiencies. We then discuss how diagnosis reliant on biomarker levels alone could lead to misleading diagnosis, as each biomarker level could be affected differently by various factors including the presence of inflammation or infection, risk profile of the patient and timing relative to dietary exposure.

1.3.1 Standard biomarkers

Selecting nutritional biomarkers that accurately and reliably reflect the nutrient exposure, status and effect is challenging and there is currently a limited availability of these biomarkers.[20] This has been identified by the Institute of Medicine (IOM) as a knowledge gap that requires further research, and is being addressed by the National Institute of Child Health and Human Development (NICHD) through the creation of the Biomarkers of Nutrition for Development (BOND) program.[21] Despite the challenges, the tremendous progress in the areas of nutritional biomarkers, medicine, metabolism and genetics has led to the discovery of useful nutritional biomarkers over the years. Table 1.1 briefly outlines the standard biomarkers that have been studied and widely accepted for use in the status assessment of micronutrients such as iron, zinc, vitamins A, D, and B_{12} (Table 1.1). A more comprehensive information can be found elsewhere.[22]

1.3.2 Sample types and naturally occurring form of biomarkers

Following the selection of a proper biomarker, the PON device should consider for sample type in which the biomarker reference values are defined. As such they should often be able to process blood samples, which are complex to work with but contains the richest level of physiological information. Nonetheless, there are other bodily fluids like urine, saliva, breast milk, and sweat that could be suitable for assessment of certain biomarkers (see Table 1.1). Further, many nutrients are under homeostatic control in blood and their concentration in blood may not be indicative of true status or reflect shorter time periods of intake, necessitating analysis in other body fluids or tissues. For example, decreased levels of folate in serum (<7nM) may indicate vitamin B_9 deficiency, however deficiency is more accurately diagnosed by looking for RBC folate levels below 305nM. As there exist different processing requirements for each sample type, the diagnostic device should be developed accordingly. Another key consideration should be on what natural form the biomarkers are found in within the sample. For example, blood 25-hydroxyvitamin D [25(OH)D] exist 95-99% bound to the vitamin D binding proteins (VDBP).[23] As this hinders the immunoassay interactions that most vitamin D tests are based on, an essential sample processing to liberate the 25(OH)D from the VDBP has to be incorporated into the diagnostic device design.

Table 1.1: Summary of micronutrients, biomarkers & levels of deficiency/insufficiency, and health consequences[22]

Micronutrient	Biomarker	Levels of deficiency/insufficiency	Compatible sample types	Health consequences
Vitamin A	Retinol, Retinol-binding protein	<0.7 µM: deficiency; <1.05 µM: insufficiency[24]	Blood, breastmilk	Night blindness, delayed growth, ocular lesions and xerophthalmia, impaired immune functions
Vitamin B_7	Biotin	<140 pM in serum: deficiency; 140-365 pM; normal range[25]	Blood, urine	Dermatitis, depression, alopecia, seizures, developmental delay, poor skin and hair quality
Vitamin B_9	Folate (serum or RBC),	<7 nM in serum: insufficiency <305 nM in RBC: insufficiency	Blood	Tiredness, loss of appetite, megaloblastic anaemia, neural tube defects
Vitamin B_{12}	Serum vitamin B_{12},	<150 pM: deficiency; <221 pM: insufficiency	Blood	Neurological (paraesthesia, cognitive impairment) and hematological (anaemia) disorders
	Methylmalonic acid,	>376 nM: insufficiency		
	Homocysteine	>21.3 µM: insufficiency		
Vitamin C	Vitamin C	<11 µM in plasma: deficiency; <28 µM: insufficiency	Blood, urine	Scurvy, vitamin C hypovitaminosis
Vitamin D	Serum 25-hydroxyvitamin D,	<50 nM: deficiency; <75 nM: insufficiency	Blood	Rickets in children, osteomalacia in adults, osteoporosis
	Serum vitamin D binding protein*	300-600 µg/ml: normal range[26]; direct correlation to D deficiency has not yet been determined		
Vitamin E	Serum vitamin E	<5 µg/ml: deficiency; 5-20 µg/ml: normal range[27]	Blood	Neuromuscular and neurological disorders, retinopathy, anaemia
Zinc	Zinc	<10.7µM in serum: deficiency[28]	Blood, hair	Anorexia, lethargy, diarrhoea, growth restriction (delayed bone maturation), impaired immune function
Iron	Serum ferritin,	<12 ng/mL: deficiency in children under 5 years of age; <15 ng/mL: deficiency in adults	Blood	Anaemia, insufficient energy metabolism, impaired muscle strength and endurance, impaired collagen synthesis, increased anxiety, impaired memory, low birth weight and premature delivery (pregnant women)
	Serum soluble transferrin receptor,	>4.4µg/ml: deficiency[29]		
	Hemoglobin*	<110 mg/mL: deficiency in pregnant women; <120 mg/mL: deficiency in non-pregnant women; <130 mg/mL: deficiency in men (>15 years)		
Iodine	Urinary iodine,	<99 ng/mL in: insufficiency in children; <150 ng/mL: insufficiency in pregnant women	Urine, blood	Goiter, impaired mental function, hypothyroidism, delayed physical development
	Serum TSH	>5 IU/mL: deficiency		
Selenium	Selenium	<80 ng/mL in serum or plasma: deficiency[30]; >1µg/mL: excess [31]	Blood, urine, toe nails, scalp hair[32]	Selenosis (excess selenium; hair loss, brittle nails, nausea, diarrhea, fatigue), Keshan disease (deficient selenium)
CRP**,	Serum CRP	>5 µg/mL[33]: inflammation	Blood	Increased risk of diabetes and cardiovascular disease (chronic inflammation); presence of infection and/or trauma (acute inflammation)
AGP**	Serum AGP	>1 mg/mL[33]: inflammation		

* non-specific markers
** inflammation markers needed for accurate iron and vitamin A status evaluation

1.3.3 Presence of infection or inflammation.

Biomarker levels of certain micronutrient deficiencies will be affected by the presence of infection or inflammation in the patient. The failure to take this into account has caused major problems in the current methods used to identify vitamin A and iron deficiencies. Being acute phase reactants, the RBP and ferritin concentrations change (i.e. RBP levels decrease and ferritin levels increase) during an infection or any underlying inflammation.[34] Therefore without accurate assessment of inflammation, the estimates of iron and vitamin A deficiency are biased – false overdiagnosis of iron deficiency and underdiagnosis of vitamin A deficiency. For the detection of such micronutrients, the PON device design should eliminate false outputs by incorporating inflammation and infection markers such as C-reactive protein (CRP) or α1-acid glycoprotein (AGP).[33,35]

1.3.4 Risk group

Health consequences of some micronutrient deficiencies could represent a higher threat for certain population groups based on gender, age, race, or location. As such, cut-off values and reference ranges of nutritional biomarker levels may be defined differently for each population group. For example, iron deficiency is defined by serum ferritin concentrations below 12 ng/mL and 15 ng/mL in children less than five years of age and adults, respectively.[36] Such understanding should be incorporated in the design of the diagnostic device for more accurate diagnosis of one's nutritional status.

1.3.5 Timing relative to dietary exposure

Biomarkers can be classified into short term (representing intake over past hours/days), medium-term (representing intake over weeks/months) and long-term markers (representing intake over months/years).[37] As such the knowledge of the user's recent/usual micronutrient intake, as well as acute/chronic exposure should be incorporated into the operation timing of the nutritional diagnostic devices. For example, analysis of selenium in urine provides information on recent intake, and that in hair or toenails gives a more reliable assessment of long-term selenium status.

1.4 State-of-the-art lap-on-chip biosensor systems for nutritional biomarkers

Currently there is a need for the development of accurate and reliable PON devices for nutrition diagnostics that can: (1) detect nutritional biomarkers directly from bodily fluids with a matching performance to that of the gold standard methods, where the device's limit-of-detection and sensitivity can provide an in-depth, quantitative information about one's nutritional status, and (2) multiplex the detection to a handful of biomarkers, in which the device is able to autonomously process and deliver the samples/reagents to and from the regions of appropriate biochemical events as required for the detection of each biomarker. Realization of such aims in PON has been the idea behind the development of "lab-on-chip (LOC)" or microfluidic based diagnostics technology[38], and there recently have been demonstrations of such devices for the rapid biochemical detection of some nutritional biomarkers including: iron, vitamins A, B_7, B_{12} and zinc. In the following sections we review the technological state of the art, while categorizing them by the underlying biochemical detection principle. While immunoreactions represent the standard method of detection for many, special molecular characteristics of some biomarkers enable their detection through other approaches using electrochemical, affinity-based and chemiluminescent reactions. We also discuss how the recent advancements of smartphone technology could facilitate the PON deployment of many of these LOC sensor systems.

1.4.1 Immunosensing of nutritional biomarkers in point-of-need

Immunoreactions (i.e. specific binding interactions between the biomarkers and their respective antibodies) have been the underlying detection principle of many gold standard methods including enzyme-linked immunosorbent assays (ELISA) and immunofluorescence assays (IFA). The biomarker-to-antibody interactions are easily transferrable onto the miniaturized features on LOC platforms, which have led to their widespread use in the PON detection of nutritional biomarkers.

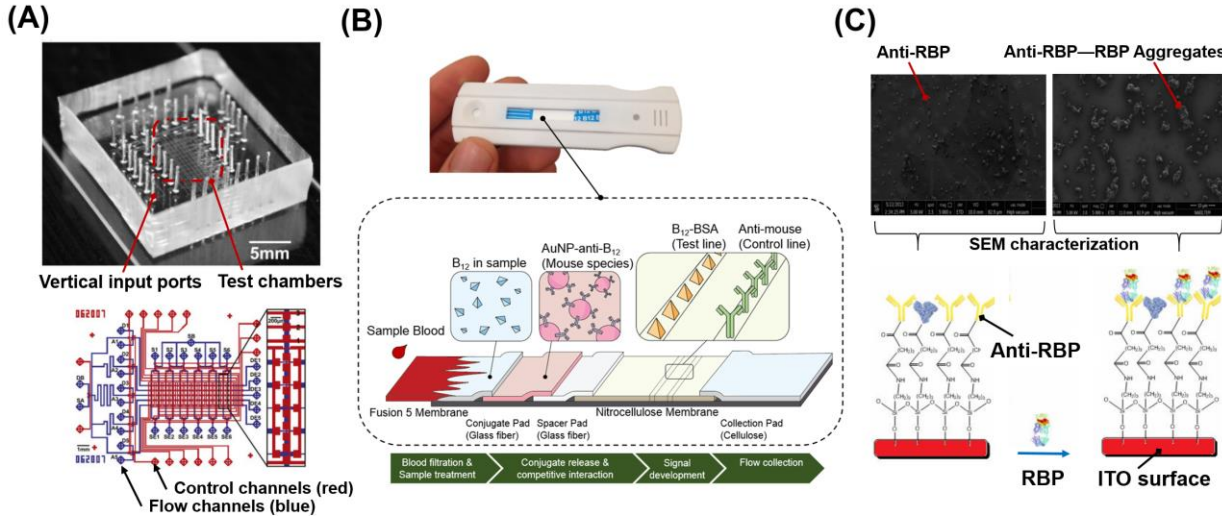

Figure 1.1: Immunosensing of nutritional biomarkers. **(A)** Microfluidic fluorescent immunoassay for the 5-plex detection of ferritin, CRP and other blood proteins **(B)** Lateral flow colorimetric immunoassay for vitamin B_{12} detection in PON **(C)** ITO-based label-free electrochemical immunosensor for RBP detection. Figures adapted with permission from: (A) Ref. 39 Copyright 2009 John Wiley and Sons, (C) Ref. 46 Copyright 2014 John Wiley and Sons.

1.4.1.1 Labelled immunosensors.

Labelled immunoassays are characterized by the use of detection labels on the antigen or antibody for producing discernible signals in an immunoreaction, and may be further classified by the specific label type (e.g. fluorescent, colorimetric, enzymatic, chemiluminescent etc.). **Figure 1.1**a shows a disposable microfluidic fluorescent immunoassay for the 5-plex detection of ferritin, CRP and other blood proteins in human serum samples.[39] In this work, in-parallel detection of 5 different target molecules is achieved on-chip by the incorporation of: the micromechanical values for controlling the reagent flow by pressure, the microchannels for directing the reagents within the chip, and the microchambers for hosting the fluorescent sandwich immunoassay. The device can sensitively measure serum ferritin levels in the range of 350–3500pg/ml, which could be combined with its CRP measurements to provide an accurate iron deficiency diagnosis. While this represents a promising step towards a PON detection of multiple nutritional biomarkers, there remains major limitations including the absence of on-chip filtration mechanism for blood

samples, and the requirement for a laboratory-scale microscope and computing platform for the fluorescent signal analysis.

Rapid diagnostic tests (RDTs), widely known for their lateral flow detection principles, are another example of a labelled immunosensor where gold nanoparticles (AuNP) are used as the colorimetric detection labels in an immunoreaction. They have been successfully deployed at the consumer level for the diagnosis of various diseases and medical conditions (e.g. ref. [40]), but their application in nutrition has been limited. The recent development of a RDT for vitamin D (Test4D™; Nanospeed Diagnostics) demonstrates the growing demand for these tests which are rapid, cheap, and capable of accepting whole blood samples directly for autonomous processing, transport and biochemical analysis. Here the Test4D™ can effectively act as a PON binary test using 32ng/ml of 25(OH)D levels as the vitamin D deficiency cut-off. More recently our group has demonstrated a novel lateral flow assay for vitamin B_{12} (Figure 1.1b) that achieves the detection of sub-ng/ml levels of vitamin B_{12} through the use of silver enhancement and the "spacer pad" that increases the duration of a key immunoreaction.[41i] This has the potential to extend the applicability of RDTs for the detection of other key nutritional biomarkers that are physiologically found in sub-ng/ml concentrations (e.g. vitamin B_7 or biotin; 140-365 pM). Despite their exceptional suitability for PON applications and the recent performance advancements, the RDTs are typically limited in two main ways. First is the binary nature of the results which are insufficient for fully describing one's micronutrient status. Second is the simple one-directional nature of the sample/reagent flow which hampers the multiplexing of distinctly different biomarkers that demand varying levels of sample processing, biochemical reaction and/or signal amplification.

1.4.1.2 Label-free immunosensors.

Detection of nutritional biomarkers can also be achieved using label-free immunosensors based on the transduction of biomarker-to-antibody binding events into measurable signals that may be electrochemical,

[i] This work is detailed in Chapter 3 of this Thesis

optical, piezoelectric or thermometric.[39,42,43] Among the methods based on different transduction schemes, electrochemical label-free immunosensors have shown the biggest potential for PON sensing applications as they are low-cost, highly sensitive, biocompatible, and easily miniaturized.[44,45] Recently a disposable, label-free electrochemical immunosensor for vitamin A deficiency diagnosis was reported. [46] As shown in Figure 1.1c, Indium Tin Oxide (ITO) surface with an immobilized layer of anti-RBP acted as the transducer that changed its impedance in response to the binding events between the anti-RBP and the sample RBP. Analysing the impedance data using the single Frequency Impedance technique, Şimşek *et al.* quantified purified RBP in artificial serum samples with a limit-of-detection of 2.5ag/mL. While the presented immunosensor required laboratory infrastructure for its operation, ultrasensitive electrochemical immunosensors that are better suited for PON nutrition diagnostics may be developed by integrating the sensors into compact microfluidics systems as demonstrated in other works for the detection of non-nutritional biomarkers.[47,48]

1.4.2 Chemical sensing of nutritional biomarkers.

Special molecular characteristics of some nutritional biomarkers offer additional sensing strategies to be exploited even when the associated antibodies are non-existent or not readily available. These are often minerals and water-soluble vitamins that can easily be incorporated into: a part of known protein-ligand affinity interactions, or a chain of chemical reactions as reactants or catalysts. In the following sections we discuss how these principles have been used to enable the PON detection of biotin (vitamin B_7), zinc and cobalt (II) ions in vitamin B_{12}.

1.4.2.1 Protein-ligand affinity sensors.

Extremely high affinity between biotin and streptavidin has been well known and exploited in numerous purification and sensing applications by tagging biotin to target proteins and subsequently capturing them with streptavidin modified with various reporters (e.g. enzymes, fluorophores).[49] For the special case where biotin is the target molecule itself, its detection using streptavidin can be more convenient and direct. Dimov

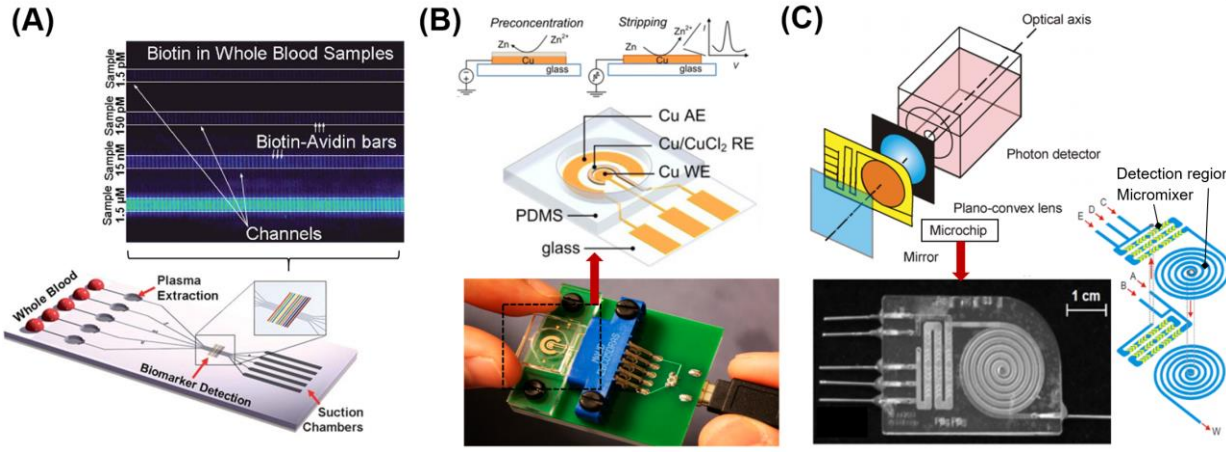

Figure 1.2: Chemical sensing of nutritional biomarkers. **(A)** SIMBAS system exploiting streptavidin-biotin affinity pair for detection of biotin **(B)** electrochemical sensor for detection of zinc **(C)** chemiluminescent sensor for detection of cobalt (II) ions in vitamin B_{12}. Figures adapted with permission from: (A) Ref. 50 Copyright 2011 The Royal Society of Chemistry, (B) Ref. 51 (direct link: http://pubs.acs.org/doi/abs/10.1021/ac500277j) Copyright 2014 The American Chemical Society, (C) Ref. 52 Copyright 2012 The Royal Society of Chemistry.

et al. has previously demonstrated a "Stand-alone self-powered integrated microfluidic blood analysis system (SIMBAS)" which used the biotin-streptavidin affinity pair to quantify pM of biotin levels in whole blood.[50] As shown in **Figure 1.2**a, the PDMS-based SIMBAS system has 3 key parts: the filter that extracts plasma from whole blood samples by sedimentation, detector that captures sample biotin via an immobilized layer of streptavidin, and suction chamber that sucks in and drives the sample flow with the vacuum pressure created by degassing. For operation, the authors ran SIMBAS with blood samples spiked with various concentrations of fluorescently tagged biotin, and demonstrated quantification of biotin down to 1.5pM after 10min. The effective use of microfluidics in SIMBAS has led to numerous advantages including: the low sample volume requirement of 5μl, rapidity, self-powered blood sample processing and flow activation, and the ability to run 5 in-parallel tests. Despite the strengths, the key limitation of the SIMBAS is that it required the fluorescent labels to be on the biotin for quantitation, whereas the naturally occurring biotin in human blood will be without labels. Furthermore, the future application of the SIMBAS to other biomarkers necessitates the detection using other affinity pairs that likely have weaker interactions

than those between biotin and streptavidin, which will evidently lead to reduced sensor performance. Ultimately for the current system, the requirement for a microscope to analyze fluorescence signals at the end hampers its deployment for PON quantification of biotin.

1.4.2.2 Electrochemical sensors.

Several nutritional biomarkers of the ionic form may be detected using an electrochemical principle known as anodic stripping voltammetry (ASV). Recently, a disposable copper-based electrochemical sensor that uses the ASV method for the PON detection of zinc in serum was demonstrated.[51] As shown in Figure 1.2b, the zinc in the sample undergoes two steps, namely: preconcentration step in which zinc is electroplated on a copper electrode of the electrochemical sensor, and stripping step in which zinc is oxidized to generate current that can be measured and correlated with sample zinc concentrations. Their novel sensor showed a limit-of-detection of 140nM zinc and operated in the physiologically relevant range of 10-15μM zinc with a total analysis time under 15min. Furthermore, the presented sensor has a number of attributes that make it attractive for PON applications including: the choice of low-cost copper as the new electrode material, sensor integration with miniature potentiostat/galvanostat system, and disposability. However, the sensor operation in this work was limited by the laboratory-based sample extraction, and could be advanced by incorporating microfluidics technology to perform sample processing on-chip. Additionally, copper as a working electrode may not be as robust as the carbon-based electrode choices.

1.4.2.3 Enzymatic sensors.

On the other hand, some nutritional biomarkers may be known catalysts of reactions that emit detectable signals of various forms including chemiluminescence. Recently, a continuous-flow microfluidic LOC device based on luminol-peroxide chemiluminescent reactions was demonstrated for the determination of vitamin B_{12}.[52] In this work, Lok *et. al* exploited the finding that the cobalt (II) ions in vitamin B_{12}, when liberated via acidification, are effective catalysts for the oxidation of luminol in the presence of hydrogen peroxide (H_2O_2) under alkaline conditions. The chemiluminescent signal produced could be correlated to

the cobalt (II) ion concentrations, which are directly correlated to the sample B_{12} concentrations[53]. As shown in Figure 1.2c, the microchip device contains two passive micromixers with 5 inlets (correlating to vitamin B_{12} sample, hydrochloric acid (HCl), sodium hydroxide (NaOH), luminol and H_2O_2), and double spiral microchannels as optical detection regions. In operation, sample B_{12} and HCl were inputted into the micromixer in order to free the cobalt (II) ions from the B_{12} via acidificaiton, subsequently followed by the supplies of NaOH, luminol and H_2O_2 which initiated the chemiluminescent signal production. While the device has demonstrated an excellent LOD of 0.368 pg/mL B_{12}, the performance was only demonstrated using B_{12} supplements and egg yolk which were processed and prepared off-chip as samples. Furthermore, the requirements for laboratory-scale detector system and infusion pumps represent hurdles for its PON vitamin B_{12} determination.

1.5 Challenges in deployment of lap-on-chip diagnostics

As discussed for the field of nutrition diagnostics (Section 1.4), making complex biochemical measurements in PON settings is being enabled by the technological advancement in the LOC systems that enhance the: throughput, parallelity, sensitivity/specificity, or other analytical metrics for biochemical assays conducted within research or centralized lab facilities. Such advancements have not been limited to nutrition diagnostics, and there have been numerous successes in the development of LOC devices for other health-related applications ranging from cancer diagnostics to detection of general markers of infectious diseases. Unfortunately however, only a few have successfully transitioned to the consumer diagnostics market. While there are numerous successful biomedical consumer products that contain microscale channels or similar features (e.g. inhalers for asthmatics), most of these are at least conceptually different from the traditional vision of a LOC device.

There may be two reasons for this. The first is the difficulty in obtaining quantitative results with a simple one-off test. The majority of commercially available tests for the consumer market are Rapid Diagnostic Tests (RDTs) based on the lateral flow principle (e.g. ref. [40]). Such products are popular because the user

only needs to insert the sample and the fluid transport, sample processing, and detection reaction all occur autonomously. Unfortunately, these types of tests are typically only able to provide non-quantitative information and thus are only useful when the desired result is binary (e.g. pregnant/not pregnant). Obtaining a quantitative result requires a more complex sensor system and sample handling technique, which typically must be interpreted and displayed by a reusable and often research grade instrument. While some simple visual feedback systems have been developed, as with colorimetric tests, these tend to rely on higher initial target number than are found in most applications and are subject to user interpretation error. A second challenge is that most of the analytes a typical consumer wants to be tested for (e.g. vitamin D) do not require frequent testing. In the consumer market the reader and consumable model has proven most successful where the user must make numerous measurements over the course of a day or week, as is done with blood glucose monitoring. In such a case the consumer is willing to spend a little more to purchase a reader since it will be used so frequently, or conversely the company may be willing to sell the reader at a loss in order to increase consumable sales. For cases where measurements are made sporadically or with much lower frequency, the cost of purchasing a personal reader system can be prohibitively high, particularly for the casual user, representing a high bar to market entry.

1.6 Role for smartphone based lap-on-chip diagnostics

We believe the extreme societal penetration of the smartphone and its ubiquity, familiarity, and functionality, can fundamentally alter this predicament. Almost 46% of American adults have a smartphone today and this number is expected to keep increasing with an anticipated 250 million smartphones in use in the US by the year 2016.[54] This means that nearly every person in the US (and by extension most developed countries) is either carrying a smartphone with them or has near immediate access to one. Not only do these devices contain state-of-the-art imaging, data analysis, communications, and social networking capabilities, they are an extremely easy to use and familiar to almost all age groups. It is common to see everyone from the elderly to pre-school children using them. This familiarity can dramatically reduce required training

requirements and potentially user errors during testing. As we and others have demonstrated, the majority of the functionality required to make and interpret a quantitative in vitro measurement is already embedded in smartphones. **Figure 1.3** shows a few examples of recently demonstrated system for colorimetric test strip analysis,[55] microscopy,[56] genetic testing,[57] and electrochemical detection.[58] As can be seen, a typical system comprises of an accessory, which is either fitted to the smartphone and interacts with the on-board camera or the communications port, and a test "chip" (or similar) which is inserted into the accessory. The key of such systems is that the vast majority of the cost and complexity is embedded in the smartphone, which the user can be expected to have and therefore need not be engineered separately into the system. This is transformative for lab-on-chip technology because now it can be relied upon that most consumers will already own a test reader/instrument in the form of a smartphone and business models can be constructed around selling the test strips at high margins with a significantly lower barrier to entry. The

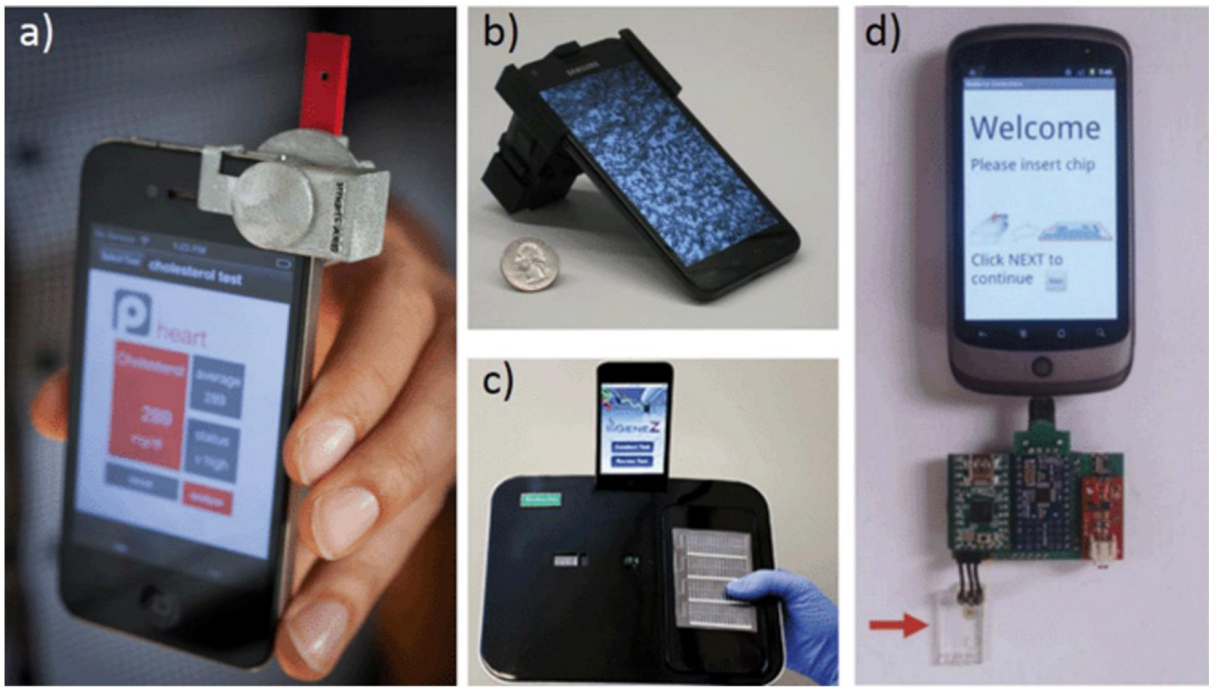

Figure 1.3 Smartphone based microfluidic and lab-on-chip technology. **(A)** colorimetric analysis for serum cholesterol detection **(B)** smartphone microscopy **(C)** genetic testing and **(D)** electrochemistry analysis. Images (B), (C), and (D) reproduced from ref. 56, 57 and 58 respectively with permission from The Royal Society of Chemistry.

opportunity is even more apparent in lower and middle income countries where the relatively low infrastructure requirements associated with establishing high-quality cellular (or mobile) networks makes smartphones one of the few widely deployed technologies.

1.7 Smartphone based lap-on-chip systems for nutritional biomarkers

As reasoned in Section 1.6, the worldwide update in smartphone based technology can be transformative to the deployment of LOC diagnostics by addressing the aforementioned challenges outlined in Section 1.5. In this section, we present some of the emerging smartphone based systems in the field of nutrition diagnostics.

The efficacy of smartphone based platforms in nutritional analysis was previously demonstrated by our group for vitamin D deficiency diagnosis.[59] In that work, we presented the "vitamin D AuNP immunoassay device (vitaAID)" system shown in **Figure 1.4**a which used the smartphone's imaging and computational capabilities to read and analyze colorimetric signals from a novel AuNP-based immunoreaction on the vitaAID test strips.[ii] The system accurately quantified serum 25(OH)D with an accuracy of 15nM and a precision of 10nM without the use of conventional laboratory equipment (i.e. spectrophotometer). More recently we presented the NutriPhone system, a mobile platform for personalized diagnosis of vitamin B_{12} deficiency.[41][iii] This system improved upon the limitations of the vitaAID system by incorporating a custom RDT for vitamin B_{12} capable of processing and analysing whole blood samples on-chip in less than 15min. Figure 1.4b demonstrates another example in which a simple paper based microfluidics technology was empowered to perform complex PON nutrition diagnostics by being integrated with the smartphone technology. In this work, Lee *et al.* presented the "electronics enabled microfluidic paper-based analytical

[ii] This work is detailed in Chapter 2 of this Thesis
[iii] This work is detailed in Chapter 3 of this Thesis

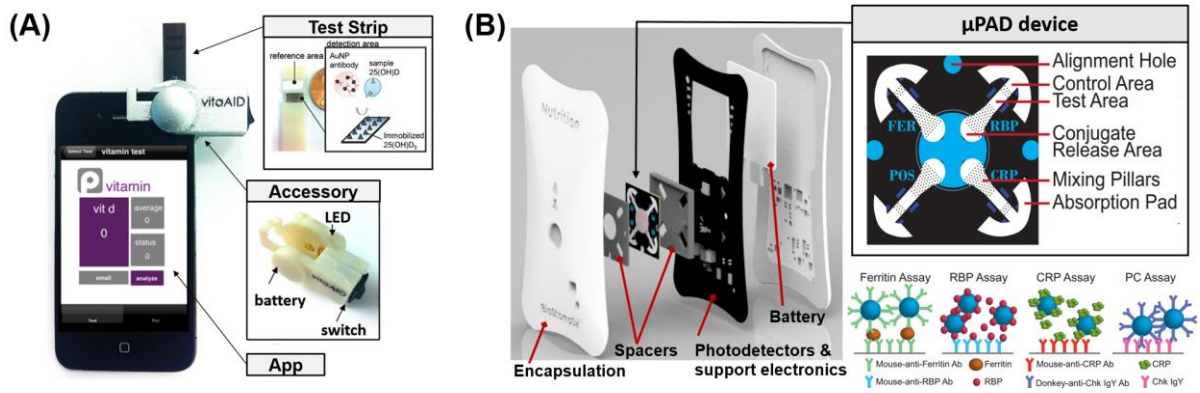

Figure 1.4: Smartphone enabled sensing of nutritional biomarkers. **(A)** vitaAID system for PON diagnosis of vitamin D deficiency **(B)** ee-μPAD system for diagnosis of vitamin A and iron deficiencies and inflammation. Figures adapted with permission from: (A) Ref. 59 Copyright 2014 The Royal Society of Chemistry, (B) Ref. 60 Copyright 2015 John Wiley and Sons.

device (EE-μPAD)" which consists of: a paper-based microfluidics device for immunodetection of ferritin, RBP and CRP in whole blood samples, and an optoelectronics system that measures light transmission through the detection regions on the paper-based device and wirelessly transmits the data to a smartphone for processing the data and communicating the results.[60] Outsourcing of the computing power and connectivity of smartphones enable the EE-μPAD to assess vitamin A, iron and inflammation status by allowing the quantification of RBP, ferritin and CRP, respectively, in the physiologically relevant ranges. The efficacy of the EE-μPAD was further demonstrated through a clinical trial where it showed comparable performance to the gold standard ELISA method in assessing 95 whole blood samples. The partial relsiance on smartphones wherein sensing is achieved by a separate optoelectronics component adds costs to the EE-μPAD, however presents benefits including its universal compatibility with different types of smartphones, and easier automation of the device operations.

1.8 Summary and future perspectives

Micronutrient deficiencies are globally prevalent and responsible for the suboptimal health of the world population, most of whom lack access to proper nutrition diagnostic systems. Development of rapid, cheap and easy-to-use system for accurate evaluation of nutritional biomarkers in PON settings has the potential

to address the challenges with current laboratory based methods, and allow for more effective management of micronutrient deficiencies. The on-going advancements in nutritional biomarkers are establishing ways to more accurately diagnose micronutrient deficiencies, which can foster the development of such diagnostic systems.

Various systems for PON diagnosis of numerous micronutrient deficiencies have been realized by miniaturizing different biochemical sensing approaches on LOC devices, which necessarily incorporate microfluidics and/or filtering mechanisms to process and handle the complex bodily fluids on-chip. While most of the aforementioned work is still limited to laboratory use due to the persisting requirements for sophisticated analytical tools, the growing ubiquity of smartphone technology with powerful sensing, computing and communication capabilities is replacing such equipment in PON settings.

So far, in the field of PON nutrition diagnostics, smartphone technology has been coupled with simple paper-based test strips, empowering them to diagnose several micronutrient deficiencies based on quantitative biomarker measurements. However, smartphone technology can also enable other types of LOC devices such as fluorescent or chemiluminescent based systems for PON nutrition diagnostics, as has been demonstrated in recent works for similar applications.[61,62] Beyond their roles as analytical systems, the smartphone based PON diagnostic systems have the potential to effectively store and communicate micronutrient status data for better epidemiological understanding and management of the micronutrient deficiencies.

1.9 References

1. Bailey, R. L., West Jr, K. P. & Black, R. E. The Epidemiology of Global Micronutrient Deficiencies. *Annals of Nutrition and Metabolism* **66(suppl 2)**, 22-33 (2015).

2. Black, R. E., Allen, L. H., Bhutta, Z. A., Caulfield, L. E., De Onis, M., Ezzati, M., Mathers, C., Rivera, J., Maternal & Group, C. U. S. Maternal and child undernutrition: global and regional exposures and health consequences. *The lancet* **371**, 243-260 (2008).

3. Black, R. Micronutrient deficiency: an underlying cause of morbidity and mortality. *Bulletin of the World Health Organization* **81**, 79-79 (2003).

4. WHO. *Micronutrient deficiencies*, <http://www.who.int/nutrition/topics/ida/en/> (2015).

5. Clarke, R., Birks, J., Nexo, E., Ueland, P. M., Schneede, J., Scott, J., Molloy, A. & Evans, J. G. Low vitamin B-12 status and risk of cognitive decline in older adults. *The American journal of clinical nutrition* **86**, 1384-1391 (2007).

6. Key, T. J., Appleby, P. N. & Rosell, M. S. Health effects of vegetarian and vegan diets. *Proceedings of the Nutrition Society* **65**, 35-41 (2006).

7. Stabler, S. P. & Allen, R. H. Vitamin B12 deficiency as a worldwide problem. *Annu. Rev. Nutr.* **24**, 299-326 (2004).

8. Ginde, A. A., Liu, M. C. & Camargo, C. A. Demographic Differences and Trends of Vitamin D Insufficiency in the US Population, 1988–2004. *Archives of internal medicine* **169**, 626-632, doi:10.1001/archinternmed.2008.604 (2009).

9. Gennari, C. Calcium and vitamin D nutrition and bone disease of the elderly. *Public health nutrition* **4**, 547-559 (2001).

10. Wang, T. J., Pencina, M. J., Booth, S. L., Jacques, P. F., Ingelsson, E., Lanier, K., Benjamin, E. J., D'Agostino, R. B., Wolf, M. & Vasan, R. S. Vitamin D deficiency and risk of cardiovascular disease. *Circulation* **117**, 503-511 (2008).

11. Mehta, S., Giovannucci, E., Mugusi, F. M., Spiegelman, D., Aboud, S., Hertzmark, E., Msamanga, G. I., Hunter, D. & Fawzi, W. W. Vitamin D status of HIV-infected women and its association with HIV disease progression, anemia, and mortality. *PLoS One* **5**, e8770, doi:10.1371/journal.pone.0008770 (2010).

12. Mehta, S., Hunter, D. J., Mugusi, F. M., Spiegelman, D., Manji, K. P., Giovannucci, E. L., Hertzmark, E., Msamanga, G. I. & Fawzi, W. W. Perinatal outcomes, including mother-to-child transmission of HIV, and child mortality and their association with maternal vitamin D status in Tanzania. *J Infect Dis* **200**, 1022-1030, doi:10.1086/605699 (2009).

13. Holick, M. F. Sunlight and vitamin D for bone health and prevention of autoimmune diseases, cancers, and cardiovascular disease. *The American journal of clinical nutrition* **80**, 1678S-1688S (2004).

14. *Copenhagen Consensus: Results*, <http://copenhagenconsensus.com/Files/Filer/CC08/Presse%20%20result/CC08_results_FINAL.pdf> (2008).

15. *Bill and Melinda Gates Foundation, Nutrition: Strategy Overview*, <https://docs.gatesfoundation.org/Documents/nutrition-strategy.pdf> (2011).

16. Müller, O. & Krawinkel, M. Malnutrition and health in developing countries. *Canadian Medical Association Journal* **173**, 279-286 (2005).

17. Potischman, N. & Freudenheim, J. L. Biomarkers of nutritional exposure and nutritional status: an overview. *The Journal of nutrition* **133**, 873S-874S (2003).

18. Blössner M, d. O. M. Malnutrition: quantifying the health impact at national and local levels. *WHO Environmental Burden of Disease Series* **12** (2005).

19. Solomons, N. W. & Allen, L. H. The Functional Assessment of Nutritional Status: Principles, Practice and Potential. *Nutrition Reviews* **41**, 33-50, doi:10.1111/j.1753-4887.1983.tb07456.x (1983).

20. Black, R. E., Allen, L. H., Bhutta, Z. A., Caulfield, L. E., de Onis, M., Ezzati, M., Mathers, C. & Rivera, J. Maternal and child undernutrition: global and regional exposures and health consequences. *The Lancet* **371**, 243-260, doi:10.1016/S0140-6736(07)61690-0.

21. Combs, G. F., Trumbo, P. R., McKinley, M. C., Milner, J., Studenski, S., Kimura, T., Watkins, S. M. & Raiten, D. J. Biomarkers in nutrition: new frontiers in research and application. *Annals of the New York Academy of Sciences* **1278**, 1-10, doi:10.1111/nyas.12069 (2013).

22. Erdman Jr, J. W., MacDonald, I. A. & Zeisel, S. H. *Present knowledge in nutrition*. (John Wiley & Sons, 2012).

23. D. Carter, G. Accuracy of 25-Hydroxyvitamin D Assays: Confronting the Issues. *Current Drug Targets* **12**, 19-28 (2011).

24. WHO. Indicators for assessing vitamin A deficiency and their application in monitoring and evaluation intervention programmes. *World Health Organization* (1996).

25. Mardach, R., Zempleni, J., Wolf, B., Cannon, M. J., Jennings, M. L., Cress, S., Boylan, J., Roth, S., Cederbaum, S. & Mock, D. M. Biotin dependency due to a defect in biotin transport. *The Journal of Clinical Investigation* **109**, 1617-1623, doi:10.1172/JCI13138 (2002).

26. Blanton, D., Han, Z., Bierschenk, L., Linga-Reddy, M. V. P., Wang, H., Clare-Salzler, M., Haller, M., Schatz, D., Myhr, C., She, J.-X., Wasserfall, C. & Atkinson, M. Reduced Serum Vitamin D–Binding Protein Levels Are Associated With Type 1 Diabetes. *Diabetes* **60**, 2566-2570, doi:10.2337/db11-0576 (2011).

27. Packer, L. *Vitamin E in Health and Disease: Biochemistry and Clinical Applications*. (CRC Press, 1992).

28. Cole, C. R., Grant, F. K., Swaby-Ellis, E. D., Smith, J. L., Jacques, A., Northrop-Clewes, C. A., Caldwell, K. L., Pfeiffer, C. M. & Ziegler, T. R. Zinc and iron deficiency and their interrelations in low-income African American and Hispanic children in Atlanta. *The American Journal of Clinical Nutrition* **91**, 1027-1034, doi:10.3945/ajcn.2009.28089 (2010).

29. CDC. Trace Elements: Iron-Stats Indicators. *Second National Report on Biochemical Indicators of Diet and Nutrition in the U.S. Population* (2012).

30. NIH. Selenium: Dietary Supplement Fact Sheet. (2016).

31. Column, H. C. ASPEN Dietetics Section Newsletter January 2001. (2001).

32. Blaurock-Busch, E., Amin, O. R., Dessoki, H. H. & Rabah, T. Toxic Metals and Essential Elements in Hair and Severity of Symptoms among Children with Autism. *Mædica* **7**, 38-48 (2012).

33. Thurnham, D. I. & McCabe, G. P. Influence of infection and inflammation on biomarkers of nutritional status with an emphasis on vitamin A and iron. *WHO. Report: priorities in the assessment of vitamin A and iron status in populations, Panama City, Panama*, 15-17 (2010).

34. Thurnham, D. I., McCabe, G. P., Northrop-Clewes, C. A. & Nestel, P. Effects of subclinical infection on plasma retinol concentrations and assessment of prevalence of vitamin A deficiency: meta-analysis. *Lancet* **362**, 2052-2058 (2003).

35. Tomkins, A. Assessing micronutrient status in the presence of inflammation. *J Nutr* **133**, 1649S-1655S (2003).

36. CDC. *National Report on Biochemical Indicators of Diet and Nutrition in the U.S. Population: Iron Status Indicators* (1999-2002).

37. Potischman, N. Biologic and methodologic issues for nutritional biomarkers. *J Nutr* **133 Suppl 3**, 875s-880s (2003).

38. Manz, A., Graber, N. & Widmer, H. M. Miniaturized total chemical analysis systems: a novel concept for chemical sensing [op.9]. *Sensors and actuators B: Chemical* **1**, 244-248 (1990).

39. Kartalov, E. P., Lin, D. H., Lee, D. T., Anderson, W. F., Taylor, C. R. & Scherer, A. Internally calibrated quantification of protein analytes in human serum by fluorescence immunoassays in disposable elastomeric microfluidic devices. *Electrophoresis* **29**, 5010-5016, doi:10.1002/elps.200800297 (2008).

40. Wongsrichanalai, C., Barcus, M. J., Muth, S., Sutamihardja, A. & Wernsdorfer, W. H. A review of malaria diagnostic tools: microscopy and rapid diagnostic test (RDT). *The American journal of tropical medicine and hygiene* **77**, 119-127 (2007).

41. Lee, S., O'Dell, D., Hohenstein, J., Colt, S., Mehta, S. & Erickson, D. NutriPhone: a mobile platform for low-cost point-of-care quantification of vitamin B12 concentrations. . *Under Review* (2016).

42. Moina, C. & Ybarra, G. Fundamentals and applications of immunosensors. *Advances in immunoassay technology*, 65-80 (2012).

43. Vestergaard, M. d., Kerman, K. & Tamiya, E. An Overview of Label-free Electrochemical Protein Sensors. *Sensors (Basel, Switzerland)* **7**, 3442-3458 (2007).

44. Daniels, J. S. & Pourmand, N. Label-Free Impedance Biosensors: Opportunities and Challenges. *Electroanal* **19**, 1239-1257, doi:10.1002/elan.200603855 (2007).

45. Wan, Y., Su, Y., Zhu, X., Liu, G. & Fan, C. Development of electrochemical immunosensors towards point of care diagnostics. *Biosensors and Bioelectronics* **47**, 1-11, doi:http://dx.doi.org/10.1016/j.bios.2013.02.045 (2013).

46. Şimşek, Ç. S., Teke, M. & Sezgintürk, M. K. An ITO Based Disposable Biosensor for Ultrasensitive Analysis of Retinol Binding Protein. *Electroanal* **26**, 328-339, doi:10.1002/elan.201300443 (2014).

47. Kellner, C., Botero, M. L., Latta, D., Drese, K., Fragoso, A. & O'Sullivan, C. K. Automated microsystem for electrochemical detection of cancer markers. *ELECTROPHORESIS* **32**, 926-930, doi:10.1002/elps.201000667 (2011).

48. Tan, F., Leung, P. H. M., Liu, Z.-b., Zhang, Y., Xiao, L., Ye, W., Zhang, X., Yi, L. & Yang, M. A PDMS microfluidic impedance immunosensor for E. coli O157:H7 and Staphylococcus aureus detection via antibody-immobilized nanoporous membrane. *Sensors and Actuators B: Chemical* **159**, 328-335, doi:http://dx.doi.org/10.1016/j.snb.2011.06.074 (2011).

49. Dundas, C. M., Demonte, D. & Park, S. Streptavidin–biotin technology: improvements and innovations in chemical and biological applications. *Applied microbiology and biotechnology* **97**, 9343-9353 (2013).

50. Dimov, I. K., Basabe-Desmonts, L., Garcia-Cordero, J. L., Ross, B. M., Ricco, A. J. & Lee, L. P. Stand-alone self-powered integrated microfluidic blood analysis system (SIMBAS). *Lab on a Chip* **11**, 845-850, doi:10.1039/C0LC00403K (2011).

51. Pei, X., Kang, W., Yue, W., Bange, A., Heineman, W. R. & Papautsky, I. Disposable Copper-Based Electrochemical Sensor for Anodic Stripping Voltammetry. *Analytical chemistry* **86**, 4893-4900 (2014).

52. Lok, K. S., Abdul Muttalib, S. Z., Lee, P. P., Kwok, Y. C. & Nguyen, N. T. Rapid determination of vitamin B12 concentration with a chemiluminescence lab on a chip. *Lab Chip* **12**, 2353-2361, doi:10.1039/c2lc00037g (2012).

53. Zhou, Y. K., Li, H., Liu, Y. & Liang, G. Y. Chemiluminescence determination of vitamin B12 by a flow-injection method. *Anal Chim Acta* **243**, 127-130, doi:http://dx.doi.org/10.1016/S0003-2670(00)82550-7 (1991).

54. Pew Internet and American Life Project. (2012).

55. Oncescu, V., Mancuso, M. & Erickson, D. Cholesterol testing on a smartphone. *Lab on a Chip* **14**, 759-763, doi:10.1039/C3LC51194D (2014).

56. Navruz, I., Coskun, A. F., Wong, J., Mohammad, S., Tseng, D., Nagi, R., Phillips, S. & Ozcan, A. Smart-phone based computational microscopy using multi-frame contact imaging on a fiber-optic array. *Lab on a Chip* **13**, 4015-4023, doi:10.1039/C3LC50589H (2013).

57. Stedtfeld, R. D., Tourlousse, D. M., Seyrig, G., Stedtfeld, T. M., Kronlein, M., Price, S., Ahmad, F., Gulari, E., Tiedje, J. M. & Hashsham, S. A. Gene-Z: a device for point of care genetic testing using a smartphone. *Lab on a Chip* **12**, 1454-1462, doi:10.1039/C2LC21226A (2012).

58. Lillehoj, P. B., Huang, M.-C., Truong, N. & Ho, C.-M. Rapid electrochemical detection on a mobile phone. *Lab on a Chip* **13**, 2950-2955, doi:10.1039/C3LC50306B (2013).

59. Lee, S., Oncescu, V., Mancuso, M., Mehta, S. & Erickson, D. A smartphone platform for the quantification of vitamin D levels. *Lab on a Chip* **14**, 1437-1442 (2014).

60. Lee, S., Aranyosi, A. J., Wong, M. D., Hong, J. H., Lowe, J., Chan, C., Garlock, D., Shaw, S., Beattie, P. D., Kratochvil, Z., Kubasti, N., Seagers, K., Ghaffari, R. & Swanson, C. D. Flexible opto-electronics enabled microfluidics systems with cloud connectivity for point-of-care micronutrient analysis. *Biosensors & bioelectronics* **78**, 290-299, doi:10.1016/j.bios.2015.11.060 (2016).

61. Yu, H., Tan, Y. & Cunningham, B. T. Smartphone Fluorescence Spectroscopy. *Analytical chemistry* **86**, 8805-8813, doi:10.1021/ac502080t (2014).

62. Wei, Q., Qi, H., Luo, W., Tseng, D., Ki, S. J., Wan, Z., Göröcs, Z., Bentolila, L. A., Wu, T.-T., Sun, R. & Ozcan, A. Fluorescent Imaging of Single Nanoparticles and Viruses on a Smart Phone. *ACS Nano* **7**, 9147-9155, doi:10.1021/nn4037706 (2013).

Chapter 2:

A smartphone platform for the quantification of vitamin D levels[†]

2.1 Abstract

Vitamin D deficiency has been linked to a number of diseases and adverse outcomes including: osteoporosis, infections, diabetes, cardiovascular diseases, and even cancer. At present the vast majority of vitamin D testing is performed in large-scale laboratories at the request of a physician as part of an annual panel of blood tests. Here we present a system for rapid quantification of vitamin D levels on a smartphone. The system consists of a smartphone accessory, an app, and a test strip that allows the colorimetric detection of 25-hydroxyvitamin D using a novel gold nanoparticle-based immunoassay. We show that the system can be used to accurately measure physiological levels of 25-hydroxyvitamin D with accuracy better than 15nM and a precision of 10nM. We compare our system with well-established ELISA test kits for serum samples of unknown concentration and demonstrate equivalency of the results. We envision this as the first step towards the development of the NutriPhone, a comprehensive system for the analysis of multiple vitamins and micronutrients on a smartphone.

[†] This Chapter was published as: **Lee, S.**, Oncescu, V., Mancuso, M., Mehta, S., Erickson, D. (2014) "A smartphone platform for the quantification of vitamin D levels" **Lab on a Chip**. 14: 1437

2.2 Introduction

Vitamin D deficiency is prevalent worldwide[1] and has been linked to diabetes[2], cardiovascular diseases[3,4], infections[5,6], and cancer[7,8] in addition to bone diseases such as osteoporosis[9] and rickets[10]. Deficiency is commonly defined in humans by measuring serum concentrations of 25-hydroxyvitamin D, or 25(OH)D, the circulating form of vitamin D. The currently recommended cutoffs for vitamin D deficiency and insufficiency are defined by 25(OH)D levels below 50nM and 80nM respectively. Low levels of vitamin D can usually be improved by consuming supplements and increasing skin exposure to sunlight.[11] However, many people are unaware of their vitamin D status due to the lack of simple methods for diagnosing and tracking 25(OH)D concentrations in the blood. The ability to monitor vitamin D levels may help those at risk to detect low levels at an earlier stage and enable corrective interventions before the occurrence of potentially irreversible damage. Reliance on supplements alone without knowledge of true vitamin D status may fall short in addressing severe vitamin D deficiencies (<20nM) or in some cases lead to possible vitamin D intoxication.[11,12] At present, most 25(OH)D tests are conducted using high-performance liquid chromatography (HPLC), liquid chromatography-tandem mass spectrometry (LC-MS) techniques, or certain immunoassays such as radioimmunoassay (RIA) and enzyme-linked immunosorbent assay (ELISA).[13-15] These methods are time consuming, costly and difficult to perform in most settings outside sophisticated laboratories. Recently, a lateral flow assay for vitamin D (Test4D; Nanospeed Diagnostics) has been introduced[16], demonstrating the commercial need for such rapid, point-of-care vitamin D analysis. Smartphone based diagnostics offer additional advantages over lateral flow assays including the abilities to quantify results, track changes with time, and provide user-free error tracking.

We present here the vitaAID – *vita*min AuNP-based Immunoassay Device – a system for rapid quantification of vitamin D levels on a smartphone. This is achieved through the development of: a smartphone accessory, app, and novel gold nanoparticle (AuNP) based colorimetric competitive direct-antigen immunoassay. This assay enables us to quantify 25(OH)D molecules whose small size (~400g/mol) restricts their binding to more than one antibody at a time.[17,18]. Gold nanoparticle based colorimetric

assays[19,20] coupled with smartphone technology have previously been used for the quantification of mercury contamination in water samples as demonstrated by Wei *et al.*[21] In addition, smartphone platforms were used for the detection of biomarkers in complex bodily fluids[22-25], thereby demonstrating the ability to do rapid, personalized diagnostics.

In this Chapter we describe the vitaAID and show how 25(OH)D levels can be quantified by evaluating brightness differences between the detection area and a reference area on the vitaAID test strip. We then demonstrate that the vitaAID system can be used to quantify vitamin D levels by evaluating serum samples with unknown 25(OH)D concentrations and comparing the results to those obtained using a commercial ELISA method.

2.3 Results

2.3.1 vitaAID system and test strip surface chemistry

The vitaAID system consists of a smartphone accessory and custom test strip as shown in **Figure 2.1**a. The accessory has been designed to minimize the effect of variability in external lighting conditions with a 5mm amber LED (λ=592nm) embedded in a polydimethylsiloxane (PDMS) diffuser used to illuminate the back

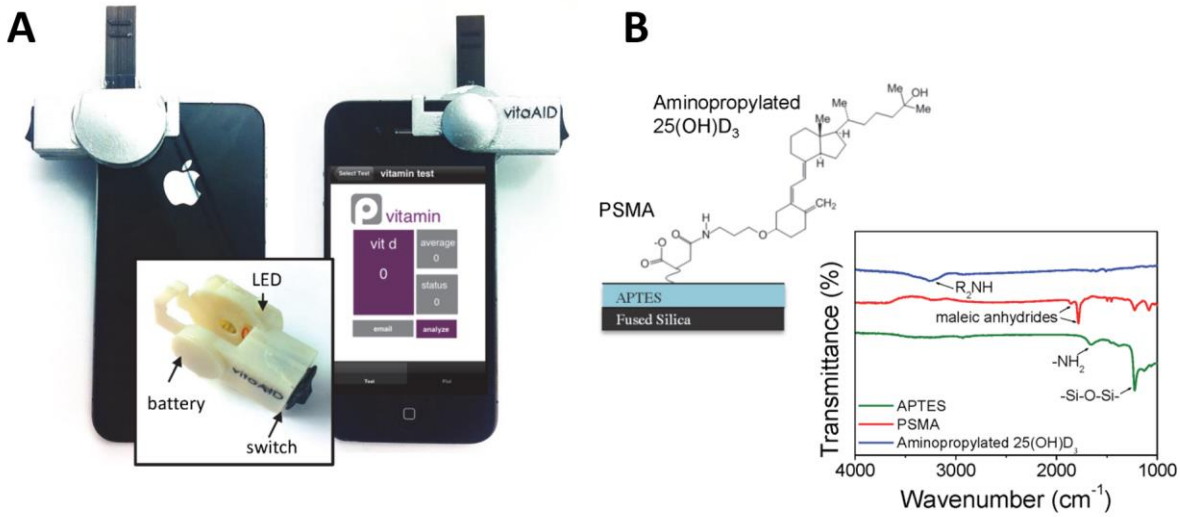

Figure 2.1: vitaAID system overview. **(A)** vitaAID accessory on a iPhone with the inset showing the components of the accessory (**B)** FT-IR spectra showing the chemical composition of the APTES, maleic anhydride and aminopropylated 25(OH)D_3 layers that constitute the detection area

of the test strip. The test strip is composed of a detection area and reference area. The reference area allows the algorithm to further adjust to differences in smartphone cameras. The detection area that enables the colorimetric reaction to occur consists of a surface-immobilized layer of 25(OH)D. There is currently no standard method for obtaining a chemically stable coating layer of 25(OH)D due to the small size and absence of linkable functional groups on the 25(OH)D. We addressed this by developing a novel 25(OH)D coating process onto a fused Si-based substrate that serves as the detection area on the test strip. As shown in Figure 2.1b, we coated the 3-aminopropyltriethoxysilane (APTES) and polystyrene-*co*-maleic anhydride (PSMA) layers sequentially on a fused Si substrate and covalently linked aminopropylated 25(OH)D to achieve a stable 25(OH)D coating. In order to validate this method, the surface treatments were characterized by Fourier-transform infrared spectroscopy (FT-IR) as shown in Figure 2.1b. The initial introduction of APTES layer on the Si substrate is evident from the transmittance peak at 1654cm^{-1} that is associated with primary amine groups (-NH_2).[26] The PSMA coating is confirmed by the appearance of peaks at 1850 and 1780cm^{-1} which have been linked with maleic anhydrides in other studies.[26-28] Lastly, the peak at 3300cm^{-1} corresponds to the formation of the secondary amine (R_2NH) bond between the PSMA and aminopropylated 25(OH)D and verifies the 25(OH)D immobilization.[29]

3.3.2 Surface-based gold nanoparticle immunoassay

The colorimetric reaction on the detection area of the test strip is based on a novel surface-based gold nanoparticle-based immunoassay as shown in **Figure 2.2**a. When a sample is applied onto the detection area of the test strip, only the antibody conjugates that are not bound to the 25(OH)D present in the initial sample are captured by the coated 25(OH)D on the surface. The colorimetric signals from the immobilized AuNP-antibody conjugates are then amplified using a silver enhancement scheme as the silver ions undergo reduction on the surface of the AuNP to increase their size and thereby increase the sensitivity of the system. For samples with high vitamin D levels, most of the antibody conjugates are occupied with 25(OH)D from the initial sample, resulting in only a subtle change in the colorimetric signal on the test strip. For samples with low vitamin D levels, the test strip develops an intense color that reflects the high number of antibody

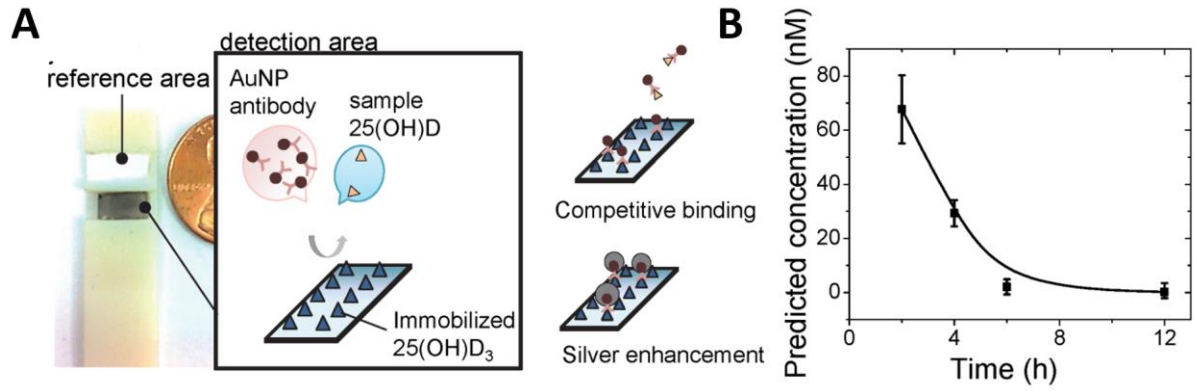

Figure 2.2 viatAID test strip. **(A)** Test strip and schematic of the gold nanoparticle-based immunoassay reaction on the detection area **(B)** variation in predicted concentration at different AuNP-anti-25(OH)D_3 incubation times on the detection area for 0nM sample 25(OH)D

conjugates bound on the surface. The steps involved in the preparation of the AuNP-anti-25(OH)D conjugate solution and the detection area are discussed in the Methods section.

A critical step during testing is the incubation of the AuNP-anti-25(OH)D sample solution on the test strip's detection area. It is important to characterize the time it takes for the AuNP-anti-25(OH)D to immobilize in order to minimize the total assay time and to improve accuracy. In Figure 2.2b ,we show the effect of different incubation times on the brightness difference between the detection and reference areas of the test strip (ΔH) for a sample without 25(OH)D. After 6h the brightness difference is within 10% of that obtained after a typical 12h overnight incubation. This indicates that a 6h incubation time is sufficient in order to obtain accurate results during such vitamin D measurements. The incubation time can however be significantly reduced by using the obtained negative exponential relationship to determine the minimum incubation time for ensuring that sufficient conjugate binding events have occurred on the detection area. In a recent study, Kai *et al*.[30] have demonstrated that the incorporation of microfluidic channels could further reduce such incubation times to the order of minutes through improved binding kinetics.

2.3.3 Quantification of colorimetric reaction

Once the competitive binding of AuNP-anti-25(OH)D was performed on the test strip, the quantification of the 25(OH)D levels in the initial sample can be achieved using the vitaAID smartphone platform. First, the

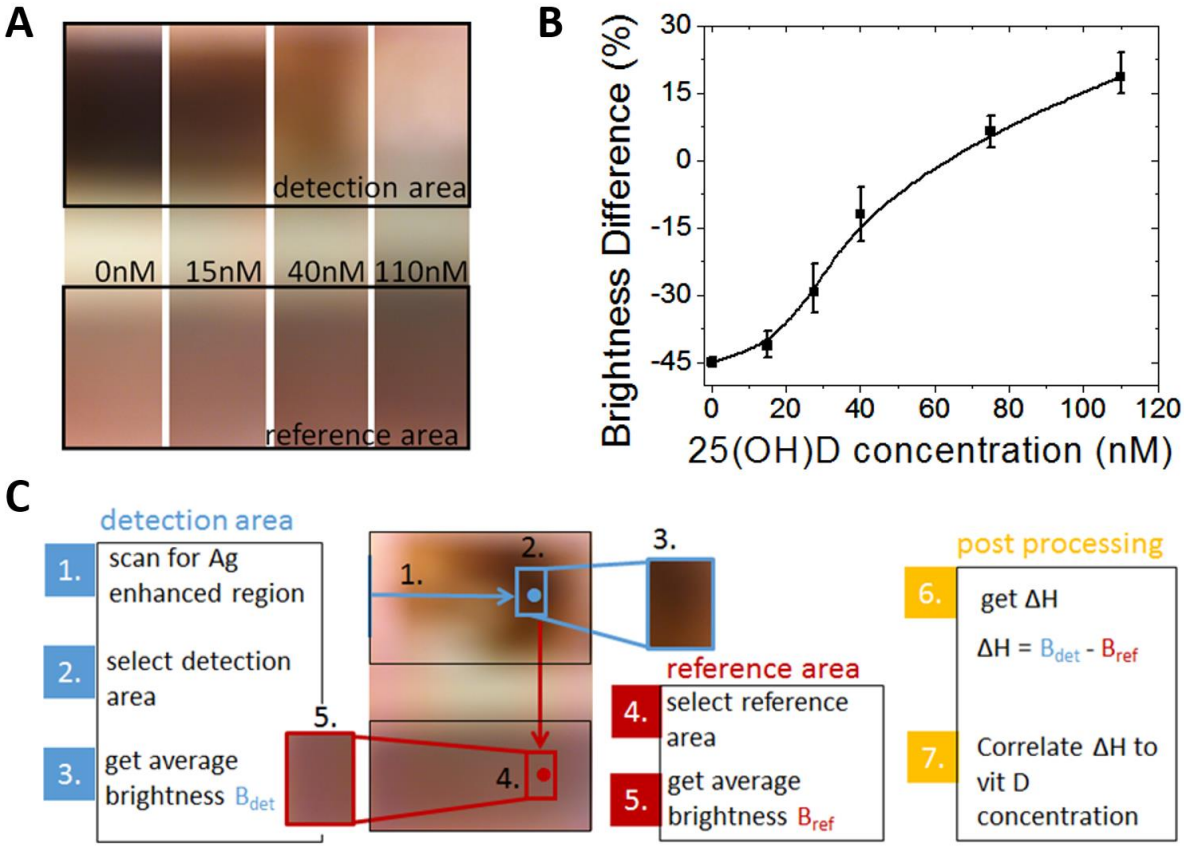

Figure 2.3 vitaAID algorithm overview. **(A)** colorimetric variation on the test strip at different known 25(OH)D concentrations **(B)** calibration curve showing brightness difference between the detection area and reference area ΔH at different known 25(OH)D concentrations **(C)** algorithm used in quantifying 25(OH)D levels on test strip

colorimetric change is captured using the smartphone's camera after inserting the test strip in the vitaAID accessory. In **Figure 2.3**a we show the colorimetric change in the transparent fused silica detection region at different known concentrations of 25(OH)D and the colorimetric change on the white reference region due to changes in exposure time of the camera. The iPhone automatically adjusts its camera exposure times in response to the amount of light passing through the detection region. Therefore, by comparing the differences in brightness between the detection area (B_{det}) and reference area (B_{ref}) we can estimate the concentration of 25(OH)D independent of the exposure setting of the iPhone camera. In Figure 2.3b we show that $\Delta H = B_{det} - B_{ref}$ can be correlated to the 25(OH)D concentration in the initial sample. A second

order polynomial was then fitted onto this calibration curve in order to obtain a function such that [25(OH)D] = f(ΔH).

Figure 2.3c shows the algorithm that allows the quantification of 25(OH)D across the entire range of physiological values. First, the detection area is scanned for silver enhanced regions where AuNP-anti-25(OH)D is bound. This is important because at higher 25(OH)D concentrations in the initial sample, the detection area rarely exhibits a uniform colorimetric change. A 100px by 100px area around the high intensity silver enhanced region is taken and the brightness is averaged across all the pixels in that area. The brightness is a coordinate in the Hue Saturation Brightness (HSB) color model and is computed from the Red Green Blue (RGB) average values as described elsewhere.[31] The same steps are then performed on the reference region and an average brightness is calculated. Once the brightness difference between the detection area and the reference area is computed, the algorithm uses a second order polynomial [25(OH)D] = f(ΔH) derived from Figure 2.3b to calculate the 25(OH)D concentration in the initial sample.

3.3.4 Accuracy and precision compared to ELISA

The accuracy of the vitaAID system was characterized by quantifying 25(OH)D in solutions of known concentrations and comparing them to results obtained using a commercial ELISA kit. In **Figure 2.4**a we

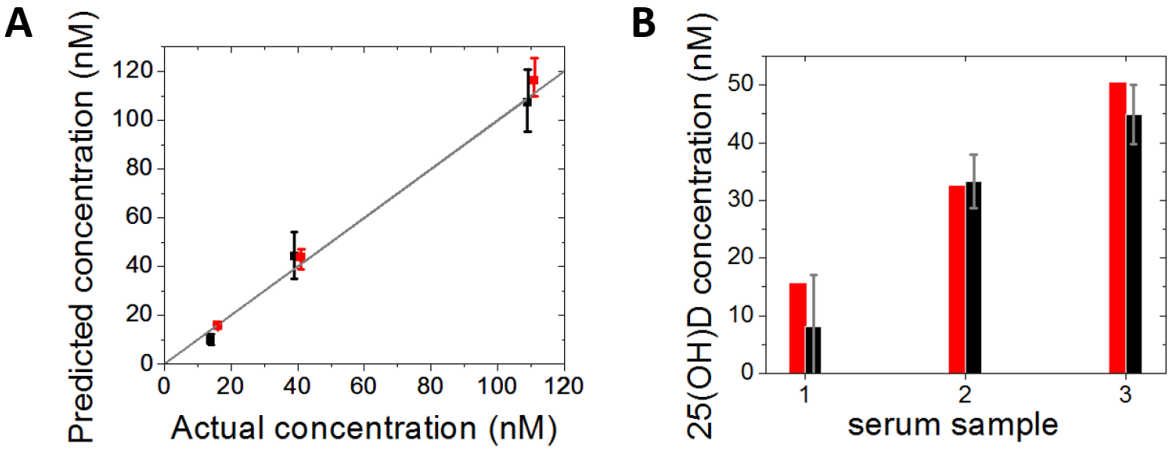

Figure 2.4 vitaAID performance. **(A)** predicted concentration vs. actual concentration (grey line) for calibration solutions at 15nM, 40nM and 110nM using vitaAID system (black) and ELISA kit (red) **(B)** predicted concentrations of 25(OH)D in serum samples and comparison to the average ELISA result

show variations in predicted 25(OH)D levels for 3 standard solutions of 15nM, 40nM and 110nM. At each concentration, 3 test strips were used and the maximum error across all the samples and concentrations was measured as 14.1nM at a concentration of 40nM. The maximum average inter-sample difference was 9.8nM also at 40nM. These errors are of the same order as those of ELISA methods for the quantification of 25(OH)D levels.

In Figure 2.4b, 3 serum samples of unknown 25(OH)D concentration are evaluated using both the vitaAID system and an ELISA method. As indicated previously, 25(OH)D levels below 50nM indicate vitamin D deficiency while level below 20nM indicate a severe deficiency. Both methods are in agreement that 2 of the samples are 25(OH)D deficient, while the other is borderline deficient. Moreover, 2 of the ELISA measurements fall within the range of values measured using the vitaAID system and one is within 2nM of that range.

2.4 Discussion

In this Chapter we presented the vitaAID system which allows for the fast and accurate quantification of 25(OH)D levels. This system uses a novel gold nanoparticle-based immunoassay in order to produce a surface colorimetric reaction that can be quantified directly on a smartphone. We have demonstrated that we can measure physiological levels of 25(OH)D in solution with accuracy better than 15nM and a precision of 10nM. Moreover we show that the results obtained using the vitaAID system are comparable with that of commercial ELISA kits. By analyzing 3 serum samples with unknown 25(OH)D concentration we were able to determine accurately the extent of vitamin D deficiency in each case. These results represent a promising step in the development of an accurate system for determining vitamin D levels which has many potential applications as a point-of-care tool both in the developed and the developing world.

In the future, this method for vitamin D quantification can be further improved in terms of precision and accuracy. Here, we used a specific form of 25(OH)D for coating and detection, namely 25(OH)D_3 and anti-25(OH)D_3. The monoclonal anti-25(OH)D_3 has 68% cross reactivity with 25(OH)D_2 and 100% with

25(OH)D_3. The use of 25(OH)D_3 for the detection zone coating allows for the capturing of all the unbound AuNP-anti-25(OH)D_3 conjugates after the initial interaction with the sample. Nonetheless, this difference in the antibody affinity inevitably causes our method to underestimate the total 25(OH)D level which is the sum of the 25(OH)D_2 and 25(OH)D_3 levels. This represents the shortcoming of most immunoassays for vitamin D (e.g. ELISA kit; Alpco, radioimmunoassay; DiaSorin) as demonstrated through clinical comparison studies with other detection standards such as HPLC and LC-MS.[13,14,32]

2.5 Materials and Methods

2.5.1 Sample preparation

For a vitamin D deficiency test, once the sample has been acquired, several steps are performed in solution prior to its application onto the vitaAID test strip. First, the filtered serum sample is mixed 1:10 (v/v) with 0.78g/ml acetonitrile (Thermo Fisher Sceintific Inc.) in order to liberate the 25(OH)D molecules that are in proportion of 95-99% bound to vitamin D binding proteins (DBP).[33,34] The sample is then mixed with AuNP-anti-25(OH)D conjugate solution for 30min. This ensures that all the 25(OH)D initially present in the blood sample is bound to AuNP-anti-25(OH)D before being applied onto the test strip.

2.5.2 AuNP-anti-25(OH)D_3 conjugate preparation

The spherical AuNP (Nanopartz Inc., 30nm) came pre-treated with N-hydroxysuccinimide ester terminal (NHS) groups which specifically reacted with the primary amines of monoclonal anti-25(OH)D_3 IgG (Raybiotech Inc.) to form the AuNP-antibody conjugates. The antibody was first purified using the Pierce Antibody Clean-up Kit (Thermo Fisher Scientific Inc.) because 2% bovine serum albumin (BSA) stabilizers in anti-25(OH)D_3 are known to interfere with the amine-reactive conjugation.[35] The antibody solution was placed into the Melon Gel-based purification support which binds non-antibody proteins while allowing the IgG antibody to flow through in a purified form during the one-minute centrifugation at 6000g. The successful removal of BSA was checked by performing sodium dodecyl sulfate polyacrylamide gel electrophoresis (SDS-PAGE). For conjugation, the AuNP were mixed with the purified anti-25(OH)D_3 at

0.1mg/ml in 0.01M amine-free phosphate buffer saline (PBS) buffer at pH 7.4. The mixture was sonicated for 30s to re-suspend AuNP into solution, followed by vortexing for 30min at room temperature.[36] The centrifugation was performed at 15000g for 10min to remove the excess antibody in supernatant form and the final conjugates were reconstituted in 0.01M PBS with 0.1% Tween-20 at pH 7.4. The successful conjugation was confirmed through surface plasmon resonance changes using ultraviolet-visible spectroscopy. The conjugates were diluted to 10µg/ml and stored at 4°C until use.

2.5.3 Detection area preparation

The covalent immobilization of 25(OH)D was achieved by obtaining 25(OH)D_3, 3'-Aminopropyl Ether (Toronto Research Chemicals Inc.) and using its primary amines as linkers to the test strip surface. Immobilization of the peptides to surface using maleic anhydride chemistry has been demonstrated previously by others.[37,38] Here, the aminopropylated 25(OH)D_3 was immobilized on a flat Si substrate other than on a typical well-plate which represents a compatibility improvement for use in our smartphone-based detection. Briefly, 4" fused Si wafers were cleaned in piranha solution, immersed in 20mM APTES (Sigma-Aldrich Co. LLC) in isopropanol for 2h and annealed at 120°C for 1h. The APTES coating acted as an activation layer for the binding of 1% PSMA (Sigma-Aldrich Co. LLC) dissolved in tetrahydrofuron, which was spin-coated at 3500rpm for 30s followed by curing at 120°C for 2h. The treated Si wafer was cooled and immersed in acetone for 10min and subsequently diced into 4 by 7mm strips. Finally, the 25(OH)D immobilization was achieved by incubating the PSMA-treated strips with 20µg/ml aminopropylated 25(OH)D_3 in the coating buffer (0.1M carbonate/bicarbonate buffer at pH 9.4) for 1h at 37°C. The unreacted PSMA sites were treated by incubating the blocking buffer (0.01M PBS with 1mg/ml Casein and 0.05% Kathon preservative at pH 7.4) for 30min at room temperature, and cleaned with washing buffer (0.01M PBS with 0.05% Tween-20 at pH 7.4). The incubation procedures were performed in custom incubation chambers that housed the test strips and prevented pre-mature drying of the treatment solutions. The modified Si surfaces after each surface treatment were characterized by FT-IR using a Vertex 80-v spectrometer (Bruker Optics) equipped with a 60° germaniam attenuated total reflection (VeeMax Ge ATR)

crystal. For each spectrum, 256 scans at a spectral resolution of $4cm^{-1}$ were performed using a liquid nitrogen detector. After the 6h incubation of AuNP-antibody conjugates with the sample on the detection area, the strip was rinsed three times with the washing buffer to remove unbound conjugates and incubated with silver enhancement solution from the Silver Enhancer Kit (Sigma-Aldrich Co. LLC). After 20min, the detection area was rinsed with the washing buffer and air dried at room temperature.

2.5.4 ELISA kit procedures.

The standard and serum samples were analyzed with 25-OH Vitamin D ELISA kit (ALPCO Diagnostics) according to the provided protocol. Briefly, the samples were incubated with the releasing agent to separate 25(OH)D molecules from DBP at 37°C for 1h. The samples and anti-25(OH)D were then added onto the 25(OH)D coated microtiter plates. During an overnight (18-22h) incubation, the 25(OH)D molecules in the sample and those immobilized on the plates competitively bound to the available anti-25(OH)D. The plates were washed to remove any unbound anti-25(OH)D and peroxidase-conjugated antibody were added to form 25(OH)D─anti-25(OH)D─peroxidase antibody complex on the plate surface. After 1h incubation, the plates were washed and tetramethylbenzidine (TMB) substrates were added which resulted in a reaction causing the solution color to change. After 20min, the reaction was stopped with an acidic solution and the absorption of the solution was measured using Spectramax 384 at 450nm.

2.6 References

1. Holick, M. F. Vitamin D deficiency. *N Engl J Med* **357**, 266-281 (2007).

2. Holick, M. F. Vitamin D: importance in the prevention of cancers, type 1 diabetes, heart disease, and osteoporosis. *The American Journal of Clinical Nutrition* **79**, 362-371 (2004).

3. Wang, T. J., Pencina, M. J., Booth, S. L., Jacques, P. F., Ingelsson, E., Lanier, K., Benjamin, E. J., D'Agostino, R. B., Wolf, M. & Vasan, R. S. Vitamin D deficiency and risk of cardiovascular disease. *Circulation* **117**, 503-511, doi:10.1161/circulationaha.107.706127 (2008).

4. Anderson, J. L., May, H. T., Horne, B. D., Bair, T. L., Hall, N. L., Carlquist, J. F., Lappe, D. L. & Muhlestein, J. B. Relation of vitamin D deficiency to cardiovascular risk factors, disease status, and incident events in a general healthcare population. *The American journal of cardiology* **106**, 963-968, doi:10.1016/j.amjcard.2010.05.027 (2010).

5. Mehta, S., Giovannucci, E., Mugusi, F. M., Spiegelman, D., Aboud, S., Hertzmark, E., Msamanga, G. I., Hunter, D. & Fawzi, W. W. Vitamin D Status of HIV-Infected Women and Its Association with HIV Disease Progression, Anemia, and Mortality. *PLoS ONE* **5**, e8770, doi:10.1371/journal.pone.0008770 (2010).

6. Mehta, S., Hunter, D. J., Mugusi, F. M., Spiegelman, D., Manji, K. P., Giovannucci, E. L., Hertzmark, E., Msamanga, G. I. & Fawzi, W. W. Perinatal outcomes, including mother-to-child transmission of HIV, and child mortality and their association with maternal vitamin D status in Tanzania. *J Infect Dis* **200**, 1022-1030, doi:10.1086/605699 (2009).

7. Garland, C. F., Garland, F. C., Gorham, E. D., Lipkin, M., Newmark, H., Mohr, S. B. & Holick, M. F. The Role of Vitamin D in Cancer Prevention. *American Journal of Public Health* **96**, 252-261, doi:10.2105/AJPH.2004.045260 (2006).

8. Lappe, J. M., Travers-Gustafson, D., Davies, K. M., Recker, R. R. & Heaney, R. P. Vitamin D and calcium supplementation reduces cancer risk: results of a randomized trial. *The American Journal of Clinical Nutrition* **85**, 1586-1591 (2007).

9. XunWu, M. Vitamin D deficiency and osteoporosis. *Zhongguo Shiyong Neike Zazhi/Chinese Journal of Practical Internal Medicine* **29**, 965-967 (2009).

10. Chesney, R. Vitamin D Deficiency and Rickets. *Rev Endocr Metab Disord* **2**, 145-151, doi:10.1023/A:1010071426415 (2001).

11. Lips, P. Worldwide status of vitamin D nutrition. *J Steroid Biochem Mol Biol* **121**, 297-300 (2010).

12. Mithal, A., Wahl, D. A., Bonjour, J. P., Burckhardt, P., Dawson-Hughes, B., Eisman, J. A., El-Hajj Fuleihan, G., Josse, R. G., Lips, P. & Morales-Torres, J. Global vitamin D status and determinants of hypovitaminosis D. *Osteoporos Int* **20**, 1807-1820, doi:10.1007/s00198-009-0954-6 (2009).

13. Roth, H. J., Schmidt-Gayk, H., Weber, H. & Niederau, C. Accuracy and clinical implications of seven 25-hydroxyvitamin D methods compared with liquid chromatography-tandem mass spectrometry as a reference. *Annals of clinical biochemistry* **45**, 153-159, doi:10.1258/acb.2007.007091 (2008).

14. Wallace, A. M., Gibson, S., de la Hunty, A., Lamberg-Allardt, C. & Ashwell, M. Measurement of 25-hydroxyvitamin D in the clinical laboratory: current procedures, performance characteristics and limitations. *Steroids* **75**, 477-488, doi:10.1016/j.steroids.2010.02.012 (2010).

15. Hollis, B. W. & Horst, R. L. The assessment of circulating 25(OH)D and 1,25(OH)2D: Where we are and where we are going. *The Journal of Steroid Biochemistry and Molecular Biology* **103**, 473-476, doi:http://dx.doi.org/10.1016/j.jsbmb.2006.11.004 (2007).

16. Gupta, R. & Gupta, S. Lateral flow immunoassay for detecting vitamins. Report No. WO/2012/129650, (2012).

17. Fu, E., Nelson, K. E., Ramsey, S. A., Foley, J. O., Helton, K. & Yager, P. Modeling of a competitive microfluidic heterogeneous immunoassay: sensitivity of the assay response to varying system parameters. *Analytical chemistry* **81**, 3407-3413, doi:10.1021/ac802672v (2009).

18. Pradelles, P., Grassi, J., Creminon, C., Boutten, B. & Mamas, S. Immunometric assay of low-molecular-weight haptens containing primary amino-groups. *Analytical chemistry* **66**, 16-22 (1994).

19. Lei, K. & Butt, Y. C. Colorimetric immunoassay chip based on gold nanoparticles and gold enhancement. *Microfluid Nanofluid* **8**, 131-137, doi:10.1007/s10404-009-0490-x (2010).

20. Yeh, C.-H., Hung, C.-Y., Chang, T., Lin, H.-P. & Lin, Y.-C. An immunoassay using antibody-gold nanoparticle conjugate, silver enhancement and flatbed scanner. *Microfluid Nanofluid* **6**, 85-91, doi:10.1007/s10404-008-0298-0 (2009).

21. Wei, Q., Nagi, R., Sadeghi, K., Feng, S., Yan, E., Ki, S. J., Caire, R., Tseng, D. & Ozcan, A. Detection and Spatial Mapping of Mercury Contamination in Water Samples using a Smart-Phone. *ACS nano* (2014).

22. Coskun, A. F., Nagi, R., Sadeghi, K., Phillips, S. & Ozcan, A. Albumin testing in urine using a smart-phone. *Lab on a Chip* **13**, 4231-4238 (2013).

23. Coskun, A. F., Wong, J., Khodadadi, D., Nagi, R., Tey, A. & Ozcan, A. A personalized food allergen testing platform on a cellphone. *Lab on a Chip* **13**, 636-640, doi:10.1039/C2LC41152K (2013).

24. Oncescu, V., Mancuso, M. & Erickson, D. Cholesterol testing on a smartphone. *Lab on a Chip* **14**, 759-763, doi:10.1039/C3LC51194D (2014).

25. Oncescu, V., O'Dell, D. & Erickson, D. Smartphone based health accessory for colorimetric detection of biomarkers in sweat and saliva. *Lab on a Chip* **13**, 3232-3238 (2013).

26. Wang, J. H., Zhu, L. P., Zhu, B. K. & Xu, Y. Y. Fabrication of superhydrophilic poly(styrene-alt-maleic anhydride)/silica hybrid surfaces on poly(vinylidene fluoride) membranes. *J Colloid Interface Sci* **363**, 676-681 (2011).

27. Chitanu, G. C., Popescu, I. & Carpov, A. Synthesis and characterization of maleic anhydride copolymers and their derivatives. *Revue Roumaine de Chimie* **51**, 923-929 (2006).

28. Jeong, J.-H., Byoun, Y.-S. & Lee, Y.-S. Poly (styrene-alt-maleic anhydride)-4-aminophenol conjugate: synthesis and antibacterial activity. *Reactive and Functional Polymers* **50**, 257-263 (2002).

29. Lin, R.-H. & Hsu, J.-H. In situ FT-IR and DSC investigation on the cure reaction of the dicyanate/diepoxide/diamine system. *Polymer international* **50**, 1073-1081 (2001).

30. Kai, J., Puntambekar, A., Santiago, N., Lee, S. H., Sehy, D. W., Moore, V., Han, J. & Ahn, C. H. A novel microfluidic microplate as the next generation assay platform for enzyme linked immunoassays (ELISA). *Lab on a Chip* **12**, 4257-4262 (2012).

31. Bigun, J. in *Vision with Direction: A Systematic Introduction to Image Processing and Computer Vision* Ch. 2, 31-32 (Springer, 2006).

32. Højskov, C. S., Heickendorff, L. & Møller, H. J. High-throughput liquid–liquid extraction and LCMSMS assay for determination of circulating 25(OH) vitamin D3 and D2 in the routine clinical laboratory. *Clinica Chimica Acta* **411**, 114-116, doi:http://dx.doi.org/10.1016/j.cca.2009.10.010 (2010).

33. Wootton, A. M. Improving the measurement of 25-hydroxyvitamin D. *Clinical Biochemist Reviews* **26**, 33 (2005).

34. D Carter, G. Accuracy of 25-hydroxyvitamin D assays: confronting the issues. *Current drug targets* **12**, 19-28 (2011).

35. Grodzki, A. C. & Berenstein, E. in *Immunocytochemical Methods and Protocols* 15-26 (Springer, 2010).

36. Ljungblad, J. (Linköping University, Department of Physics, Chemistry and Biology, 2009).

37. Tasso, M., Cordeiro, A. L., Salchert, K. & Werner, C. Covalent immobilization of subtilisin A onto thin films of maleic anhydride copolymers. *Macromolecular bioscience* **9**, 922-929 (2009).

38. Cordeiro, A. L., Pompe, T., Salchert, K. & Werner, C. in *Bioconjugation Protocols* 465-476 (Springer, 2011).

Chapter 3:

NutriPhone: a mobile platform for low-cost point-of-care quantification of vitamin B_{12} concentrations[†]

3.1 Abstract

Vitamin B_{12} is necessary for formation of red blood cells, DNA synthesis, neural myelination, brain development, and growth. Vitamin B_{12} deficiency is often asymptomatic early in its course; however, once it manifests, particularly with neurological symptoms, reversal by dietary changes or supplementation becomes less effective. Access to easy, low cost, and personalized nutritional diagnostics could enable individuals to better understand their own deficiencies as well as track the effects of dietary changes. In this work, we present the NutriPhone, a mobile platform for the analysis of blood vitamin B_{12} levels in 15 minutes. The NutriPhone technology comprises of a smartphone accessory, an app, and a competitive-type lateral flow test strip that quantifies vitamin B_{12} levels. To achieve the detection of sub-nmol/L physiological levels of vitamin B_{12}, our assay incorporates an innovative "spacer pad" for increasing the duration of the key competitive binding reaction and uses silver amplification of the initial signal. We demonstrate the efficacy of our NutriPhone system by quantifying physiologically relevant levels of vitamin B_{12} and performing human trials where it was used to accurately evaluate blood vitamin B_{12} status of $_{12}$ participants from just a drop (~40µl) of finger prick blood.

[†] This chapter was reproduced from:

Lee, S., O'Dell, D., Hohenstein, J., Colt, S., Mehta, S., Erickson, D. (2016) "NutriPhone: a mobile platform for low-cost point-of-care quantification of vitamin B_{12} concentrations" Under Review in Nature Scientific Reports

3.2 Introduction

Vitamin B_{12} is a water-soluble vitamin that is necessary for DNA synthesis, the metabolism of amino acids and fatty acids[1] which are required for normal blood formation[2], cell synthesis[3], and neurological functions[4,5] in the human body. Low levels of vitamin B_{12} can consequently lead to a wide range of hematologic and neurological abnormalities.[6,7] Specifically, poor vitamin B_{12} status has been associated with several acute and chronic conditions including anaemia[7,8], paraesthesia[1,9] , and cognitive impairments[10]. Vitamin B_{12} deficiency during pregnancy and early in life is also associated with neural tube defects, poor infant growth and psychomotor function, and impaired brain development.[11] The primary dietary sources of vitamin B_{12} are meats, fish, shellfish, and dairy products and as such the deficiency has been reported to be the highest among populations with predominantly a vegetarian or vegan diet.[12,13] In the US, the deficiency rate among vegetarians has been estimated at 60%[14], while the rate as high as 81% has been reported in India[15] where there is a high percentage of vegetarians and vegans.[16]

Depending on the severity, underlying cause, and if detected early, the manifestations of vitamin B_{12} deficiency can often be reversed by consuming supplements and/or by changes in diet, as recommended by a healthcare practitioner. In an attempt to reduce the barrier to diagnosis of micronutrient deficiencies, our group has previously developed the vitaAID – vitamin AuNP-based Immunoassay Device – a system for colorimetric quantification of vitamin D levels on a smartphone.[17] In that work a novel gold nanoparticle (AuNP) based immunoassay for vitamin D was developed and anlayzed by our smartphone platform, enabling quantification of serum samples without the need of sophisticated laboratory equipment such as spectrophotometers. However its deployment for point-of-care (POC) applications was limited by the persisting requirements for off-chip blood sample processing, multiple pipetting steps and the non-trivial incubation time (~3 h).

A possible solution to the aforementioned limitations is the adaptation of lateral flow immunoassay principles to diagnose micronutrient deficiencies. Lateral flow assays are widely used in diagnosing numerous diseases[18-20] and medical conditions[21-23] in POC settings because they are rapid, simple and

produce simple qualitative results that can be interpreted by untrained personnel. Development of lateral flow test for B_{12} however is significantly more challenging due to the extremely low limit of detection that is required. One of the recommended cut-offs for vitamin B_{12} insufficiency is defined in humans by serum vitamin B_{12} below 221 pmol/L[24] (compared with 50-75 nmol/L 25(OH)D for vitamin D[25]). Traditionally commercial lateral flow assays have lower limits of detection in the tens of nmol/L range.[26]

Here we present a novel POC vitamin B_{12} assessment test, implement it on our "NutriPhone" mobile platform, and demonstrate its performance in a series of human trials. The test uses a finger-stick of blood and comprises of a novel competitive-type lateral flow assay which is able to process whole blood samples, store the necessary reagents, and has built-in flow control directly on the test strip. Controlled and repeatable imaging of the B_{12} test strips with the smartphone platform, and computational image processing via the smartphone app enable the NutriPhone system to provide quantitative information from traditionally non-quantitative lateral flow test strips. As in other smartphone based diagnostics systems, our system inherits the abilities to track changes with time, provide user-free error tracking, and communicate results via e-mail or social networking service.[27-31]

In this paper we describe the NutriPhone system and demonstrate how the incorporation of an innovative "spacer pad" for an extended competitive binding interaction, silver enhancement of the initial colorimetric signal[32], and optical detection via a smartphone platform push the limit-of-detection (LOD) of our B_{12} lateral flow assay into the required range. We show that vitamin B_{12} levels in standard solutions can be accurately quantified in less than 15 min by evaluating the ratio of test to control line signals (T/C ratio). We then validate the performance of our vitamin B_{12} assay in a small trial with human participants.

3.3 Results

3.3.1 NutriPhone system and vitamin B_{12} test operation

The NutriPhone system consists of: a reusable smartphone accessory, a disposable custom test strip for vitamin B_{12}, and a smartphone app. The accessory has been designed to accept test strips and align them to

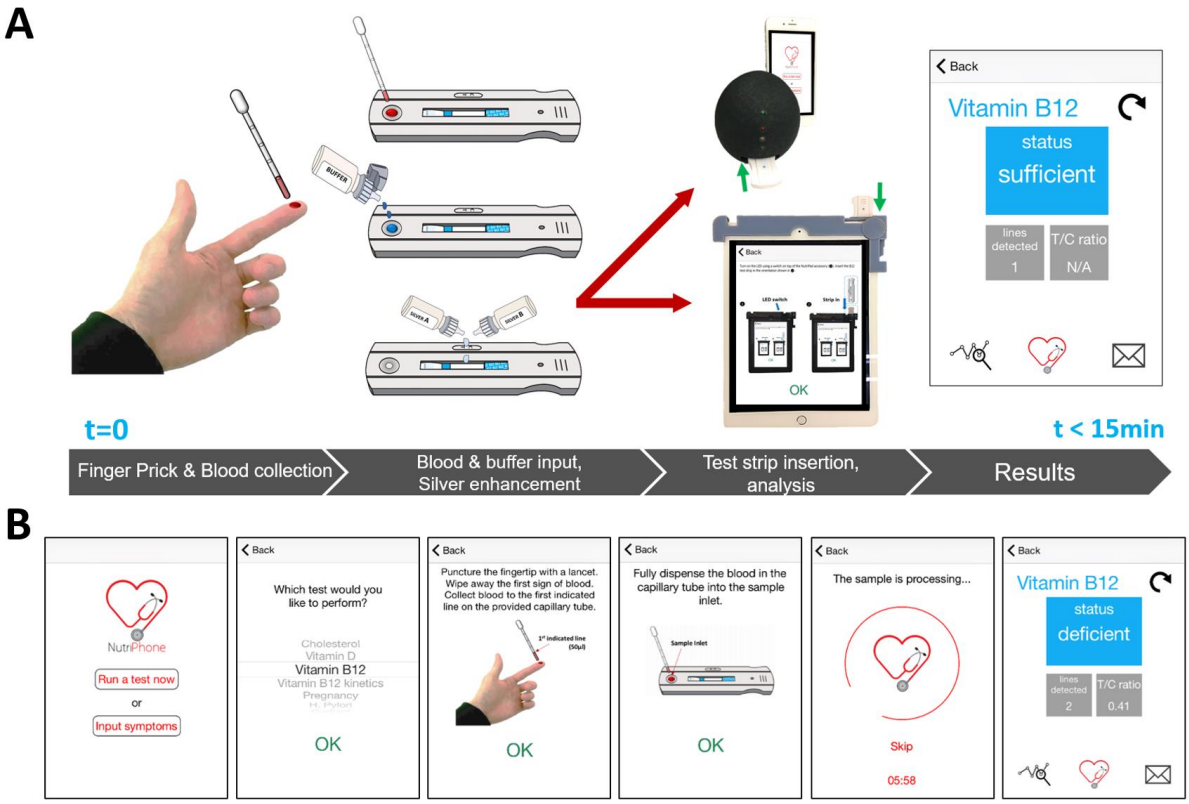

Figure 3.1: NutriPhone system for PON vitamin B_{12} analysis. **(A)** System overview showing the custom B_{12} test strip that accepts and anlayzes whole blood samples, two versions of the smartphone based accessory that accurately read the test strips, and smartphone app **(B)** NutriPhone app for guiding the users step-by-step through the test protocol and displaying the B_{12} results at the end

a CMOS camera with an embedded focusing lens (f=12 mm) in the optical path, which allows for capturing focused images of test strip signals in a compact accessory space (in Supplementary Fig. A1.1.). In order to minimize the variability caused by the different external lighting conditions, the accessory relies on two white surface mount LEDs (placed 10 mm on either sides focusing lens, facing the test strip 12 mm away) to uniformly illuminate the front of the test strip while blocking the ambient light entrance. While more LEDs could be adapted (e.g. to illuminate from other angles) to improve the uniformity further, they were compromised for longer accessory operation using two AA batteries at 3V.

To run a vitamin B_{12} deficiency test in POC settings as shown in **Figure 3.1**a, the user starts the NutriPhone app on his or her smartphone and follows the step-by-step instructions as shown in Figure 3.1b. Briefly, the

user collects a whole blood sample via a finger prick and applies it directly onto the test strip's inlet. After allowing for 4 min of incubation, the user initiates the sample flow by applying droplets of the chase buffer from the dropper bottle. The colorimetric signal develops in the subsequent 6 min after which the signals are amplified by applying a droplet of silver enhancement solution from the respective dropper bottles. The user then inserts the test strip into the NutriPhone accessory, and the amplified colorimetric signals are captured by the smartphone camera after 2 min and anlayzed by the smartphone app for the total start-to-results time of less than 15 min.

3.3.2 Vitamin B_{12} lateral flow assay architecture and principles

The custom vitamin B_{12} test strip shown in **Figure 3.2**a was developed as a lateral flow assay which integrates: a whole blood filtration membrane (FR-1), a conjugate pad that dry-stores the AuNP-anti-B_{12} conjugates, a novel spacer pad that allows for longer sample interaction with AuNP-anti-B_{12} conjugates, a nitrocellulose membrane that immobilizes the vitamin B_{12}-BSA molecules and secondary antibodies as test and control lines respectively, and a cellulose fibre absorbent pad that collects the waste sample at the end. This architecture represents a competitive-type lateral flow assay which was used here to accommodate the small size of vitamin B_{12} molecules (~1355 g/mol) that prevents their binding to more than one antibody at time.[33,34]

When a blood sample is applied onto the sample pad of our vitamin B_{12} assay, the blood cells are filtered and only the plasma proceeds to the conjugate pad and releases the AuNP-anti-B_{12} conjugates that become free to interact with the B_{12} in the sample. The sample to AuNP-anti-B_{12} interaction is the critical step in our assay, where there are limited binding regions on the AuNP-anti-B_{12} and their interaction with the sample B_{12} determines their availability downstream for binding to the BSA-B_{12} on the test line. In conventional lateral flow assays, such interaction occurs over tens of seconds which is too short for an accurate and thorough binding reactions to occur, especially when the target molecules are found in low (i.e. sub-nmol/L) concentrations. The innovation in our NutriPhone B_{12} assay that enables the detection of sub-nmol/L B_{12} has been the addition of the spacer pad between the conjugate pad and the nitrocellulose

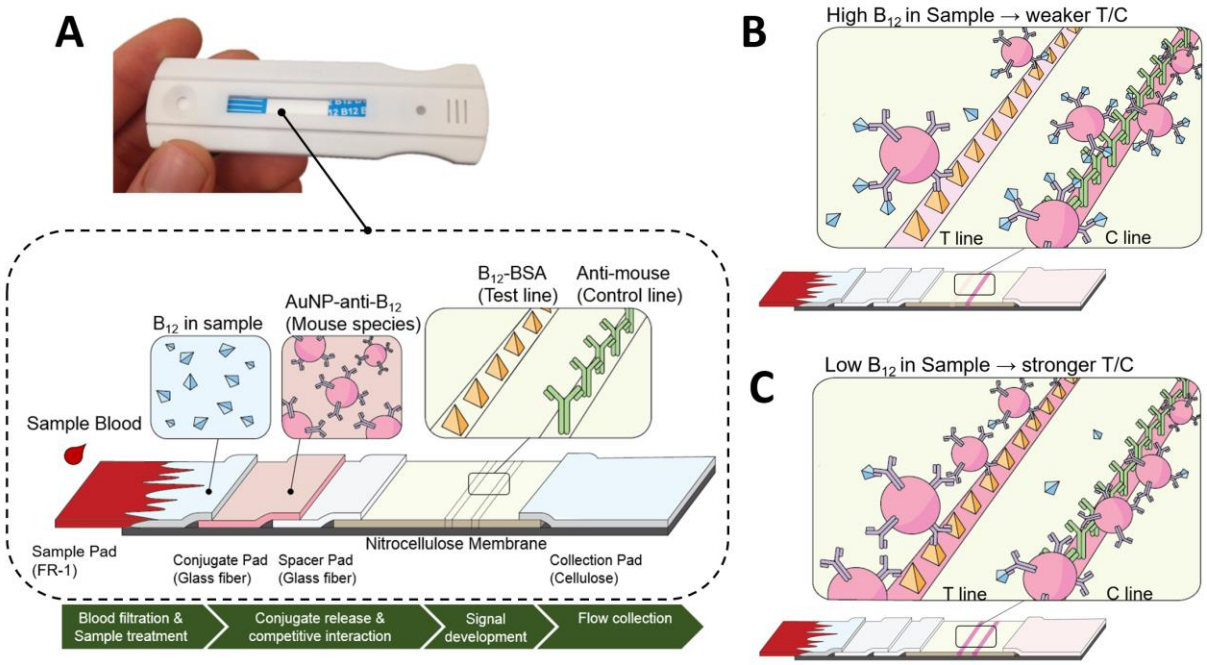

Figure 3.2: NutriPhone vitamin B_{12} lateral flow assay. **(A)** Strip image and schematic of the custom B_{12} test strip architecture and components **(B)** Competitive interaction between the sample B_{12} and bound BSA-B_{12} at test line for a limited binding regions on AuNP-anti-B_{12} results in a weak T/C signal intensity for high B_{12} in the sample, and **(C)** strong T/C signal intensity for low B_{12} in the sample.

membrane. This spacer pad effectively prevents the sample—AuNP-anti-B_{12} mixture from flowing onto the nitrocellulose membrane before additionally activated by the user, thereby allowing for a more thorough interaction. In our optimized NutriPhone protocol, the user allows an additional 4 min of interaction time between the sample B_{12} and the AuN-anti-B_{12} before adding chase buffers to complete the test. For samples with high B_{12} levels as shown in Figure 3.2b, most of the AuNP-anti-B_{12} conjugates are occupied with B_{12} molecules from the initial sample, resulting in only a subtle change in the colorimetric signal at the test line. Here the preoccupied AuNP-anti-B_{12} that pass the test line without binding are still captured by the secondary antibodies on the control line to exhibit a strong signal, which leads to weak T/C ratios for testing high B_{12} samples. For samples with low B_{12} levels as shown in Figure 3.2c, the test line develops an intense color that reflects the high number of AuNP-anti-B_{12} bound at the test line. This leads to a weak control line signal which is indicative of the depleted number of AuNP-anti-B_{12} reaching the control line, and

consequently strong T/C ratios are observed for testing low B_{12} samples. For the earlier versions of our B_{12} strips under the same preparation and operating conditions but without the spacer pad incorporation, the T/C ratio remained insensitive to the increase in the sample B_{12} concentrations up until tens of nmol/L which demonstrates the significance of the spacer pad in the B_{12} detection in the sub-nmol/L ranges.

3.3.3 Vitamin B_{12} quantification in standard solutions

Once the competitive binding of AuNP-anti-B_{12} conjugates on the test and control lines was performed, the resulting colorimetric signals were silver enhanced and captured by our NutriPhone system. In **Figure 3.3**a, we show the colorimetric change of the test and control lines at different known concentrations of vitamin B_{12} standards. The captured images were then processed by our NutriPhone app based on the algorithm shown in Figure 3.3b. Briefly, a noisy 2D image was filtered and converted to the grayscale, followed by a

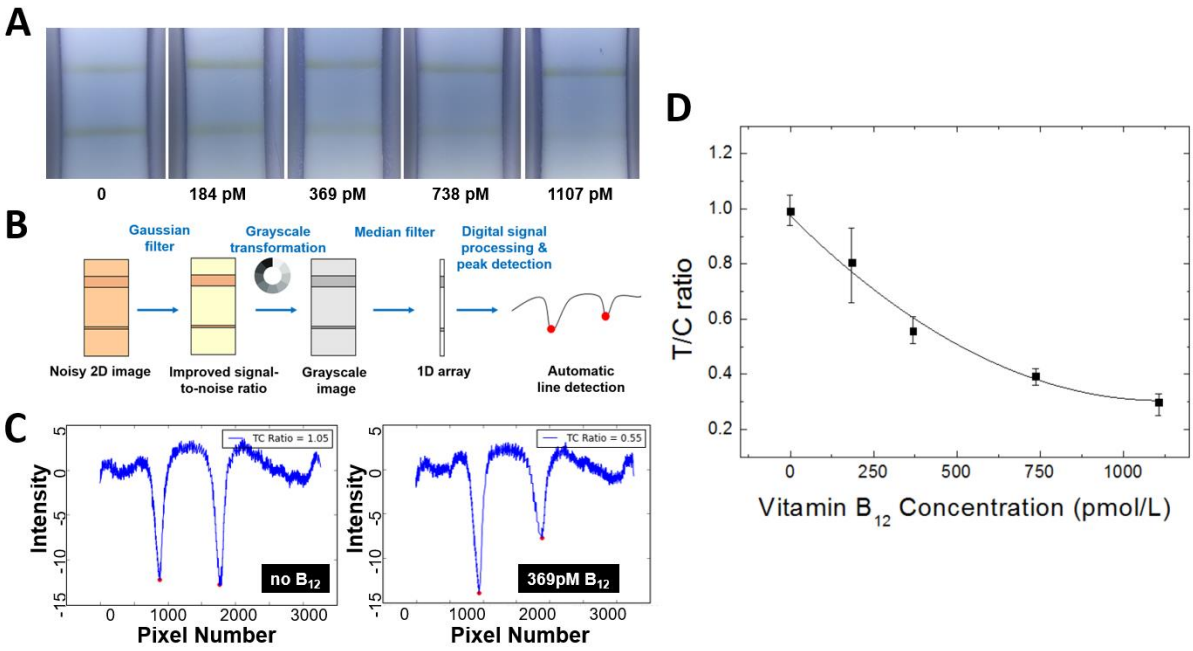

Figure 3.3: NutriPhone image acquisition and processing for vitamin B_{12} quantification. **(A)** Colorimetric variation of the test and control line regions on the silver enhanced B_{12} lateral flow test strip at different known concentrations of standard vitamin B_{12} samples **(B)** image processing algorithm used by our NutriPhone platform **(C)** Test and control line signals detected by the NutriPhone app as local intensity minima for 0 and 369 pmol/L of B_{12} standard samples **(D)** Calibration curve showing the T/C ratios of the colorimetric signals at different standard B_{12} concentrations

median filtering to reduce the 2D image into a 1D array which simplified our task to a 1D digital signal processing problem. As shown in in Figure 3.3c, the test and control regions of highly concentrated AuNP-anti-B_{12} were detected as local minima on the grayscale intensity plot, and the respective peak values could be used to calculate T/C ratios. In Figure 3.3d we show that T/C ratios can be correlated to the vitamin B_{12} concentration in the standard solutions. At each concentration, three test strips were used and the maximum lower and upper deviations were shown. We then fitted a second order polynomial onto this calibration curve to obtain a function such that $[B_{12}] = f(T/C)$. This function was stored and used by the NutriPhone app to predict B_{12} concentrations from the T/C ratios, where the calibration was performed for each batch of test strips in order to account for the batch-to-batch variations.

3.3.4 Vitamin B_{12} deficiency testing using whole blood samples

The performance of our NutriPhone system in POC settings was evaluated by using it to diagnose the vitamin B_{12} status of human participants. Here, a single finger prick of blood was collected from each of the 12 participants and used as direct inputs to our NutriPhone B_{12} test strips. In **Figure 3.4**a we show the colorimetric change on the B_{12} test strips for the two participant samples with sufficient (>738 pmol/L B_{12}) and deficient (186.7 pmol/L B_{12}) levels of vitamin B_{12}. As expected for our competitive B_{12} strips, the T/C ratio for a deficient B_{12} case appears to be significantly greater than that for a sufficient B_{12} case, and this difference could be quantified by our NutriPhone app. Figure 3.4b demonstrates the vitamin B_{12} levels of the 12 participants as predicted by our NutriPhone B_{12} system based on a calibration curve pre-determined for the tested batch of B_{12} test strips and compares them to the levels as determined by the laboratory standard method (Chemiluminescence Immunoassay on the IMMULITE 2000 Immunoassay system, Siemens Medical Solutions Diagnostics, Deerfield , IL). The comparison shows that our system has a median bias of -0.3%, and a high correlation at +0.93 ($p<0.0001$). The NutriPhone system in the current state has a cut-off of 332 pmol/L B_{12}, in which it can accurately distinguish eight participants with B_{12} levels less than 332 pmol/L from the other four participants with B_{12} levels greater than 332 pmol/L. The current NutriPhone system shows a reduced sensitivity/specificity when lower cut-offs are imposed, however it

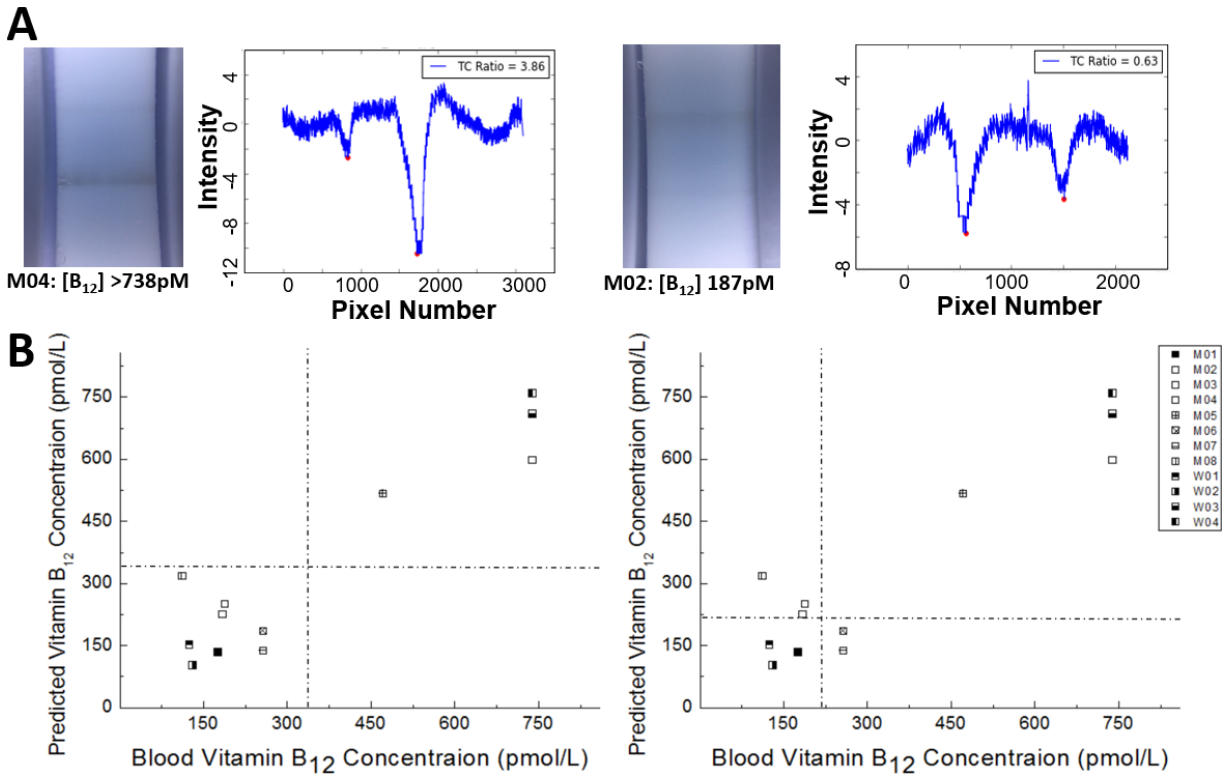

Figure 3.4: NutriPhone vitamin B_{12} human trials. **(A)** B_{12} test strip images and the corresponding T/C signals as illustrative results from the human trials **(B)** Blood vitamin B_{12} concentrations of 12 human participants as predicted by the NutriPhone system and comparison to the standard method results, where B_{12} deficiency cut-off was set differently at 332 pmol/L (left) and 221 pmol/L (right)

maintains a high sensitivity and specificity of 87% and 100% respectively using a 258 pmol/L cut-off. The NutriPhone's performance for other cut-off concentrations can also be found from the Receiver operating characteristic (ROC) curve in Supplementary Fig. A1.2.

3.4 Discussion

In this Chapter we have demonstrated a NutriPhone system which allows for the POC determination of vitamin B_{12} status in under 15 min. This is achieved by developing a novel competitive-type lateral flow assay for vitamin B_{12} which produces colorimetric test and control line signals that can be anlayzed by our system to give quantitative T/C ratios, which can then be correlated with sample vitamin B_{12} concentrations. We further validate the system in a human trial where it was used to diagnose vitamin B_{12} status of 12

human participants using a single drop of finger prick blood as the input to the system. Our device can immediately have an impact in some situations that require screening of <369 pmol/L B_{12} samples and B_{12} quantification in the higher concentration region[35]; however we plan to enable better quantification in the future and tune the device to operate with a lower cut-off of 150 pmol/L B_{12}, one of the cut-off points used to diagnose vitamin B_{12} deficiency[24]. These results represent a significant step in the development of a POC tool for accurate and rapid quantification of blood vitamin B_{12} levels, with great potential for deployment in the direct consumers market as well as for clinical and community health care settings in developing countries.

In the near future, the NutriPhone system for B_{12} can be improved in terms of both performance and usability. Currently, the accurate quantification of B_{12} levels in the range 0-332 pmol/L of B_{12} is demonstrated only in standard solutions, whereas the reduced performance in whole blood is likely due to its constituents that interfere with our test's key binding reaction between the sample B_{12} and the AuNP-anti-B_{12}. This could be improved by treating our sample pad to include more effective detergents to facilitate the binding interaction, and/or further optimizing the current incubation time after the initial sample application. On the other hand, the limiting step that prevents our vitamin B_{12} assay from being a complete sample-in-answer-out test is the silver enhancement step which additionally requires the user to apply silver enhancer solutions onto the test strip. For better usability by the end users, the next generation B_{12} test strips could dry-store the silver enhancing reagents on-chip as has been demonstrated elsewhere.[36] With these improvements, we hope to extend the human trials in populations with a wider range of B_{12} status to ensure adequate replicates at the lower end of the physiological and the deficient range of vitamin B_{12}.

3.5 Materials and Methods

3.5.1 AuNP-anti-B_{12} conjugate pad preparation

The monoclonal anti-vitamin B_{12} IgG produced in mouse (CalBioreagents Inc.) came in >95% purity and was conjugated with 40 nm AuNPs using the InnovaCoat Gold Conjugation Kit (Innova Bioscinces Ltd.).

Briefly, 0.23 μg AuNP in freeze dried form was mixed with 1μg anti-vitamin B_{12} IgG in 0.01 M amine-free phosphate buffer saline (PBS) buffer at pH 7.4. The anti-vitamin B_{12} IgG attached stably to the surface of AuNP via lysine residues during the 15 min incubation and the reaction was terminated by adding 0.1 M tris-buffered saline (TBS) with 0.1% Tween 20. To remove any excess antibodies, 0.01 M TBS with 0.1% Tween 20 was added in 10 times the volume of the conjugate mixture and was centrifuged at 9000g for 10 min. Upon removal of the supernatants, the final AuNP-anti-B_{12} conjugates were reconstituted in 0.01M TBS containing 2% bovine serum albumin (BSA) and the final optical density (O.D.) was checked using Spectramax 384 at 530 nm. The conjugates were stored at 4°C until use.

To prepare the conjugate pads for the B_{12} assay, the AuNP-anti-B_{12} conjugates were first diluted to 0.060 O.D. in the conjugate buffer (2mM borate buffer with 5% sucrose) which contained the preservative and resolubilization agents.[37] The Glass Fibre Conjugate Pads (EMD Millipore) with 30cm x 5mm dimensions were soaked in the diluted conjugate solution for 1 min, followed by drying at 37°C for 10h.

3.5.2 Vitamin B_{12} lateral flow assay preparation

High Flow Plus 180 Membrane Cards (HF180; EMD Millipore) with a 2 mm clear polyester film backing was used as the assay platform, housing the nitrocellulose membrane and the adhesive parts where the conjugate, sample and absorbent pads could be attached. Before the assembly, the test and control lines were prepared on the nitrocellulose membrane using the Lateral Flow Reagent Dispenser (Claremont Biosolution) to dispense 0.325 mg/ml Vitamin B_{12}-BSA conjugate (CalBioreagents Inc.) and 0.75 mg/ml anti-mouse IgG produced in goat (Sigma-Aldrich Co. LLC), respectively. The two lines are separated by 3 mm and uniform line widths of 1 mm could be obtained by operating the Legato 200 Dual Syringe Pump (Claremont Biosolution) at 6.4 μl/min. The membrane cards were subsequently dried for 2 h at 37°C, then at room temperature overnight. The B_{12} lateral flow assay was assembled into its final form shown in Fig. 1a by first attaching the spacer pad (i.e. untreated Glass Fibre Conjugate Pads with 30 cm x 5 mm

dimensions) to the adhesive region of the assay platform below the nitrocellulose membrane with an overlap of 0.5 mm. The AuNP-anti-B_{12} treated conjugate pad was then attached below the spacer pad with 0.5 mm overlap. The FR-1 Membrane (035; MDI Membrane Technologies) with 30 cm x 13.5 mm dimensions was then attached below the AuNP-anti-B_{12} conjugate pad with the 2 mm overlap to serve as the sample pad of the assay. The FR-1 membrane has a thickness of 0.35 mm and whole blood holding capacity of 30 µl/cm^2. Notably the 5mm length of the spacer pad was such that the gap created between the nitrocellulose membrane and the conjugate pad is sufficiently long to prevent the sample—AuNP–anti-B_{12} mixture from entering the nitrocellulose membrane at the initial 40 µl sample application. While the 5 mm length can be increased and retain the proper function of the spacer pad, this would necessarily decrease the length of the FR-1 membrane (where the total available length below the nitrocellulose was set by the HF180 platform's backing length of 20mm) and thereby decrease the blood holding capacity for the test. As done for the commercial rapid diagnostic tests, a specialized covertape (Kenosha C.V.) with arrows printed to indicate the sample input location, was attached on the top of these membranes and ensured proper contact between the membranes during the sample flow. The Cellulose Fibre Sample Pad (EMD Millipore) was attached above the nitrocellulose membrane with the 2 mm overlap to serve as the absorbent pad of the assay. The assembled assay was cut into individual strips of 4 mm width using a rotary paper trimmer (Dahle). The strips were then kept sealed in a plastic container to prevent contamination from dirt/dust, at room temperature. Also, silica gel desiccants (Dry-Packs™) were added for moisture control, where condensing water vapour could displace the immobilized agents on the nitrocellulose and/or negatively affect the AuNP–anti B_{12} conjugate stability by causing sugar complexes to form.[37,38] Storage up to 4 weeks without loss in strip performance has been observed, however longer storage times of up to one year have been widely used for similar, commercial strips (e.g. strips from AccuBioTech Co., Ltd) that use additional control measures (e.g. lamination of pads and membranes) and proprietary additives for lengthened reagent stability.

3.5.3 NutriPhone test strip protocol and human trials

In a NutriPhone test for vitamin B_{12} deficiency, the use of capillary tubes and dropper bottles allows the users to apply appropriate amounts of key reagents in POC settings. First, vitamin B_{12} samples (Abcam) in the range from 0 to 1107 pmol/L were prepared in standard 1x PBS buffer solutions. To initiate the B_{12} assay, the user collects the sample up to an indicated line on the capillary tube (~40 µl) and dispenses it fully onto the test inlet. This is followed by applying 2 droplets (~40 µl) of the chase buffer (1x TBS with 1% BSA, 1.5% Tween20, 0.1% sodium azide) from the dropper bottle. The addition of the chase buffer allows the sample to fully wet the conjugate pad and begin the sample B_{12} interaction with AuNP-anti-B_{12}, while the presence of the spacer pad prevents the sample from entering the nitrocellulose membrane. After waiting for 4 min, the user adds additional 4 droplets (~80 µl) of chase buffer to allow the sample to proceed beyond the spacer pad and complete the flow through the assay by being collected at the absorbent pad upstream. The initial colorimetric signal develops in the subsequent 6 min at which point the user applies a droplet (~20 µl) each from the silver enhancers A and B (Ted Pella Inc.) directly on the test/control regions on the nitrocellulose membrane. The NutriPhone app automatically takes a test strip image after waiting for an additional 3 min for amplification of the initial colorimetric signal, and computes a T/C ratio. Here, using a stop solution to quench the silver enhancement reaction is a viable option, however it would represent an additional step in our testing procedures which is undesirable for the intended point-of-care applications. We therefore did not use a stop solution, and instead computed T/C ratios from the images taken at the same time point. Throughout the procedures, the NutriPhone app incorporates the step-by-step instructions and timers to prevent its users from the common operation errors.

Our human trials were approved by the Institutional Review Board for Human Subjects at Cornell University, and carried out in accordance with their guidelines and regulations. The informed consent was obtained from all participants. In the trials, the participants were finger-pricked for a drop of blood (~40 µL) which was collected using a capillary tube and dispensed onto the inlet of the B_{12} test strip for carrying out the NutriPhone B_{12} test as described in the protocol above. A trained and certified phlebotomist then

drew ~5 mL of blood via venipuncture. Following 1 hour incubation at room temperature, serum was separated from whole venous blood by centrifugation at 2000 rpm for 10 min. Serum vitamin B_{12} was measured by chemiluminescence immunoassay on the Immulite 2000 platform (Siemens Healthcare Laboratory Diagnostics). The Siemens vitamin B_{12} kit reports normal reference values between 142-724 pmol/L with a lower limit of detection at 92 pmol/L.

3.5.4 Image processing algorithm

The majority of the iOS app was written in Objective-C. The image processing algorithm was written in pure C to improve speed and performance. There were no major 3rd party libraries used in the final version of the app; everything was either the default iOS libraries, or written by the authors. After an image was captured by the NutriPhone app, a series of image processing steps as shown in Figure 3.3b were performed to improve the limit of detection and accuracy over the conventional visual inspection. First, a 3x3 Gaussian filter was applied to the raw image to smooth out some of the noise. The image was then converted to the grayscale, so that the grayscale intensity could be used as a single-channel measurement that distinguishes the background from the colorimetric lines. The grayscale intensity of the colored control and test lines are lower than the hue of the background, so that the presence of a line could be detected by finding a local minimum in the hue data. After the grayscale conversion, the 2D image was reduced to a 1D array by replacing each row in the 2D image with the median hue value along that row. The median filtering reduces the noise, and the lower dimensionality reduces the process of peak detection to a 1D digital signal processing problem. The local minima corresponding to the test and control lines were located by stepping through the 1D array and storing all points which are at least 10 intensity values below the last inflection point on both sides. The values of local minima were then compared to yield T/C ratios, which were lastly converted into vitamin B12 concentrations based on the pre-determined calibration curve, [B12] = f(T/C).

3.6 References

1. Allen, R. H., Stabler, S. P., Savage, D. G. & Lindenbaum, J. Metabolic abnormalities in cobalamin (vitamin B12) and folate deficiency. *The FASEB journal* **7**, 1344-1353 (1993).

2. Baik, H. & Russell, R. Vitamin B12 deficiency in the elderly. *Annual review of nutrition* **19**, 357-377 (1999).

3. Dror, D. K. & Allen, L. H. Effect of vitamin B12 deficiency on neurodevelopment in infants: current knowledge and possible mechanisms. *Nutrition reviews* **66**, 250-255 (2008).

4. Fenech, M. The role of folic acid and vitamin B12 in genomic stability of human cells. *Mutation Research/Fundamental and Molecular Mechanisms of Mutagenesis* **475**, 57-67 (2001).

5. Hall, C. A. Function of vitamin B12 in the central nervous system as revealed by congenital defects. *American journal of hematology* **34**, 121-127 (1990).

6. Stabler, S. P. Vitamin B12 Deficiency. *New England Journal of Medicine* **368**, 149-160, doi:doi:10.1056/NEJMcp1113996 (2013).

7. Oh, R. & Brown, D. L. Vitamin B12 deficiency. *American family physician* **67**, 979-986 (2003).

8. Stabler, S. P. & Allen, R. H. Vitamin B12 deficiency as a worldwide problem. *Annu Rev Nutr* **24**, 299-326, doi:10.1146/annurev.nutr.24.012003.132440 (2004).

9. WOKES, F., Badenoch, J. & Sinclair, H. Human dietary deficiency of vitamin B12. *American Journal of Clinical Nutrition* **3**, 375-382 (1955).

10. Moore, E., Mander, A., Ames, D., Carne, R., Sanders, K. & Watters, D. Cognitive impairment and vitamin B12: a review. *International psychogeriatrics* **24**, 541-556 (2012).

11. Finkelstein, J. L., Layden, A. J. & Stover, P. J. Vitamin B-12 and Perinatal Health. **6**, 552-563, doi:10.3945/an.115.008201 (2015).

12. Zeuschner, C. L., Hokin, B. D., Marsh, K. A., Saunders, A. V., Reid, M. A. & Ramsay, M. R. Vitamin B_{12} and vegetarian diets. *Med J Aust* **199**, S27-32 (2013).

13. Pawlak, R., Parrott, S. J., Raj, S., Cullum-Dugan, D. & Lucus, D. How prevalent is vitamin B(12) deficiency among vegetarians? *Nutr Rev* **71**, 110-117, doi:10.1111/nure.12001 (2013).

14. Crane, M. G., Sample, C., Patchett, S. & Register, U. Vitamin B12 Studies in Toal Vegetarians (Vegans). *Journal of Nutritional Medicine* **4**, 419-430 (1994).

15. Yajnik, C., Deshpande, S. S., Lubree, H. G., Naik, S., Bhat, D., Uradey, B. S., Deshpande, J. A., Rege, S. S., Refsum, H. & Yudkin, J. Vitamin B12 deficiency and hyperhomocysteinemia in rural and urban Indians. *JAPI* **54**, 775-782 (2006).

16. Pawlak, R., Lester, S. E. & Babatunde, T. The prevalence of cobalamin deficiency among vegetarians assessed by serum vitamin B12: a review of literature. *Eur J Clin Nutr* **68**, 541-548, doi:10.1038/ejcn.2014.46 (2014).

17. Lee, S., Oncescu, V., Mancuso, M., Mehta, S. & Erickson, D. A smartphone platform for the quantification of vitamin D levels. *Lab on a Chip* **14**, 1437-1442 (2014).

18. Blacksell, S. D. Commercial dengue rapid diagnostic tests for point-of-care application: recent evaluations and future needs? *BioMed Research International* **2012** (2012).

19. Jackowska, T., Grzelczyk-Wielgorska, M. & Pawlik, K. in *Respiratory Regulation - The Molecular Approach* Vol. 756 *Advances in Experimental Medicine and Biology* (ed Mieczyslaw Pokorski) Ch. 33, 263-269 (Springer Netherlands, 2013).

20. Organization, W. H. *Malaria rapid diagnostic test performance: results of WHO product testing of malaria RDTs: round 5 (2013)*. (World Health Organization, 2014).

21. Allin, K. H. & Nordestgaard, B. G. Elevated C-reactive protein in the diagnosis, prognosis, and cause of cancer. *Critical reviews in clinical laboratory sciences* **48**, 155-170 (2011).

22. Wagner, T. A., Gravett, C. A., Gravett, M. G. & Rubens, C. E. A global health opportunity: The potential of multiplexed diagnostics in low-resource settings. *Journal of global health* **1**, 138 (2011).

23. Monno, R., Fumarola, L., Mercadante, G., Tzakis, G., Battista, M. & Miragliotta, G. Evaluation of a rapid test for the diagnosis of pneumococcal pneumonia. *Journal of microbiological methods* **92**, 127-131 (2013).

24. Malouf, R. & Areosa Sastre, A. Vitamin B12 for cognition. *Cochrane Database Syst Rev* **3** (2003).

25. Lips, P. Worldwide status of vitamin D nutrition. *The Journal of Steroid Biochemistry and Molecular Biology* **121**, 297-300, doi:http://dx.doi.org/10.1016/j.jsbmb.2010.02.021 (2010).

26. Posthuma-Trumpie, G. A., Korf, J. & Amerongen, A. Lateral flow (immuno)assay: its strengths, weaknesses, opportunities and threats. A literature survey. *Analytical and Bioanalytical Chemistry* **393**, 569-582, doi:10.1007/s00216-008-2287-2 (2008).

27. Oncescu, V., Mancuso, M. & Erickson, D. Cholesterol testing on a smartphone. *Lab Chip* **14**, 759-763, doi:10.1039/C3LC51194D (2014).

28. Berg, B., Cortazar, B., Tseng, D., Ozkan, H., Feng, S., Wei, Q., Chan, R. Y.-L., Burbano, J., Farooqui, Q. & Lewinski, M. Cellphone-Based Hand-Held Microplate Reader for Point-of-Care Testing of Enzyme-Linked Immunosorbent Assays. *ACS nano* **9**, 7857-7866 (2015).

29. Gallegos, D., Long, K. D., Yu, H., Clark, P. P., Lin, Y., George, S., Nath, P. & Cunningham, B. T. Label-free biodetection using a smartphone. *Lab on a Chip* **13**, 2124-2132 (2013).

30. Erickson, D., O'Dell, D., Jiang, L., Oncescu, V., Gumus, A., Lee, S., Mancuso, M. & Mehta, S. Smartphone technology can be transformative to the deployment of lab-on-chip diagnostics. *Lab on a Chip* **14**, 3159-3164 (2014).

31. Feng, S., Caire, R., Cortazar, B., Turan, M., Wong, A. & Ozcan, A. in *Frontiers in Optics 2015.* FM2B.2 (Optical Society of America).

32. Anfossi, L., Di Nardo, F., Giovannoli, C., Passini, C. & Baggiani, C. Increased sensitivity of lateral flow immunoassay for ochratoxin A through silver enhancement. *Analytical and Bioanalytical Chemistry* **405**, 9859-9867, doi:10.1007/s00216-013-7428-6 (2013).

33. Fu, E., Nelson, K. E., Ramsey, S. A., Foley, J. O., Helton, K. & Yager, P. Modeling of a Competitive Microfluidic Heterogeneous Immunoassay: Sensitivity of the Assay Response to Varying System Parameters. *Anal. Chem.* **81**, 3407-3413, doi:10.1021/ac802672v (2009).

34. Pradelles, P., Grassi, J., Creminon, C., Boutten, B. & Mamas, S. Immunometric assay of low molecular weight haptens containing primary amino groups. *Analytical chemistry* **66**, 16-22, doi:10.1021/ac00073a005 (1994).

35. Travica, N., Ried, K., Bujnowski, R. & Sali, A. Integrative health check reveals suboptimal levels in a number of vital biomarkers. *Advances in Integrative Medicine*, doi:http://dx.doi.org/10.1016/j.aimed.2015.11.002.

36. Cho, I.-H., Seo, S.-M., Paek, E.-H. & Paek, S.-H. Immunogold–silver staining-on-a-chip biosensor based on cross-flow chromatography. *Journal of Chromatography B* **878**, 271-277, doi:http://dx.doi.org/10.1016/j.jchromb.2009.07.016 (2010).

37. Millipore. Rapid Lateral Flow Test Strips: Considerations for Product Development. (2008).

38. Wong, R. & Tse, H. *Lateral Flow Immunoassay*. (HUmana Press, 2009).

Chapter 4:

Two-color lateral flow assay for multiplex detection of causative agents behind acute febrile illnesses †

4.1 Abstract

Acute undifferentiated febrile illnesses (AFIs) represent a significant health burden worldwide. AFIs can be caused by infection with a number of different pathogens including dengue (DENV) and Chikungunya viruses (CHIKV), and their differential diagnosis is critical to the proper patient management. While rapid diagnostic tests (RDTs) for the detection of IgG/IgM against a single pathogen have played a significant role in enabling the rapid diagnosis in the point-of-care settings, the state-of-the-art assay scheme is incompatible with the multiplex detection of IgG/IgM to more than one pathogen. In this paper we present a novel assay scheme that uses two-color latex labels for rapid multiplex detection of IgG/IgM. Adapting this assay scheme, we show that 4-plex detection of the IgG/IgM antibodies to DENV and CHIKV is possible in 10 minutes by using it to correctly identify 12 different diagnostic scenarios. We also show that blue, mixed and red colorimetric signals corresponding to IgG, IgG/IgM, and IgM positive cases respectively can be associated with distinct ranges of hue intensities, which could be exploited by analyzer systems in the future for making accurate, automated quantification and diagnosis. This represents the first steps towards the development of a single RDT-based system for the differential diagnosis of numerous AFIs of interest.

† This chapter was reproduced from:

- **Lee, S.**, Mehta, S., Erickson, D. (2016) "Two-color lateral flow assay for multiplex detection of causative agents behind acute febrile illnesses" Under Review in Biosensors and Bioelectronics

4.2 Introduction

Acute undifferentiated febrile illnesses (AFIs) are responsible for substantial morbidity and mortality globally and impose a considerable economic cost, primarily in developing countries.[1-3] In order to treat patients of febrile illnesses appropriately and effectively, the AFIs need to be differentially diagnosed by identifying the causative infectious agents, examples of which include Chikungunya (CHIKV) and Dengue (DENV).[4,5] CHIKV is a re-emerging mosquito-borne alphavirus responsible for a severe epidemic in countries of the Indian Ocean region with an estimated 7.5 million cases over five years.[6] DENV is the most rapidly-spreading mosquito vector disease worldwide, with an estimated 50–100 million new dengue infections occurring every year in over 100 countries.[7]

In many settings, the initial diagnosis of patients presenting with febrile illness is done with the use of a standard rapid diagnostic test (RDT) based on lateral flow principles. These tests can be easily administered and yield quick results with relatively high sensitivities and specificities.[8-11] For the AFI diagnosis, most of these tests rely on detecting the Immunoglobulin M (IgM) antibodies to the infectious agent, which is supplemented by the Immunoglobulin G (IgG) antibody detection for the indication of a past infection.[12] In such cases the current state-of-the-art is a single RDT strip for the duplex IgG/IgM detection using two test lines (one for IgG and one for IgM detection). In these cases detection is limited to that associated with a single infectious agent, and the detection of IgG/IgM to the other pathogens would require additional pathogen-specific strips to be used in parallel. Multiplexing the IgG/IgM detection of several AFIs on a single strip can have an immediate, significant impact by facilitating its deployment, lowering the cost, and allowing much more rapid differential AFI diagnosis.[13]

For the detection of several antigens, as opposed to antibodies, multiplexing on a single strip has previously been achieved by introducing additional detection antibodies of the same label (e.g. gold nanoparticle labelled antibody for new target antigens) and adding the associated test lines that are spatially separated from each other for developing multiple test line signals.[14,15] Unfortunately, such approach cannot be adapted in multiplexing antibody RDTs whose test lines comprise of anti-IgG and anti-IgM and are not

pathogen specific. This represents a challenge for multiplexing because even if multiple detection probes with different pathogen specificity are used, they would all be captured on a single test line; as such when a test line signal develops color, the information about the causative pathogen would still be unknown. Therefore under this format, multiplexing requires the encoding of each detection probe with a different characteristic color (i.e. associating a distinct color with a certain pathogen), and subsequently analyzing the composition of the test region color as recently demonstrated for a similar application.[16] This approach has practical drawbacks including the requirements for distinctly different color labels (*n*-plex test would require *n* differently colored probes), and the complexity of analyzing the color development as *n* becomes large.

In this Chapter we present a novel lateral flow assay scheme for multiplexing the detection of several pathogens-specific IgG/IgM on a single strip using just two color labels. This method uses blue and red encodings to discriminate between the IgGs and IgMs, while the pathogen specificity is determined by observing the test line location of the color development. We first show that our assay can achieve the duplex IgG/IgM detection for CHIKV using just a single test region. We then demonstrate the 4-plex detection of anti-CHIKV IgG/IgM and anti-DENV IgG/IgM on the same test strip, and expand on opportunities for further multiplexing.

4.3 Experimental

4.3.1 Blue and Red latex based detection probe preparation

The latex based detection probes used in the study were prepared by labelling the anti-IgG antibodies (goat anti-rabbit IgG secondary antibody, γ-chain specific; Jackson ImmunoResearch Laboratories, Inc.) with Blue latex beads (LATEX conjugation kit – 400nm Blue; Innova Biosciences Ltd.), and anti-IgM antibodies (goat anti-mouse IgM secondary antibody, μ-chain specific; Sigma Aldrich Co.) with Red latex beads (LATEX conjugation kit – 400nm Red; Innova Biosciences Ltd.). Before the conjugation procedures, a buffer exchange for the antibody solutions (AbPure Antibody Concentration and Clean-up Kit; Innova

Biosciences Ltd.) was performed which removed small interfering substances such as azide and tris from the solutions, and transferred the antibodies to an amine-free buffer (10mM MES buffer at pH 7) that is compatible with the subsequent conjugation procedures. The conjugation was carried out by adding 40µl of the anti-IgG at 0.1mg/ml to the 0.4mg of the pre-treated 400nm Blue polystyrene latex beads. The antibodies covalently bound to the surface of the latex beads via lysine residues during the 15min incubation at room temperature, and the reaction was quenched by adding 1mL of 0.01M tris-buffered saline (TBS) with 0.1% Tween 20. The Blue latex–anti-IgG conjugates were spun at 10,000 rpm for 9 min to remove any of the unbound antibodies, reconstituted to 1% and stored at 4°C until use. The above conjugated steps were repeated for anti-IgM and 400nm Red polystyrene latex beads, yielding 1% red latex–anti-IgM conjugates. The choice of our anti-IgG and anti-IgM probes that have affinities towards rabbit IgGs and mouse IgMs, respectively, has been to demonstrate our assay scheme using the commercially available IgGs and IgMs of DENV and CHIKV. In order for this assay to be useful in the diagnosis of AFIs in humans, the current anti-IgG and anti-IgM probes would need to be replaced with those with human IgG/IgM affinities, however the probe preparation steps would remain the same.

To prepare the conjugate pad that dry-stores the red and blue latex based probes, the probes were first diluted to 0.4% in the conjugate buffer (2mM borate buffer with 5% sucrose), and then used to fully immerse the Glass Fibre Conjugate Pads (EMD Millipore) with 10cm x 5mm dimensions. The conjugate pad was dried at 37°C for 5h and stored until being assembled in to the lateral flow assay.

4.3.2 Two-color Lateral flow assay preparation

The lateral flow assay was prepared by assembling the sample, conjugate, and absorbent pads onto the adhesive parts of the plastic-backed Hi-Flow Plus 90 Membrane Cards (EMD Millipore), which contained the nitrocellulose membrane that housed various test and control regions. To ensure proper wicking of the sample solution through the assembled assay, the components were assembled via the adhesive regions of the membrane card in the following order: (1) the latex-bead-treated conjugate pad was first attached below the nitrocellulose membrane with a 0.5mm overlap, (2) the FR-1 Membrane (MDI Membrane

Technologies) as the sample pad was attached below the conjugate pad with a 0.5mm overlap, and (3) the Cellulose Fiber Membrane (EMD Millipore) as the absorbent pad was attached above the nitrocellulose membrane also with a 0.5mm overlap. The assembled membrane card was cut manually into individual strips of 5 mm width (Figure 4.1a) using a rotary paper trimmer (Dahle North America, Inc.).

The control regions of the test strip were prepared by dispensing 0.4µl of 0.5mg/ml anti-goat IgG secondary antibody (LifeSpan Biosciences, Inc.) onto the center of the nitrocellulose membrane, 3mm below the absorbent pads. The test regions were subsequently prepared 2mm below the control regions by dispensing 0.5µl of 1.0mg/ml: recombinant CHIKV E2 protein (RaybioTech, Inc) for the CHIKV test (Figure 4.2a), and/or recombinant dengue antigen (RaybioTech, Inc) for the DENV test. For the 4-plex test which combines the CHIKV and DENV tests, the CHIKV and DENV test regions were dispensed side-by-side with a 1mm separation distance, and 2mm below the control region (Figure 4.3). For this initial prototype version of the assay, pipetting of test and control regions provided convenient and cost-effective means to prepare the small batch of test strips (<50). For mass producing of the test strips, a lateral flow dispenser (e.g. Lateral Flow Reagent Dispenser; Claremont Biosolution) could be adapted to yield higher repeatability.

4.3.3 Assay procedures

In the testing of the two-color lateral flow assay, 10µl of the sample was first dispensed onto the sample pad of the test strip, where the sample may be: rabbit anti-CHIKV IgG (Integrated BioTherapeutics, Inc.), mouse anti-CHIKV IgM (United States Biological), rabbit anti-DENV IgG (LifeSpan BioSciences, Inc.), and/or mouse anti-DENV 4 IgM (antibodies-online). Subsequently 80µl of the chase buffer (1x TBS with 1% BSA, 1.5% Tween 20, 0.1% sodium azide) was dispensed which initiated the sample flow through the length of the test strip. For the duplex IgG/IgM detection for CHIKV (Section 4.3.2), the anti-CHIKV IgG and IgM samples of 150, 300, 450 and 600µg/ml were prepared by diluting with 1x PBS. For the 4-plex

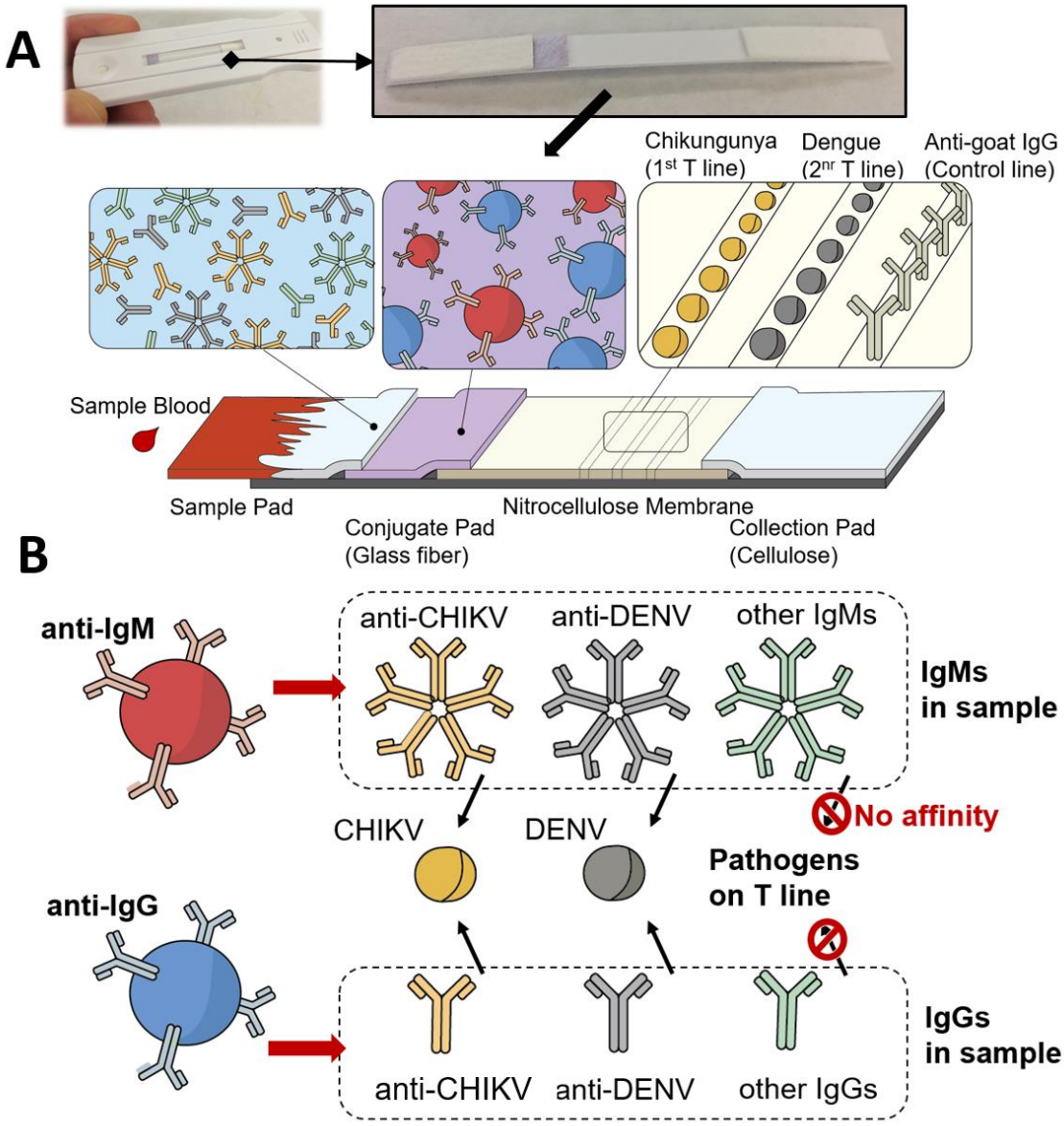

Figure 4.1: Two-color lateral flow assay for multiplex detection of causative agents behind acute febrile illnesses. **(A)** Assay architecture comprising of sample, conjugate, nitrocellulose and collection membranes. **(B)** Assay principles involving: Blue latex–anti-IgG and Red latex–anti-IgM detection probes for targeting the sample IgG and IgM respectively, and the recombinant pathogen molecules on the test line for capturing the IgG/IgM to the respective pathogens.

IgG/IgM detection for CHIKV and DENV (Section 4.3.3), the anti-CHIKV IgG/IgM and anti-DENV IgG/IgM samples at 600 µg/ml in 1x PBS were prepared and used.

4.3.4 Image acquisition and analysis

After allowing for 10min for the color development on the test and control regions, the image of the test and control regions were taken using a CMOS camera under the same room lighting conditions. The images were transferred to a standard laptop computer and red (R), green (G) and blue (B) intensities were obtained using ImageJ (National Institutes of Health). Within the test regions which typically measured 120 pixels by 120 pixels, three different areas of 40 pixels by 40 pixels were analyzed in order to examine the effect of non-uniformities of the color development. The R, G and B values were then averaged and used to calculate the hue (H) intensities (Supplementary Tables A2.1 and A2.2) based on the following equation:

$$H=4+(R-G)/(M-m) \text{ if } M=B, \text{ or } H=2+(B-R)/(M-m) \text{ if } M=G \qquad (1)$$

where M=max(R,G,B) and m=min(R,G,B). Here the use of hue channel to investigate the test region color is convenient as in the range of our interest, hue intensity is found to increase monotonically as the ratio of red to blue color increases. The other advantages of using hue channels have been discussed elsewhere.[17] In our analysis, the test regions that did not develop any color were not considered.

4.4 Results and Discussion

4.4.1 Two-color multiplex assay operation principles

Our two-color lateral flow assay consists of: the sample pad for accepting the sample, the conjugate pad for storing the detection probes, the nitrocellulose membrane for immobilizing the test and control region reagents, and the absorbent pad for collecting the waste mixtures (**Figure 4.1**a). To operate our test, the sample and chase buffer solutions are added to the sample pad sequentially as typically done for other traditional RDTs. Once wetted, the blue and red detection probes that have been dry-stored on the conjugate pad are released and become free to interact with all the sample IgGs and IgMs, respectively, including those associated with the AFIs of interest (Figure 4.1b). When the sample–probe mixture flows over the test regions, only the IgGs and IgMs to the targeted pathogens are captured at the respective test regions, and develops color due to the accompanying blue and red detection probes from the earlier interaction.

Further downstream, the control region immobilizes the secondary antibodies (i.e. anti-goat IgG) that capture both the blue anti-IgG and red anti-IgM detection probes based on their host species (i.e. goat), and develops mixed colors to confirm that the test has completed successfully. Thus after checking to find the mixed color development on the control region, the operator can obtain diagnostic AFI information from the two-color assay by: (1) observing the color development on the test region where red, blue and mixed colors indicate the presence of IgGs, IgMs or both, respectively, and (2) determining the pathogen specificity of the detected IgG/IgM by noting the location of the test region under observation (e.g. two spatially separated test regions associated with DENV and CHIKV are shown as examples in Figure 1b). Here, such multiplexing is enabled by our use of anti-IgG and anti-IgM probes that serve as common agents in the IgG/IgM detection of different AFIs. This signifies that the two-color assay can be further multiplexed simply by introducing additional test regions (i.e. dispensing other recombinant pathogen molecules of interest such as Malaria, Chagas, Leptospirosis and Typhoid fever) and ensuring that the anti-IgG and anti-IgM probes do not become limited during their interaction with the sample.

4.4.2 Two-color duplex detection of anti-CHIKV IgG/IgM

In **Figure 4.2**a, we first demonstrate our assay scheme for the duplex detection of anti-CHIKV IgG/IgM. As expected, only the blue color can be observed on the CHIKV test region when the sample contains the significant concentrations of anti-CHIKV IgG only. The blue color on the CHIKV test region is indicative of the blue latex–anti-IgG probes that have bound to the anti-CHIKV IgG in the sample, which in turn has been captured by the CHIKV molecules on the test region (Figure 4.2b). As the sample concentration of anti-CHIKV IgG is decreased and that of anti-CHIKV IgM is increased, the blue color diminishes and the red color begins to emerge which correlates to the increasing number of red latex–anti-IgM probes accumulating on the CHIKV test region. This color trend continues to the case where only the significant concentration of anti-CHIKV IgM is found in the sample, and the red color dominates the CHIKV test region. In Figure 4.2c, we confirm this trend by acquiring the R and B intensities from the CHIKV test regions. In addition, we show that hue intensity of the test region increases as expected when red color

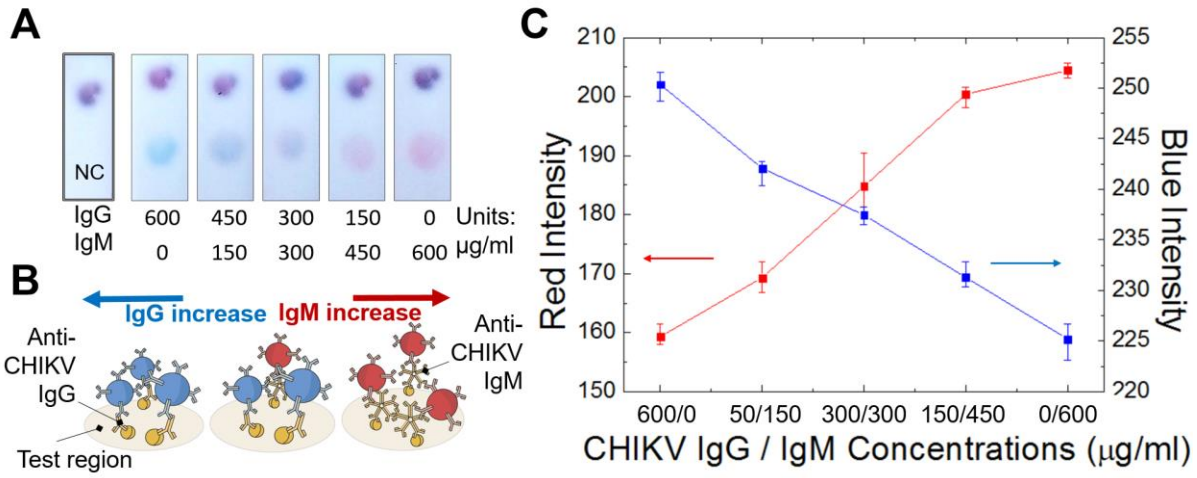

Figure 4.2: Single-spot duplex IgG/IgM test for chikungunya. **(A)** Color development on the test region of the two-color assay. **(B)** Schematic details of the test region interactions where blue and red colors correspond to the colored probes that have interacted with the anti-CHIKV IgG and IgM, respectively. **(C)** Image analysis for red and blue intensities on the test regions at different anti-CHIKV IgG/IgM concentrations.

shows a stronger presence over blue (Supplementary Figure A2.1). These results suggest that as currently optimized, our two-color lateral flow assay develops distinguished blue/red colors when the concentrations of anti-CHIKV IgG/IgM, respectively, are above 300µg/ml. As the concentrations of AFI related IgG/IgM in human blood are elevated significantly beyond 300µg/ml for those infected and found in much lower concentrations otherwise,[18] this version of our assay has the potential to diagnose the presence of anti-CHIKV IgG/IgM in point-care settings. Our novel assay scheme, in comparison to the commercial RDTs for duplex anti-CHIKV IgG/IgM detection that requires two separate test regions, is able to achieve the same level of multiplexing on just a single test region, which could lead to the reductions in the strip dimensions and material cost. [16]

4.4.3 Two-color 4-plex detection of anti-CHIKV IgG/IgM and anti-DEV IgG/IgM

In **Figure 4.3**a, we demonstrate the multiplexing capabilities of our novel assay scheme that enables the 4-plex detection of the IgG/IgM to the two distinct AFIs – CHIKV and DENV – on a single strip. The

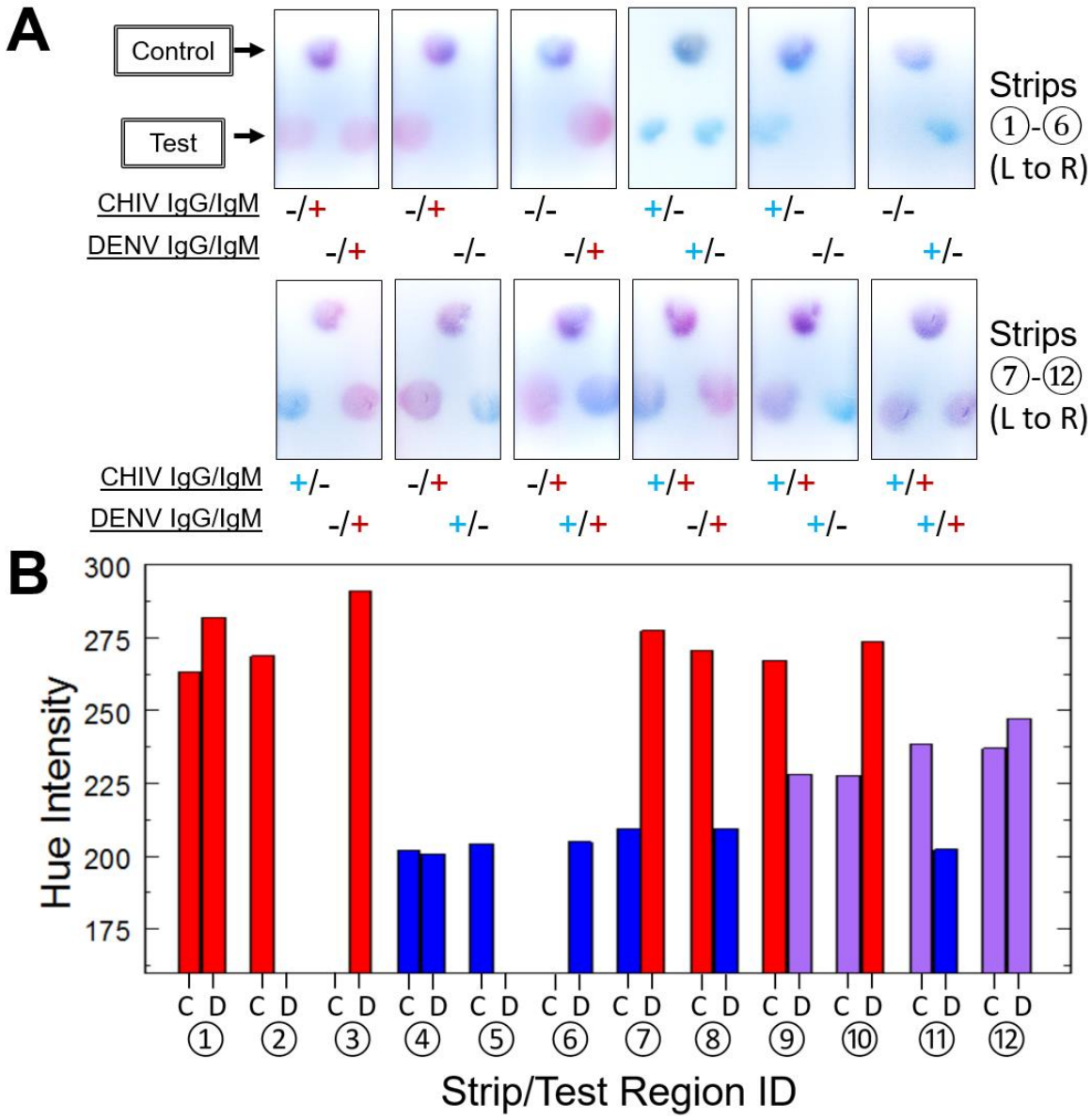

Figure 4.3: 4-plex IgG/IgM test for Chikungunya and Dengue on a single strip. **(A)** CHIKV test region (C; left) and DENV test region (D; right) developing red, blue or mixed colors for different diagnostic scenarios **(B)** Hue intensity of CHIKV and DENV test regions for the 4-plex strips

colorimetric development on the CHIKV test region (left) can be observed to indicate the presence of anti-CHIKV IgG and/or anti-CHIKV IgM above the pre-defined cut-off concentrations of 300µg/ml. In parallel, DENV test region (right) on the same strip provides information about the presence of anti-DENV IgG

and/or anti-DENV IgM. On both test regions, we show that blue, red or mixed colors develop when the sample contains the pathogen-specific IgGs, IgMs or both, respectively, which could be used to correctly identify 12 different diagnostic scenarios involving anti-CHIV and anti-DENV IgG/IgM. In Figure 4.3b, we quantitatively confirm these observations by evaluating the hue intensity of the test regions. The results indicate that the presence of IgG, IgG/IgM, and IgM can be associated with three distinct ranges of hue values at 200-209, 227-247 and 262-290, respectively (summarized in Supplementary Figure A2.2). This ability to multiplex IgG/IgM tests of more than one pathogen on a single strip is unprecedented, and has the potential to facilitate the differential diagnosis of AFIs in the point-of-care settings. As the number of test regions increases and to accommodate the users with color-perception difficulties, the need for analyzer system becomes apparent. For the intended point-of-care applications, this requirement can be fulfilled using smartphone based analyzer systems that have been previously developed by our group[19,20] and the others[21,22] for similar applications. Besides the analytical capabilities, these systems could facilitate the AFI management by allowing quick communication of results via e-mail and collecting/tracking epidemiological data.[23,24]

4.5 Conclusion

In this work, we present a novel lateral flow assay scheme that relies on two-color detection probes to multiplex the detection of IgG/IgM to CHIKV and DENV on a single lateral flow assay strip. We show that by observing the color and location of the CHIKV and DENV test regions, our assay can indicate the presence of anti-CHIKV IgG/IgM and anti-DENV IgG/IgM. As our choice of the detection probes is commonly applicable in the detection schemes of different AFI-associated IgG/IgM tests, our assay could be easily multiplexed beyond the two AFIs presented here. Thus, this represents the significant step towards the development of a single point-of-care rapid test for the differential diagnosis of multiple AFIs, which could be integrated with smartphone reader systems to facilitate the results analysis and communication of diagnostic findings.

4.6 References

1. Chrispal, A., Boorugu, H., Gopinath, K. G., Chandy, S., Prakash, J. A. J., Thomas, E. M., Abraham, A. M., Abraham, O. & Thomas, K. Acute undifferentiated febrile illness in adult hospitalized patients: the disease spectrum and diagnostic predictors–an experience from a tertiary care hospital in South India. *Tropical doctor* **40**, 230-234 (2010).

2. Suaya, J. A., Shepard, D. S. & Beatty, M. E. in *TDR. Report of the Scientific Working Group Meeting on Dengue.* 35-49.

3. Lau, C., Smythe, L. & Weinstein, P. Leptospirosis: an emerging disease in travellers. *Travel Medicine and Infectious Disease* **8**, 33-39 (2010).

4. Laoprasopwattana, K., Kaewjungwad, L., Jarumanokul, R. & Geater, A. Differential Diagnosis of Chikungunya, Dengue Viral Infection and Other Acute Febrile Illnesses in Children. *The Pediatric Infectious Disease Journal* **31**, 459-463, doi:10.1097/INF.0b013e31824bb06d (2012).

5. Hofer, M., Mahlaoui, N. & Prieur, A.-M. A child with a systemic febrile illness – differential diagnosis and management. *Best Practice & Research Clinical Rheumatology* **20**, 627-640, doi:http://dx.doi.org/10.1016/j.berh.2006.04.001 (2006).

6. Schwartz, O. & Albert, M. L. Biology and pathogenesis of chikungunya virus. *Nat Rev Micro* **8**, 491-500, doi:10.1038/nrmicro2368 (2010).

7. WHO. Dengue and sever dengue [factsheet no. 117, revised May 2015]. (World Health Organization: Geneva, 2015).

8. Chappuis, F., Alirol, E., d'Acremont, V., Bottieau, E. & Yansouni, C. P. Rapid diagnostic tests for non-malarial febrile illness in the tropics. *Clinical Microbiology and Infection* **19**, 422-431, doi:http://dx.doi.org/10.1111/1469-0691.12154 (2013).

9. Andries, A.-C., Duong, V., Ngan, C., Ong, S., Huy, R., Sroin, K. K., Te, V., Y, B., Try, P. L. & Buchy, P. Field Evaluation and Impact on Clinical Management of a Rapid Diagnostic Kit That Detects Dengue NS1, IgM and IgG. *PLoS Negl Trop Dis* **6**, e1993, doi:10.1371/journal.pntd.0001993 (2012).

10. Bajani, M. D., Ashford, D. A., Bragg, S. L., Woods, C. W., Aye, T., Spiegel, R. A., Plikaytis, B. D., Perkins, B. A., Phelan, M., Levett, P. N. & Weyant, R. S. Evaluation of Four Commercially Available Rapid Serologic Tests for Diagnosis of Leptospirosis. *Journal of Clinical Microbiology* **41**, 803-809, doi:10.1128/jcm.41.2.803-809.2003 (2003).

11. Anderson, J. L., May, H. T., Horne, B. D., Bair, T. L., Hall, N. L., Carlquist, J. F., Lappe, D. L. & Muhlestein, J. B. Relation of vitamin D deficiency to cardiovascular risk factors, disease status, and incident events in a general healthcare population. *The American journal of cardiology* **106**, 963-968, doi:10.1016/j.amjcard.2010.05.027 (2010).

12. Blacksell, S. D., Jarman, R. G., Bailey, M. S., Tanganuchitcharnchai, A., Jenjaroen, K., Gibbons, R. V., Paris, D. H., Premaratna, R., de Silva, H. J., Lalloo, D. G. & Day, N. P. J. Evaluation of Six Commercial Point-of-Care Tests for Diagnosis of Acute Dengue Infections: the Need for Combining NS1 Antigen and IgM/IgG Antibody Detection To Achieve Acceptable Levels of Accuracy. *Clinical and Vaccine Immunology* **18**, 2095-2101, doi:10.1128/cvi.05285-11 (2011).

13. D'Acremont, V. & Bosman, A. WHO informal consultation on fever management in peripheral health care settings: a global review of evidence and practice. *Geneva: World Health Organization* (2013).

14. Song, S., Liu, N., Zhao, Z., Njumbe Ediage, E., Wu, S., Sun, C., De Saeger, S. & Wu, A. Multiplex Lateral Flow Immunoassay for Mycotoxin Determination. *Analytical chemistry* **86**, 4995-5001, doi:10.1021/ac500540z (2014).

15. Yang, M., Caterer, N. R., Xu, W. & Goolia, M. Development of a multiplex lateral flow strip test for foot-and-mouth disease virus detection using monoclonal antibodies. *Journal of Virological Methods* **221**, 119-126, doi:http://dx.doi.org/10.1016/j.jviromet.2015.05.001 (2015).

16. Yen, C.-W., de Puig, H., Tam, J. O., Gomez-Marquez, J., Bosch, I., Hamad-Schifferli, K. & Gehrke, L. Multicolored silver nanoparticles for multiplexed disease diagnostics: distinguishing dengue, yellow fever, and Ebola viruses. *Lab on a Chip* **15**, 1638-1641, doi:10.1039/C5LC00055F (2015).

17. Oncescu, V., O'Dell, D. & Erickson, D. Smartphone based health accessory for colorimetric detection of biomarkers in sweat and saliva. *Lab on a Chip* **13**, 3232-3238, doi:10.1039/C3LC50431J (2013).

18. Parry, J. V., Perry, K. R. & Mortimer, P. P. Originally published as Volume 2, Issue 8550SENSITIVE ASSAYS FOR VIRAL ANTIBODIES IN SALIVA: AN ALTERNATIVE TO TESTS ON SERUM. *The Lancet* **330**, 72-75, doi:http://dx.doi.org/10.1016/S0140-6736(87)92737-1 (1987).

19. Lee, S., Oncescu, V., Mancuso, M., Mehta, S. & Erickson, D. A smartphone platform for the quantification of vitamin D levels. *Lab on a Chip* **14**, 1437-1442 (2014).

20. Lee, S., O'Dell, D., Hohenstein, J., Colt, S., Mehta, S. & Erickson, D. NutriPhone: a mobile platform for low-cost point-of-care quantification of vitamin B12 concentrations. *Under Review* (2016).

21. Mudanyali, O., Dimitrov, S., Sikora, U., Padmanabhan, S., Navruz, I. & Ozcan, A. Integrated rapid-diagnostic-test reader platform on a cellphone. *Lab on a Chip* **12**, 2678-2686, doi:10.1039/C2LC40235A (2012).

22. Laksanasopin, T., Guo, T. W., Nayak, S., Sridhara, A. A., Xie, S., Olowookere, O. O., Cadinu, P., Meng, F., Chee, N. H., Kim, J., Chin, C. D., Munyazesa, E., Mugwaneza, P., Rai, A. J., Mugisha, V., Castro, A. R., Steinmiller, D., Linder, V., Justman, J. E., Nsanzimana, S. & Sia, S. K. A smartphone dongle for diagnosis of infectious diseases at the point of care. *Sci Transl Med* **7**, 273re271-273re271, doi:10.1126/scitranslmed.aaa0056 (2015).

23. Erickson, D., O'Dell, D., Jiang, L., Oncescu, V., Gumus, A., Lee, S., Mancuso, M. & Mehta, S. Smartphone technology can be transformative to the deployment of lab-on-chip diagnostics. *Lab on a chip* **14**, 3159-3164, doi:10.1039/c4lc00142g (2014).

24. Tucker, C. Public health-related apps growing in number, popularity: Smartphones, tablets used for health. *The Nation's Health* **41**, 1,14-15 (2011).

Chapter 5:

Autonomous device for application in late-phase hemorrhagic shock prevention†

5.1 Abstract

Hemorrhagic shock (HS) is the leading cause of death for people with traumatic injuries. The onset of HS is correlated with marked changes in the plasma vasopressin levels and some studies indicate that administrating vasopressin in the bloodstream can help stabilize the situation. This situation calls naturally for the use of implantable devices for both the monitoring and treatment of HS. In this work, we present a self-powered hemorrhagic-shock autonomous integrated device (hemoAID) that continuously monitors vasopressin levels and releases vasopressin automatically when levels drop below a certain threshold. The hemoAID system consists of: (1) aptamer-based biosensor for detecting pM changes of vasopressin levels, (2) on-board drug delivery system for administration of vasopressin, and (3) non-enzymatic glucose fuel cell for powering these components. We demonstrate that the device can operate at physiological concentrations of vasopressin, in sheep serum, thus paving the way towards the development of an autonomous implantable device for HS prevention.

---

† This chapter was reproduced from:

- Oncescu, V.*, **Lee, S.***, Gumus, A., Karlsson, K., Erickson, D. (2014) "Autonomous device for application in late-phase hemorrhagic shock prevention". **PloS-ONE**. 9(2): e89903 *These authors have contributed equally to the paper
- He, P., Oncescu, V., **Lee, S.**, Choi, I., and Erickson, D. (2012) Label-free electrochemical monitoring of vasopressin in aptamer-based microfluidic biosensors. **Analytica Chimica Acta**. 759: 74-80

5.2 Introduction

Over the past decade, implantable autonomous microsystems have been developed to counter life-threatening medical conditions and to improve patient care by replacing cumbersome treatment procedures[1-3]. As such, a growing number of patients now depend on implantable cardioverter defibrillators[4], gastric stimulators[5], cardiac pacemakers[6] and artificial organs[7-9] for survival. In such cases, the severity and urgency of the medical condition override the high cost and risk of the invasive surgery that is required. On the other hand, some situations call naturally for implantable medical devices to continuously monitor physiological changes in patients or to deliver treatment through pre-determined and repeated drug delivery. For instance, continuous glucose monitoring devices have found their market by increasing the efficacy of diabetes treatment and by helping patients monitor real-time variations in their blood glucose levels due to insulin and food intake, exercise, and other factors. Recently, Farra *et al.*[10] demonstrated an implantable drug delivery microchip that operates for up to 3 weeks and eliminates the need for daily physician-assisted injections for patients with osteoporosis. While these developments have been successful at independently performing sensing[11,12] and drug delivery[13], developing implantable medical devices capable of achieving both of those functions simultaneously would be suitable for a number of applications[14]. One such case is the detection and treatment of traumatic injuries such as hemorrhagic shock (HS).

Studies have correlated the onset of HS with marked changes in the plasma vasopressin levels[15,16]. Morales *et al.*[15] have conducted a set of canine experiments where vasopressin levels showed a marked increase at the onset of hemorrhage (to as much as 319pg/mL) followed by a fall to well below the normal physiological level (29pg/mL) as hemorrhage progressed. In addition, evidence suggests that replenishment of vasopressin at this stage can reverse hypotension in patients[17,18]. Krismer *et al.*[19] have reported case studies where dosages of 100 – 160 IU vasopressin led to hemodynamic stability with sinus rhythm in HS patients within 2min and patient survival without additional treatment of up to 90min. Therefore, vasopressin can serve as both a biomarker indicative of a critical injury state and a therapeutic agent for treating it.

Developing an implantable autonomous device that can provide initial medical treatment when physician care is not readily available is highly suitable in this case.

In this Chapter, we present a self-powered hemorrhagic-shock prevention autonomous integrated device (hemoAID) that continuously monitors vasopressin levels in solution and releases vasopressin automatically when vasopressin levels drop below a certain threshold. We demonstrate that the device works at physiological concentrations of vasopressin in sheep serum. This represents the first steps towards the development of an implantable, self-powered microfluidic device for late-phase HS prevention. In the next sections, we introduce the hemoAID, demonstrate the operation of the device during rapid changes in vasopressin concentration, and proceed by discussing the characteristics of the sensing, drug delivery and power units. In the "Conclusion and Future Prospective" section, we discuss some of the issues that need to be addressed in order to move toward a fully integrated autonomous implantable hemoAID.

5.3 Results and Discussion

5.3.1 hemoAID system overview

The hemoAID device shown in **Figure 5.1**a consists of a nanowire biosensor for detecting changes in vasopressin levels, an on-board electrochemically driven drug delivery system for administration of vasopressin, and a non-enzymatic glucose fuel cell for powering the system. Those three main functional components are integrated inside a $2cm^3$ package. In this prototype version the electronic control system is external to the system and uses the circuit shown in Figure 5.1b. External housing of the circuitry was done to facilitate prototype development and could be integrated into the system in the future.

5.3.2 Integrated device operation in flow network

In order to demonstrate its operation, the hemoAID device was placed inside a closed chamber within a fluid network designed to simulate the physiological vasopressin states of late-phase HS patients.

According to a clinical study by Jochberger *et al.*[20] vasopressin concentration for patients with hemorrhagic shock rises from the normal 6±3pM range to 52±30pM as the body tries to reverse hypotension by releasing vasopressin. Following this initial increase, the level of vasopressin starts decreasing, which indicates the onset of late phase hemorrhagic shock. At that point, administering a high dose of vasopressin can temporarily stabilize the situation. Here, we demonstrate the operation of the hemoAID at those physiologically relevant vasopressin concentrations. The test chamber housing the integrated device (**Figure 5.2**a) is initially filled with 100pM vasopressin solution, which corresponds to the high initial value (52±30pM) of blood vasopressin for patients prior to late-phase HS onset. The vasopressin concentration is then progressively lowered by introducing 10pM solution into the chamber using a VWR Mini-Pump at a flow-rate of 0.115mL/s. The decrease in vasopressin concentration, indicating late-phase HS, causes an increase in conductivity resulting in a voltage output drop across the nanowire sensor at constant current. The voltage drop across the sensor can be correlated to the vasopressin concentration, as we will discuss in the next section. As shown in Figure 5.2b, the sensor's voltage decreased over 14 minutes in response to

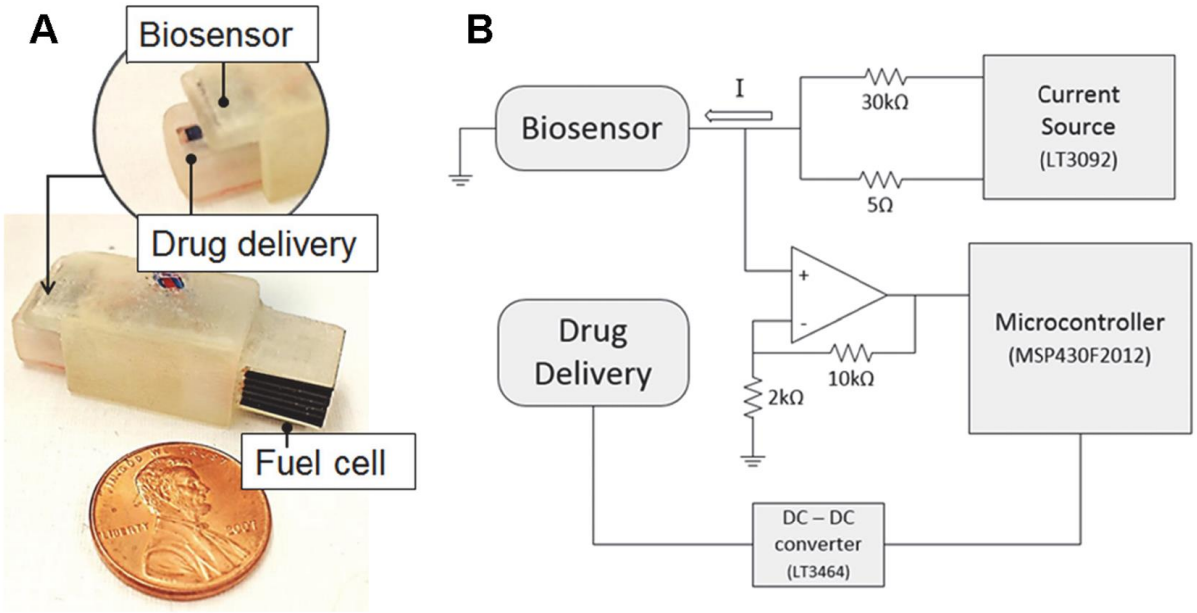

Figure 5.1: hemoAID system overview and schematic of electrical connections. **(A)** Integrated device consisting of a biosensor, drug delivery and fuel cell unit **(B)** schematic of the electrical connections between the different components of the hemoAID

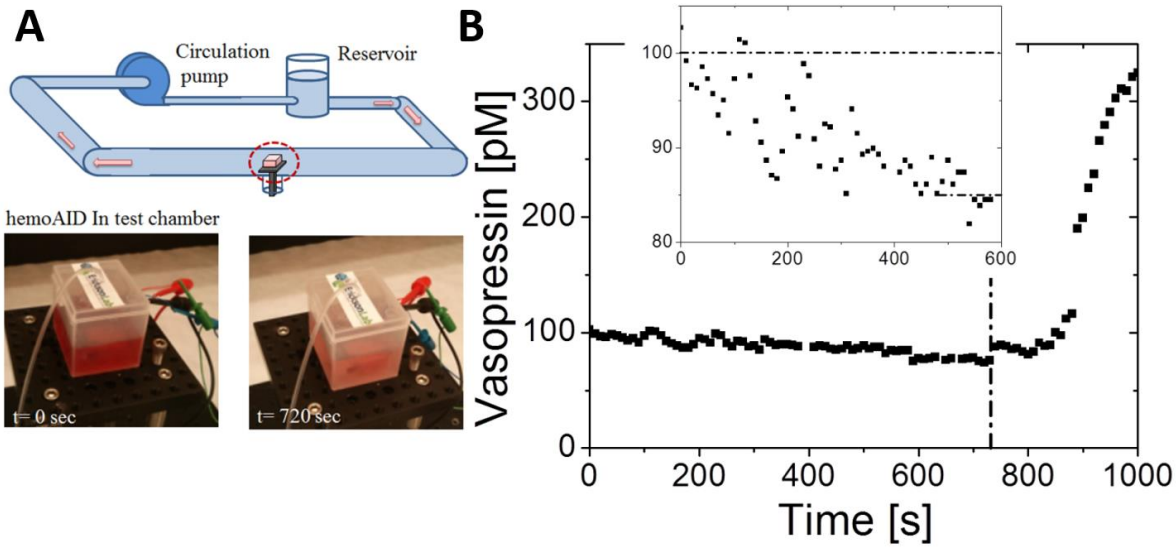

Figure 5.2: hemoAID system operation. **(A)** setup for integrated device testing **(B)** sensor detected vasopressin levels during experiment simulating decrease in vasopressin. The inset shows the vasopressin drop before the drug delivery is activated (simulating the onset of late-phase HS). The line at 720s shows the point at which drug delivery is activated

the decrease in vasopressin levels. Upon reaching a pre-determined 15% decrease in vasopressin concentration, corresponding to 0.25% voltage decrease ratio, the drug delivery is activated autonomously by the application of 35V between the top and bottom electrodes which results in the release of 16µL of highly concentrated (200µM) vasopressin. The localized vasopressin release was detected successfully by the sensor as can be seen in Figure 5.2b. This temporary increase in vasopressin would allow a patient to survive until further medical assistance can be provided.

The data obtained from the sensor is in the form of a voltage at the supplied current of 60mA. This can be transformed into a resistance change that is related to the vasopressin concentration change in solution via the following experimentally derived equation:

$$\Delta[VP] = 57.64\ \Delta R + 102.68 \qquad (1)$$

In the above equation Δ[VP] is in pM and ΔR is a % change in resistance. The relationship between changes in resistance and concentration is further discussed in the next section and is based on experiments presented elsewhere.[21]

5.3.3 Bio-sensing ability of integrated device

The nanowire biosensor we have developed and integrated in the hemoAID allows for the detection of pM changes in vasopressin concentration. Immobilized aptamer molecules on the nanowire biosensor act as electrical bioreceptors for the surrounding vasopressin. Reversible vasopressin binding leads to changes in conductivity through the carbon nanotube (CNT) detection zone (**Figure 5.3**a). The sensor is based on a device developed previously and the detailed microfabrication steps are presented elsewhere[21]. In this section, we demonstrate the sensing ability of the hemoAID to detect gradual changes in vasopressin levels by performing several characterization experiments. First, we show the reversibility of our sensor's detection mechanism by monitoring the sensor response to alternating vasopressin concentrations in a single experiment. The biosensor was placed into a custom packaging as shown with micro-channels as shown in Figure 5.3a and 0.01M Phosphate Buffer Saline (PBS) solution was introduced through one inlet until the output current was stabilized. The flow of 0.01M PBS was stopped after 20s and 10µM vasopressin was allowed to flow through the other inlet, which was again replaced by a PBS injection after another 30s. As shown in Figure 5.3b, the initial introduction of 10µM vasopressin results in a current decrease through the sensor almost instantaneously which is a consequence of depletion of charge carriers on the CNTs due to vasopressin to aptamer binding. The recovery of current upon 0.01M PBS injection at t= 50s is due to the release of vasopressin molecules from the immobilized aptamer which demonstrates the reversible nature of the binding events. The slower rate of current change during the dilution could be attributed to the low dissociation constant of aptamer-vasopressin complex, confirming the high affinity of aptamer molecules to vasopressin[22]. This experiment demonstrates the biosensor's rapid reversibility even when a high vasopressin concentration causes large changes in resistance, uncommon under normal physiological conditions.

In addition, we show that the sensor can be used to monitor physiologically relevant changes in serum vasopressin concentration. In Figure 5.3c, the biosensor is subjected to continuous variations in vasopressin by flowing sheep serum with 100pM, 50pM, 10pM and 0pM of added vasopressin in the respective order

for a period of 150s at each concentration. With each dilution, the current through the sensor increases as expected due to the release of vasopressin from the immobilized aptamers. In Figure 5.3d we show the percentage change in current from the initial no vasopressin case due to the addition of 10pM, 50pM and 100pM vasopressin. The bar graph represents the average of 5 experiments that were performed by

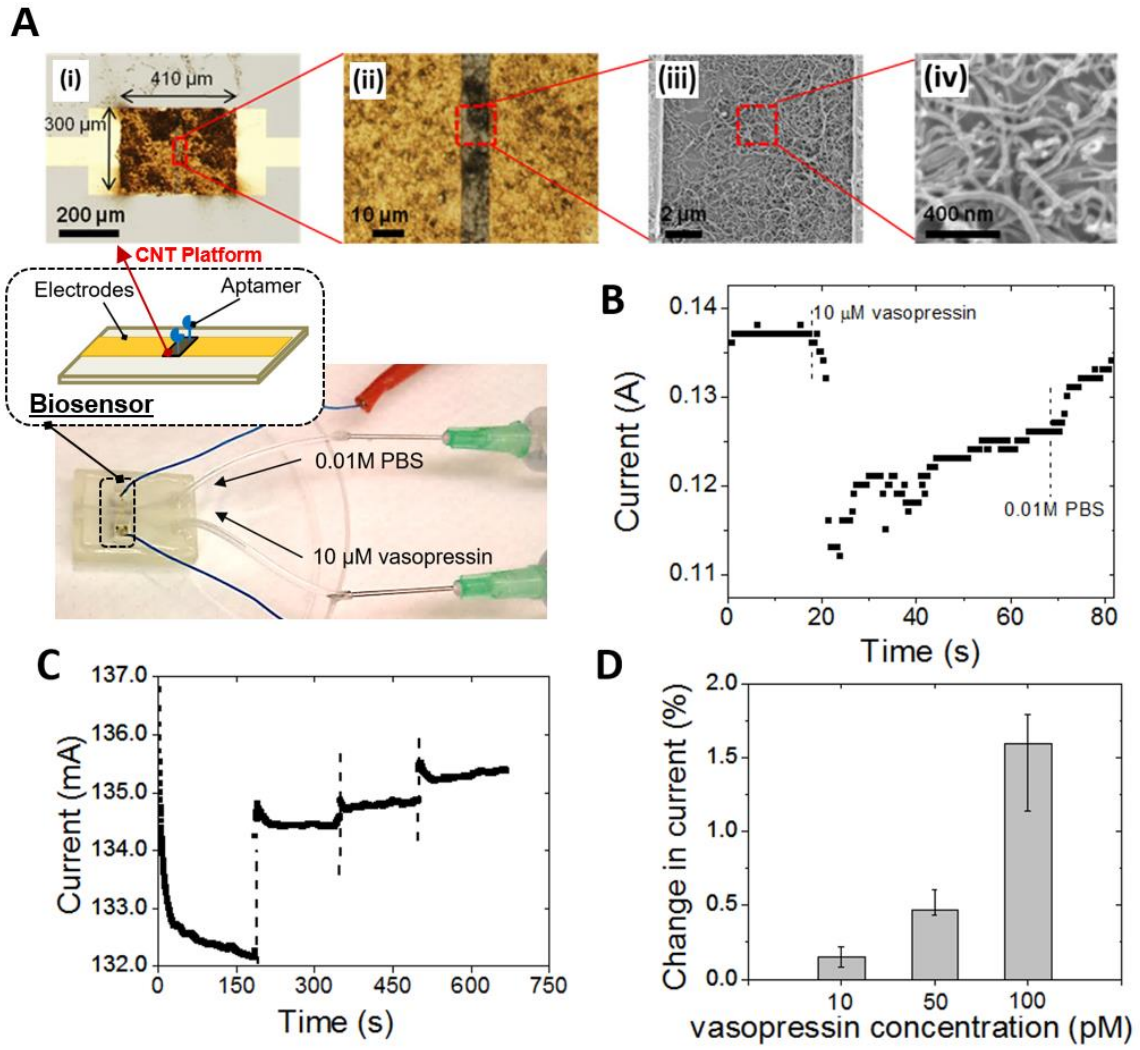

Figure 5.3: hemoAID biosensor characterization. **(A)** Schematic of the nanowire biosensor, optical images (i,ii) and SEM images (iii,iv) of the CNT patterned gold electrodes, and picture of the flow through system **(B)** demonstration of sensor reversibility **(C)** current change due to change in vasopressin concentration in sheep serum. At t=0 100pM vasopressin solution is introduces followed by 50 pM, 10pM and sheep serum with no additional vasopressin **(D)** Percentage decrease in current from the initial no vasopressin case due to different vasopressin concentration in sheep serum (average of 5 experiments)

continuously varying the concentration of vasopressin as shown in Figure 5.3c, with the error bar representing the range between the highest and lowest reading. These experiments demonstrate that the sensor can detect physiologically relevant changes in vasopressin in serum.

The high current used to increase the sensitivity of the sensor in the previous section can be decreased by changing the design of the sensor to increase its resistance either by decreasing the thickness of the nanowire sensing area on which APTMS is immobilized or by integrating several such nanowires in series. With these improvements, the sensor can be used for detection of vasopressin in interstitial fluid where changes in vasopressin are gradual and not affected by pressure changes in the bloodstream.

5.4.4 Stabilizing vasopressin levels through drug delivery

In this section we demonstrate the integrated device's mechanism to stabilize vasopressin levels through the in-parallel operation of the drug delivery system (**Figure 5.4**a) with the biosensor. Time-controlled ejection of vasopressin based on electrochemical principles as shown in Figure 5.4b has been demonstrated in previous publications.[23,24] To release vasopressin, electrical potential is applied between the top and bottom electrodes which results in two distinct reactions. The first is the electrolytic reaction in the reservoir that causes gas bubble formation and pressure build-up as a result. The second is the reaction between the chlorine ions in the buffer solution and the gold capping membrane to form a water soluble complex that gradually dissolves until it ruptures with increasing pressure of the reservoir. In the experiment presented

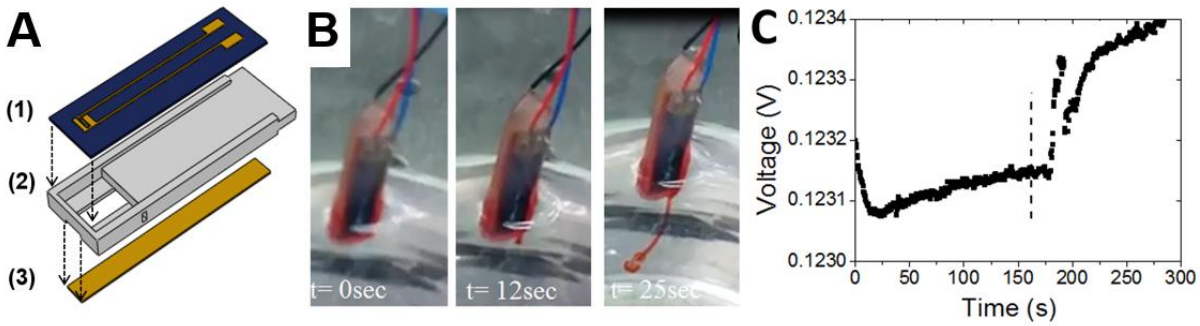

Figure 5.4: hemoAID drug delivery characterization **(A)** assembly of the drug delivery unit **(B)** vasopressin ejection over 25sec of applied voltage **(C)** increase in biosensor voltage due to drug delivery

in Figure 5.4c, the sensor and the capping membrane of the drug delivery system were aligned 50mm apart using a custom holder and immersed in a 0.01M PBS solution. After approximately 162s, the voltage output has stabilized (at t=0s on the graph), and the drug delivery was initiated by the application of a 35V potential between the top and bottom electrodes of the drug delivery system. The electrochemical ejection procedure has been imaged to suggests the onset of gold membrane rupture 5s after the potential application[24] and a sustained spike in voltage is first observed after 25s. The small magnitude of this signal (0.25mV) and the slow response of the sensor are due to large distance between the sensor and the drug delivery device. In the integrated hemoAID device, and the experiment in Fig 2b the sensor is placed 5mm in front of the sensor and the release of 16µL vasopressin solution at 200µM causes a much more rapid and larger voltage increase of 3.7%. This experiment demonstrates the ability of the sensor to monitor sudden changes in vasopressin concentration due to drug delivery by measuring the increase in voltage even when the two components are not in direct proximity.

5.4.3 Powering of integrated device

Instead of using the fuel cell unit directly to power the device, a small rechargeable battery shown in **Figure 5.5**a is used as an intermediate in order to decrease power supply fluctuations. In addition this also allows excess energy to be stored and used for the one-time operation of the drug delivery device.

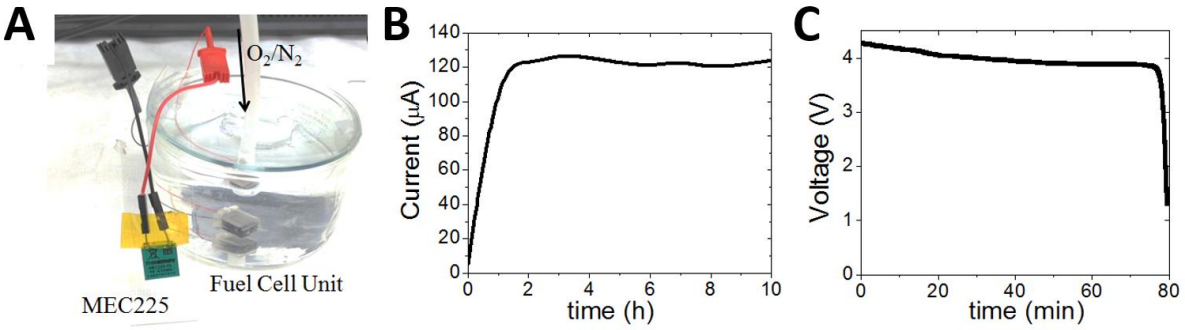

Figure 5.5: hemoAID fuel cell unit characterization. **(A)** Power unit consisting of a 1cm^3 fuel cell unit in 5mmol glucose solution at 8% O_2 saturation and an external rechargeable battery **(B)** chronoamperometric response of the fuel cell unit at 0.1 V in 0.01 M PBS solution and 5mmol glucose solution over a period of 10h **(C)** discharge profile for the rechargeable battery at an operating current of 100µA c) charging profile for the battery using the fuel cell unit

The power consumption for the integrated device with the sensor operated continuously is around 60mA at 3V. This is well above what can be supplied by a 1cm^3 fuel cell unit (20μA at 0.15V) however most of the power is required by biosensor since the change in resistivity across the detection area is directly proportional to the current applied. Although decreasing the current supply is in theory possible, this results in lower detection sensitivity. However, the microcontroller only requires 60 to 70μA at 3V to operate and we can operate the sensor at discrete time intervals, thus greatly reducing the power consumption of the system and making it possible to operate the system using a 1 cm^3 fuel cell unit. In Figure 5.5b we show the chronoamerometric response of the fuel cell unit (composed of 12 stacked single layers) at 0.1V in 0.01 M PBS solution (pH 7.4) and physiological levels of glucose and oxygen (5mmol glucose, 8% oxygen saturation) over a period of 10 hours. In Figure 5.5c we show the discharge profile of the Thinergy MEC225 with an operating current of 100μA. By continuously charging the Thinergy battery the system can operate continuously over a long period of time and avoid the power fluctuations typical of glucose fuel cell units (±4% as can be seen in Figure 5.5b).

5.4 Conclusion and Future Perspectives

In this Chapter, we have introduced the hemoAID, a device that can be used to detect a gradual drop in vasopressin concentration, corresponding to the onset of late-phase hemorrhagic shock, and deliver a highly concentrated dose of vasopressin to help stabilize the situation. We have demonstrated its operation in a controlled fluidic environment in which a 15% drop in vasopressin concentration was sensed and automatically triggered the activation of the drug delivery system. We discussed the sensor's mechanism and ability to operate in a complex medium such as sheep serum thus opening the door to the development of an implantable device for late phase hemorrhagic shock prevention.

Miniaturization and i*n-vivo* testing are the next steps in the development of an implantable hemoAID. The operation of the individual components of this device, or similar technologies, have been demonstrated elsewhere *in-vivo* or in serum. The vasopressin drug delivery system presented here is based on a device,

by Chung *et al.*, that allows controlling the rate of drug ejection and has been later shown to operate *in-vivo* in *Manduca sexta* moths[25]. In that work the drug delivery devices are sealed using biocompatible wax and implanted in the moths for over 2 days demonstrating stability of vasopressin during storage and upon electrochemical ejection. Other groups have developed similar micro-electro-mechanical-systems(MEMS) for rapid delivery of vasopressin and have demonstrated biocompatibility and long term vasopressin storage without degradation[26]. Some preliminary *in-vivo* studies in rabbits have been reported by H. L. Ho. Duc where a 20μL dose of 100μg/kg vasopressin solution is delivered subcutaneously and an increase in plasma vasopressin levels was observed to reach a stable concentration after about 1h[27]. These experiments demonstrate that such drug delivery technology is suitable for implantation and that the amount of vasopressin required is not an obstacle. The hemoAID reservoir contains approximately 16μL of concentrated vasopressin solution (200μM) or approximately 1.4 IU. When the device is loaded with a saturated solution of Arg8-vasopressin (400 IU/mg with 20 mg/ml solubility[28]) it is able to deliver a maximum of 128 IU. This falls within the range of vasopressin levels required to temporarily maintain a late-HS patient alive as discussed previously. Multiple drug delivery reservoirs can be integrated to deliver vasopressin over a longer period of time without substantially increasing the volume of the device as was done by Chung *et al.*[29]

In our previous work we have demonstrated the *in-vivo* operation of the drug delivery system after a 2 day implantation period in moths.[25] For a longer implantation period, as would be required for late phase sceptic shock prevention, a two reservoir system can be used in order to allow the drug to remain in solid lyophilized form until the device is electrochemically activated.[27] The operation principle of the drug delivery system would remain the same; however one reservoir would contain the lyophilized drug and the other the reconstruction media. The stability of vasopressin following electrochemical ejection from our device was investigated using MALDI-TOF/TOF mass spectroscopy in the appendix of a previous work.[23] Strong vasopressin peaks were observed for the ejected contents after application of a 12V potential for 5min indicating that only a small fraction of the vasopressin was oxidized during the ejection process.

In the current form, the device is integrated in a $3cm^3$ packaging with the fuel cell occupying about $1cm^3$ and the circuitry being external to the device. The miniaturization of similar circuitry has been demonstrated by Gumus *et al.* for application in *in-vivo* uric acid sensing on domestic chicken.[30] We envision the final version of the hemoAID, with multiple vasopressin drug delivery reservoirs, on-board circuitry and coated in biocompatible wax, to be suitable for sub-cutaneous implantation.

5.5 Materials and Methods

5.5.1 System design and assembly

The non-enzymatic glucose fuel cell is used to continuously charge a small rechargeable battery (Thinergy MEC225) that is then used to power a low power microcontroller (MSP430F2012, Texas Instruments, TX, USA). This set-up allows the device to operate steadily even with significant fluctuations in the power output of the fuel cell unit. During device operation, the sensor is driven by an adjustable 2-terminal current source (LT3092, Linear Technology, Milpitas, CA, USA) at 60 mA. The resistivity of the sensor changes with the amount of vasopressin in solution, which results in detectable voltage change over the biosensor. In order to improve sensitivity, the voltage is amplified using a non-inverting amplifier (Maxim Integrated, CA) before being detected using a low power microcontroller's analog to digital converter (ADC). If the voltage is lower than the pre-determined threshold, the microcontroller enables the corresponding output pin to activate the drug delivery system. In order to increase the discharge rate of vasopressin in the drug delivery device, the base voltage (3V) is converted to 35V with a micropower step-up DC/DC converter (LT3464, Linear Technology, Milpitas, CA, USA).

5.5.2 Biosensor fabrication

The detection region of the sensor was patterned on a 4-inch silicon wafer using general photolithography and surface-treated with (3-aminopropyl)trimethoxysilane (APTMS) using MolecularVapor Deposition Tool (MVD 100). The aminosilanes from the surface treatment were covalently linked with COOH-

functionalized multiwalled carbon nanotubes (Cheap Tubes Inc.) to serve as carriers of aptamer receptors. The scanning electron microscope (SEM) images of immobilized carbon nanotubes have been reported in our previous work[21]. Electrodes to the detection zone were lithographically patterned, followed by 5nm chromium/60nm gold deposition using a CHA Mark 50 e-Beam Evaporator. The wafer was diced into 0.8cm x 0.5cm pieces which represents significant size reduction from the previous design that measures 5cm x 5cm.

To immobilize the aptamer molecules on the carbon nanotube surface, an activation layer was first created by pipetting a mixture of 0.4 M 1-ethyl-3-(3-dimethylaminopropyl) carbodiimide (Geno Technology) and 0.1 M N-hydroxysuccinimide (MP Biomedicals LLC) in 1:1 volume ratio. The droplet was maintained for 3 hours at room temperature and cleaned with DI H_2O wash and N_2 dry. Subsequently, 0.1 μM aptamer solution was pipetted on the surface-treated carbon nanotubes and maintained for 24 hours at room temperature. The premature drying of the droplets for surface modifications was prevented by placing the sensors in a humidified chamber.

5.5.3 Drug delivery device fabrication

The drug delivery consists of three subcomponents: a top layer with a patterned gold electrode and suspended capping membrane, a bottom layer with a patterned gold counter-electrode and custom packaging to hold the two layers and define a microreservoir for vasopressin storage. To release vasopressin, electrical potential is applied between the top and bottom electrodes which results in two distinct reactions. The first is the electrolytic reaction in the reservoir that causes gas bubble formation and pressure build-up as a result. The second is the reaction between the chlorine ions in the buffer solution and the gold capping membrane to form a water soluble complex that gradually dissolves until it ruptures with increasing pressure of the reservoir. Fabrication procedures for the top silicon structure are described in details in a previous publication.[13] Briefly, silicon nitride was deposited on both sides of a silicon wafer using low pressure chemical vapor deposition (LPCVD) followed by gold deposition on the top and patterning for reservoir location on the bottom. The wafer was later immersed in potassium hydroxide

(KOH) overnight and reactive ion etching was used to remove the silicon nitride in the patterned reservoir location, leaving a 100μm x 100μm gold capping membrane. Modifications in our new architecture regard the other two components of the device and serve to facilitate subcomponent fabrication and assembly. The replacement of a gold deposited Pyrex layer with a single gold electrode eliminates the standard lift-off processing before the gold deposition. Furthermore, the custom packaging is used in place of PDMS in order to facilitate assembly protocol and reduce leakage of vasopressin through the PDMS. The assembled components were sealed with epoxy adhesive.

5.5.3. Power unit integration

A non-enzymatic glucose fuel cell, connected to a rechargeable battery, is used to power the microcontroller and other electrical components of the hemoAID. Lithium batteries were not used here since their short life-time makes them unsuitable for long term autonomous implantable devices with power requirements superior to that of pacemakers.[31]Non-enzymatic glucose fuel cells are promising power sources in such devices due to good long-term stability and adequate power density. Here, we are using the stacked single layer configuration that we have presented previously[32] to demonstrate integration within the autonomous integrated device. The 1 cm^2 single layer fuel cells are patterned directly on 500 μm thick fused silica substrates. A Raney-type Pt/Ni alloy was used as anode for glucose oxidation and a Pt/Al alloy as cathode for oxygen reduction because of increased selectivity as discussed elsewhere.[33,34] The fuel cell unit is composed of 12 single layer fuel cells that are connected externally in parallel to form a fuel cell stack and integrated inside of custom holder with a volume of approximately 1 cm^3.

5.6 References

1. Receveur, R. A. M., Lindemans, F. W. & de Rooij, N. F. Microsystem technologies for implantable applications. *J Micromech Microeng* **17**, R50-R80, doi:Doi 10.1088/0960-1317/17/5/R02 (2007).

2. Bazaka, K. & Jacob, M. Implantable Devices: Issues and Challenges. *Electronics* **2**, 1-34 (2012).

3. Onuki, Y., Bhardwaj, U., Papadimitrakopoulos, F. & Burgess, D. J. A review of the biocompatibility of implantable devices: current challenges to overcome foreign body response. *Journal of diabetes science and technology* **2**, 1003-1015 (2008).

4. Adler, A., Halkin, A. & Viskin, S. Wearable Cardioverter-Defibrillators. *Circulation* **127**, 854-860, doi:10.1161/circulationaha.112.146530 (2013).

5. Arriagada, A. J., Jurkov, A. S., Neshev, E., Muench, G., Andrews, C. N. & Mintchev, M. P. Design, implementation and testing of an implantable impedance-based feedback-controlled neural gastric stimulator. *Physiol. Meas.* **32**, 1103-1115, doi:10.1088/0967-3334/32/8/007 (2011).

6. Liu, S. S., Monti, J., Kargbo, H. M., Athar, M. W. & Parakh, K. Frontiers of Therapy for Patients With Heart Failure. *Am. J. Med.* **126**, 6-U45, doi:10.1016/j.amjmed.2012.04.033 (2013).

7. Ricotti, L., Assaf, T., Dario, P. & Menciassi, A. Wearable and implantable pancreas substitutes. *J. Artif. Organs* **16**, 9-22, doi:10.1007/s10047-012-0660-6 (2013).

8. Krabatsch, T., Schweiger, M., Stepanenko, A., Drews, T., Potapov, E., Pasic, M., Weng, Y., Huebler, M. & Hetzer, R. Improvements in implantable mechanical circulatory support systems. Literature overview and update. *Herz* **36**, 622-629, doi:10.1007/s00059-011-3509-5 (2011).

9. Cebotari, S., Tudorache, I., Schilling, T. & Haverich, A. Heart valve and myocardial tissue engineering. *Herz* **35**, 334-340, doi:10.1007/s00059-010-3355-x (2010).

10. Farra, R., Sheppard, N. F., McCabe, L., Neer, R. M., Anderson, J. M., Santini, J. T., Cima, M. J. & Langer, R. First-in-Human Testing of a Wirelessly Controlled Drug Delivery Microchip. *Sci Transl Med* **4**, doi:ARTN 122ra21
DOI 10.1126/scitranslmed.3003276 (2012).

11. Fojtik, M., Kim, D., Chen, G., Lin, Y.-S., Fick, D., Park, J., Seok, M., Chen, M.-T., Foo, Z. & Blaauw, D. A Millimeter-Scale Energy-Autonomous Sensor System With Stacked Battery and Solar Cells. (2013).

12. Li, H., Mu, X., Wang, Z., Liu, X., Guo, M., Jin, R., Zeng, X. & Mason, A. J. in *Engineering in Medicine and Biology Society (EMBC), 2012 Annual International Conference of the IEEE.* 503-506 (IEEE).

13. Chung, A. J., Huh, Y. S. & Erickson, D. A robust, electrochemically driven microwell drug delivery system for controlled. *D - 100887374*, T - ppublish (2009).

14. Esquivel, J. P., Colomer-Farrarons, J., Castellarnau, M., Salleras, M., del Campo, F. J., Samitier, J., Miribel-Catala, P. & Sabate, N. Fuel cell-powered microfluidic platform for lab-on-a-chip applications: Integration into an autonomous amperometric sensing device. *Lab on a Chip* **12**, 4232-4235, doi:Doi 10.1039/C2lc40946a (2012).

15. Morales, D., Madigan, J., Cullinane, S., Chen, J., Heath, M., Oz, M., Oliver, J. A. & Landry, D. W. Reversal by vasopressin of intractable hypotension in the late phase of hemorrhagic shock. *Circulation* **100**, 226-229 (1999).

16. Voelckel, W. G., Convertino, V. A., Lurie, K. G., Karlbauer, A., Schochl, H., Lindner, K. H. & Trimmel, H. Vasopressin for hemorrhagic shock management: revisiting the potential value in civilian and combat casualty care. *J Trauma* **69** (2010).

17. Anand, T. & Skinner, R. Arginine vasopressin: the future of pressure-support resuscitation in hemorrhagic shock. *J Surg Res* **178**, 321-329 (2012).

18. Wenzel, V., Raab, H. & Dunser, M. W. Arginine vasopressin: a promising rescue drug in the treatment of uncontrolled haemorrhagic shock. *Best Pract Res Clin Anaesthesiol* **22**, 299-316 (2008).

19. Krismer, A. C., Wenzel, V., Voelckel, W. G., Innerhofer, P., Stadlbauer, K. H., Haas, T., Pavlic, M., Sparr, H. J., Lindner, K. H. & Koenigsrainer, A. Employing vasopressin as an adjunct vasopressor in uncontrolled traumatic hemorrhagic shock. Three cases and a brief analysis of the literature. *Anaesthesist* **54**, 220-224 (2005).

20. Jochberger, S., Morgenthaler, N. G., Mayr, V. D., Luckner, G., Wenzel, V., Ulmer, H., Schwarz, S., Hasibeder, W. R., Friesenecker, B. E. & Dunser, M. W. Copeptin and arginine vasopressin concentrations in critically ill patients. *The Journal of clinical endocrinology and metabolism* **91**, 4381-4386, doi:10.1210/jc.2005-2830 (2006).

21. He, P., Oncescu, V., Lee, S., Choi, I. & Erickson, D. Label-free electrochemical monitoring of vasopressin in aptamer-based microfluidic biosensors. *Anal Chim Acta* **759**, 74-80, doi:DOI 10.1016/j.aca.2012.10.038 (2013).

22. Maehashi, K., Matsumoto, K., Takamura, Y. & Tamiya, E. Aptamer-Based Label-Free Immunosensors Using Carbon Nanotube Field-Effect Transistors. *Electroanal* **21**, 1285-1290, doi:DOI 10.1002/elan.200804552 (2009).

23. Chung, A. J., Huh, Y. S. & Erickson, D. A robust, electrochemically driven microwell drug delivery system for controlled vasopressin release. *Biomed Microdevices* **11**, 861-867 (2009).

24. Cordovez, B., Chung, A. J., Mak, M. & Erickson, D. A novel polymer microneedle fabrication process for active fluidic delivery. *Microfluid Nanofluid* **10**, 785-791, doi:DOI 10.1007/s10404-010-0709-x (2011).

25. Chung, A. J. & Erickson, D. Engineering insect flight metabolics using immature stage implanted microfluidics. *Lab Chip* **9**, 669-676 (2009).

26. Elman, N. M., Ho Duc, H. L. & Cima, M. J. An implantable MEMS drug delivery device for rapid delivery in ambulatory emergency care. *Biomed Microdevices* **11**, 625-631 (2009).

27. Ho Duc, H. L. *Emergency delivery of Vasopressin from an implantable MEMS rapid drug delivery device*, Massachusetts Institute of Technology, (2009).

28. Dawson, R. M. C., Elliott, D. C., Elliott, W. H. & Jones, K. M. Data for biochemical research. *Oxford University Press* **3**, 31-32 (1986).

29. Chung, A., Cordovez, B., Jasuja, N., Lee, D., Huang, X. & Erickson, D. Implantable microfluidic and electronic systems for insect flight manipulation. *Microfluid Nanofluid* **13**, 345-352, doi:10.1007/s10404-012-0957-z (2012).

30. Gumus, A., Lee, S., Karlsson, K., Gabrielson, R., Winkler, D. W. & Erickson, D. Real-time in-vivo uric acid biosensor system for biophysical monitoring of birds. *Analyst* **(Accepted)** (2013).

31. Vincent, C. A. Lithium batteries: a 50-year perspective, 1959–2009. *Solid State Ionics* **134**, 159-167, doi:http://dx.doi.org/10.1016/S0167-2738(00)00723-2 (2000).

32. Oncescu, V. & Erickson, D. High volumetric power density, non-enzymatic, glucose fuel cells. *Scientific reports* **3** (2013).

33. Kerzenmacher, S., Ducrée, J., Zengerle, R. & von Stetten, F. Energy harvesting by implantable abiotically catalyzed glucose fuel cells. *Journal of Power Sources* **182**, 1-17, doi:http://dx.doi.org/10.1016/j.jpowsour.2008.03.031 (2008).

34. Oncescu, V. & Erickson, D. A microfabricated low cost enzyme-free glucose fuel cell for powering low-power implantable devices. *Journal of Power Sources* **196**, 9169-9175, doi:http://dx.doi.org/10.1016/j.jpowsour.2011.06.100 (2011).

Chapter 6:

Conclusions and future perspectives

6.1 Summary

In this dissertation, we have discussed the development of smartphone-based biosensor systems for nutrition diagnostics and preventive care at the PON. These systems have enabled complex biochemical reactions to be carried out away from the conventional laboratories, which could be exploited for various personalized health monitoring applications.

In the first part of the thesis, we focused on the global issue of micronutrient deficiencies. In **Chapter 1**, we discussed the opportunities in PON nutrition diagnostics, nutritional biomarkers used in the assessment of nutritional status, and the state-of-the-art diagnostics technologies, some of which are being integrated with the smartphone technology for utilizing its imaging, computing and communication functionalities at the PON. In **Chapter 2** we presented our vision of the NutriPhone – a mobile platform for personalized monitoring of micronutrient deficiencies, and discussed the development of the initial prototype system for measuring vitamin D levels. The NutriPhone system consists of a test strip (i.e. biosensor system) for immunodetection of 25(OH)D, a smartphone accessory for capturing the strip images, and an app for analyzing the colorimetric signals on the test strip. We demonstrated that the system can accurately quantify physiological levels of 25(OH)D in sheep serum with an accuracy of 15nM and a precision of 10nM without the reliance on conventional laboratory equipment. In **Chapter 3**, an advanced version of the NutriPhone was demonstrated for PON vitamin B_{12} analysis of whole blood samples in 15 min. Here we developed our B_{12} biosensor as a lateral flow immunoassay and capitalized on the exceptional on-chip blood sample processing and biochemical reagent storage capabilities of these systems; furthermore, we achieved the quantification of B_{12} in the sub-nmol/ml range by incorporating a novel “spacer pad” which increased the

duration of the key immunoreaction. The effectiveness of the NutriPhone system was validated in a domestic human trial in which it was used to correctly diagnose the B_{12} status of 12 human participants.

In the second part of the thesis, we examined two areas in preventive care in which enabling early diagnosis at the PON is considered crucial for the proper patient management. One such area is that of acute febrile illnesses (AFI), which can be caused by a various infectious agents (e.g. CHIV, DENV, Malaria, Chagas, Leptospirosis, Typhoid fever, etc.). As discussed in **Chapter 4**, the rapid differential diagnosis of these agents is widely needed, and is partly being enabled by the lateral flow RDTs whose performance is currently limited to the detection of IgG/IgM against a single pathogen. Here we presented a novel lateral flow assay scheme using just two color labels for 4-plex detection of anti-CHIV and anti-DENV IgG/IgM on a single biosensor platform, and validated its performance by using it to diagnose 12 different diagnostic scenarios. We also showed that smartphones could be incorporated in the future to perform the colorimetric analysis of the biosensor outputs at the PON. The second area in preventive care that we examined in this thesis is that of traumatic injuries, example of which includes late-phase hemorrhagic shock (HS). In **Chapter 5** we discussed that for HS, vasopressin can be used as both the biomarker for its early diagnosis and the therapeutic agent for stabilizing the patients. Based on this, we demonstrated a prototype for an autonomous integrated medical device which incorporates: an aptamer-based affinity biosensor for the electrochemical detection of pM levels of vasopressin, an electrochemical active drug delivery device for automatically releasing vasopressin at the onset of HS, and a glucose fuel cell for powering the whole device.

6.2 Future Perspectives

6.2.1. Opportunities for PON vitamin D testing[i]

In Chapter 3, we realized a rapid PON test for vitamin B_{12} deficiency by developing it as a lateral flow assay with the inherent capabilities for on-chip blood processing and reagent storage. Based on a similar approach, a PON test for vitamin D deficiency could also be achieved in the near future. Currently there is a challenge in adapting the traditional lateral flow assay scheme to the vitamin D detection due to the assay's inability to perform sample pre-treatment. As discussed in Chapter 2, an essential step in the vitamin D immunoassays on the market is the separation of the 25-hydroxymolecules (25(OH)D; the best known indicator of vitamin D status in humans) from the vitamin D binding proteins (VDBP) which bind 95-99% of 25(OH)D and thereby hinder their interaction with the antibodies for 25(OH)D[1]. Although such a separation step is incompatible with traditional lateral flow assays, our innovation around the spacer pad (Chapter 3) has the potential to change this predicament, and lead to the development of lateral flow assays for vitamin D deficiency testing. As shown in **Figure 6.1**a and 6.1b, the spacer could be incorporated and allow incubation of the VDBP-bound 25(OH)D mixtures with the releasing agent (i.e. acetonitrile) to let the free 25(OH)D molecules to proceed to the test and control lines.

6.2.2 Opportunities for expanding the target nutritional biomarkers[ii]

In our most recent version of the NutriPhone, the use of smartphone technology enabled our system to obtain quantitative B_{12} information from conventionally qualitative RDT systems in PON settings. Such a detection principle could be applied to other RDT systems, NutriPhone system could be expanded for the

---

[i] The ideas behind this section are elaborated in:
Erickson, D., **Lee, S.**, Mehta, S. (Nov. 2015). Competitive lateral flow assay for point-of-care quantification of blood vitamin B_{12} and vitamin D levels. Application Number: 62/256,946.

[ii] The ideas behind this section are elaborated in:
Erickson, D., **Lee, S.**, Mehta, S. (Nov. 2015). NutriCard: multiplex point-of-care test for blood nutritional biomarkers. Application Number: 62/256,936.

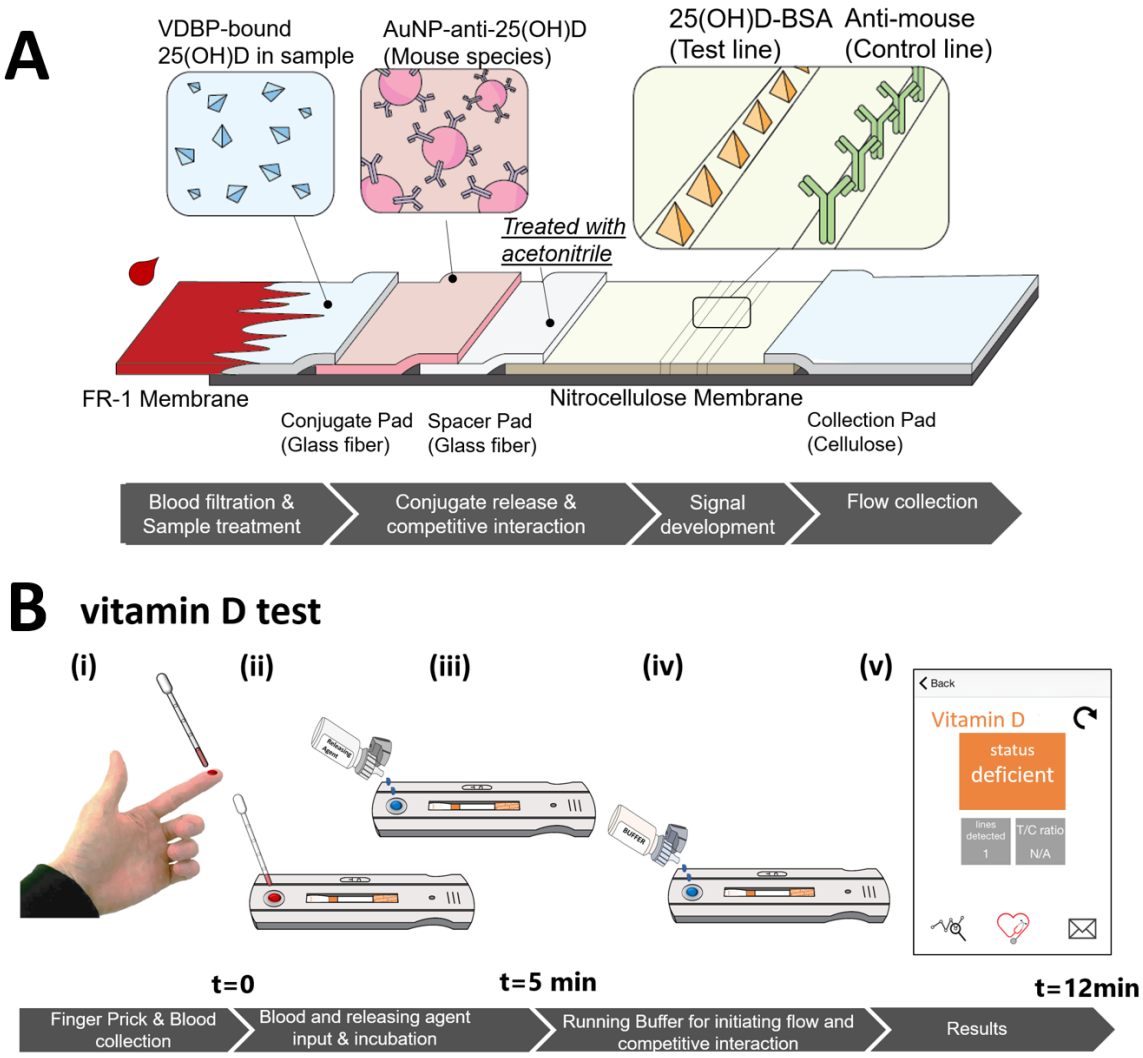

Figure 6.1: Vitamin D testing at the PON. **(A)** vitamin D lateral flow assay architecture with a acetonitrile-treated spacer pad **(B)** Vitamin D test operation where Vitamin D test in which (i) the user collects a raw blood sample using a finger prick, (ii-iii) applies the blood sample along with a releasing agent to perform the necessary sample treatment in ~5min incubation, (iv) applies the running buffer to initiates a flow onto the nitrocellulose pad where test and control lines are immobilized and (v) obtains

diagnosis of other micronutrient deficiencies simply by developing additional RDT technologies for the known nutritional biomarkers (Table 1.1). Furthermore, some of the biomarkers with similar molecular characteristics could be multiplexed into a single platform. **Figure 6.2**a demonstrates a 3-plex test for retinol-binding protein (RBP), ferritin and CRP whose considerably big molecular weights of 25, 21, 26

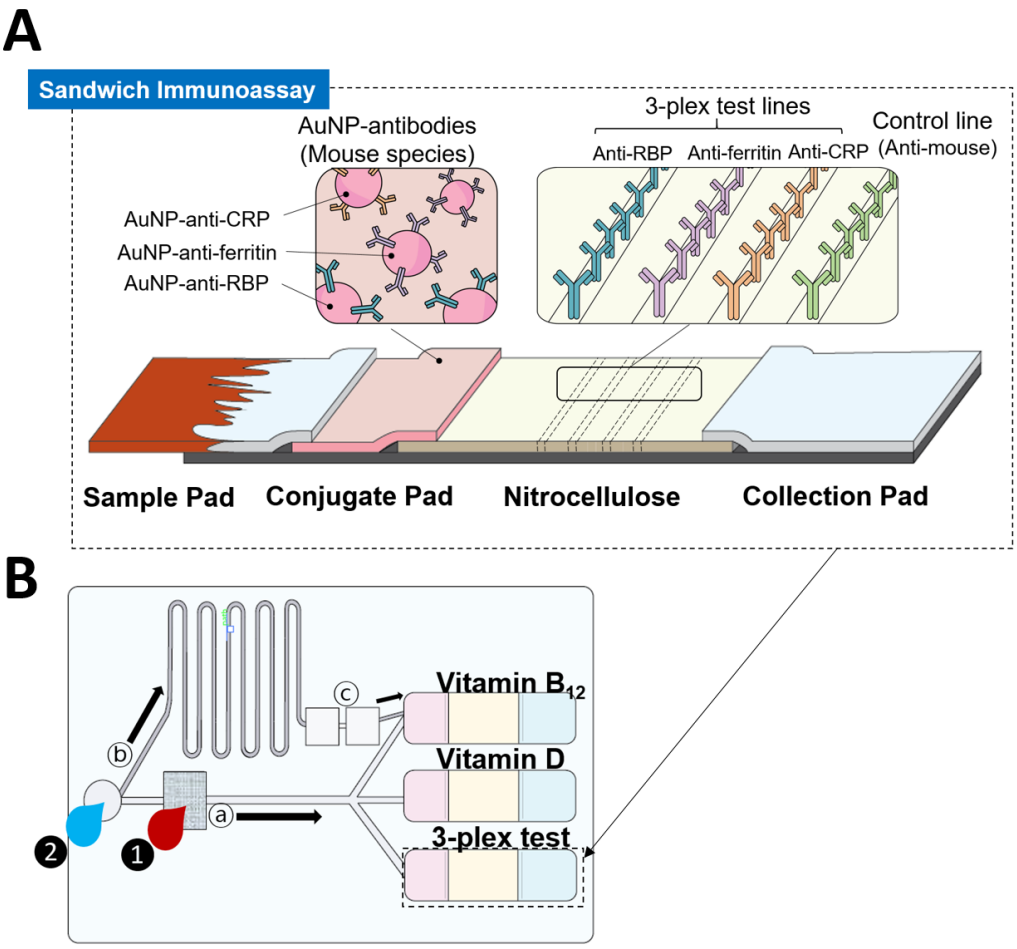

Figure 6.2: Multiplexing Strategies for NutriPhone. **(A)** 3-plex test for vitamin A, iron and C-reactive protein; developed as a sandwich-type latera flow assay where RBP, ferritin and CRP are biomarkers for vitamin A, iron and inflammation status respectively **(B)** "NutriCard" technology; composes of a plastic cartridge that incorporates lateral flow assays, and defines fluid network for distributing the

kDa respectively allow for their sandwich-type detection in a standard RDT format. The assay using this concept indicates deficiency results for vitamin A and iron based on the RBP and ferritin levels respectively, and these results are validated by checking for a presence/absence of inflammation based on the CRP levels. The limitation of the aforementioned approach is the difficulty in multiplexing the detection of biomarkers that require distinctly different levels of sample pre-processing (e.g. vitamin D assay that requires initial sample incubation with acetonitrile) and/or signal amplification (e.g. vitamin B12 assay that requires silver enhancement of the signals at the end to achieve pmol/L levels of detection).

Moving further forward, we could achieve multiplexing of these distinctly different lateral flow strips into a single "NutriCard" platform. As shown in Figure 6.2b, the test strip is composed of a plastic cartridge that houses the lateral flow assays for vitamin B_{12}, vitamin D and 3-plex test for vitamin A, iron and CRP, and defines a fluid network for distribution of key chemical reagents. Using this test, the user benefits from the speed and simplicity of the traditional rapid diagnostic tests, while at the same time having the abilities to: (1) multiplex for different targets and (2) amplify the test strip signal without the need to perform extra procedures. These enhanced capabilities would be enabled through the cartridge's microscale fluid network design which preciously controls the timing and location of the reagent delivery to and from the standard membrane components that have been widely accepted in rapid diagnostic tests (e.g. blood filtration membrane).

To operate the NutriCard test, the user applies a drop of blood onto the filtration membrane that is incorporated in the multiplex test strip. The user then applies buffer droplets onto the buffer inlet which initiates the plasma to flow to the lateral flow strips for vitamin B_{12}, vitamin D and 3-plex test via the separating fluid channels. Simultaneously the buffer application initiates a flow in the upper channel which carries the silver enhancer solutions stored within the membranes to the lateral flow strips. Because the upper channels has a longer, tortuous design, the fluid inside reaches the vitamin B_{12} lateral flow strip ~10 minutes after the plasma sample, which is the desired time delay to expose the test strips to the enhancement solutions. Here the enhancement would be used for vitamin B_{12} but not the other biomarkers as vitamin B_{12} is found in very low concentrations (pg/ml) blood[2] but not for the other biomarkers whose detection range is higher (nmol/L –µmol/L)[3,4] and allows the detection without the enhancement. The test could be expanded further to include a wider range of micronutrients and allow a comprehensive nutritional analysis from just a finger prick of blood.

6.2.3 Opportunities for the two-color assay – FeverPhone

In the near future, the exceptional multiplexing capabilities of our two-color lateral flow assay (Chapter 4) can be explored further; as discussed in Chapter 4, this can be achieved simply by introducing additional

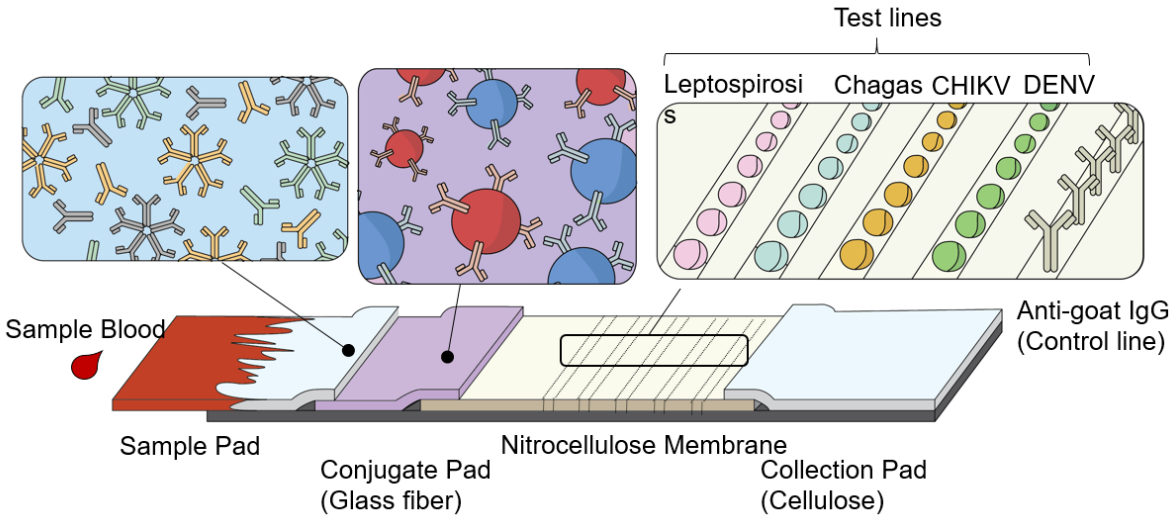

Figure 6.3: Two-color lateral flow assay for multiplex IgG/IgM detection of several febrile illnesses.

test lines of different target pathogen molecules such as Chagas, Leptospirosis, Malaria, Typhoid etc. In **Figure 6.3**, we show the two-color lateral flow assay architecture with a test line region that has been modified to enable the multiplex IgG/IgM detection against Chagas, Leptosprisois, DENV and CHIKV. As in the previous version, the assay uses blue and red encodings to discriminate between the IgGs and IgMs, while the pathogen specificity is determined by observing the test line location of the color development. Therefore for the assay presented in Figure 6.3, there is a potential to achieve 8-plex detection of IgG/IgM antibodies to Chagas, Leptosprisois, DENV and CHIKV using just two-color probes.

Ultimately, these advancements could lead to the development of FeverPhone, a smartphone-based system for rapid, comprehensive, differential diagnosis of causes behind acute febrile illnesses. The smartphone, besides its role as an analytical tool, can be used to better monitor the patients and track the diseases.

6.3 References

1. Wootton, A. M. Improving the measurement of 25-hydroxyvitamin D. *The Clinical biochemist. Reviews / Australian Association of Clinical Biochemists* **26**, 33-36 (2005).

2. Van Tiggelen, C. J., Peperkamp, J. P. & Tertoolen, J. F. Vitamin B12 levels of cerebrospinal fluid in patients with organic mental disorder. *Journal of Orthomolecular Psychiatry* **12**, 305-311 (1983).

3. Chan, T. & Gu, F. Early diagnosis of sepsis using serum biomarkers. (2011).

4. Kanai, M., Raz, A. & Goodman, D. S. Retinol-binding protein: the transport protein for vitamin A in human plasma. *Journal of Clinical Investigation* **47**, 2025 (1968).

Appendix 1:

Supplementary information for Chapter 3

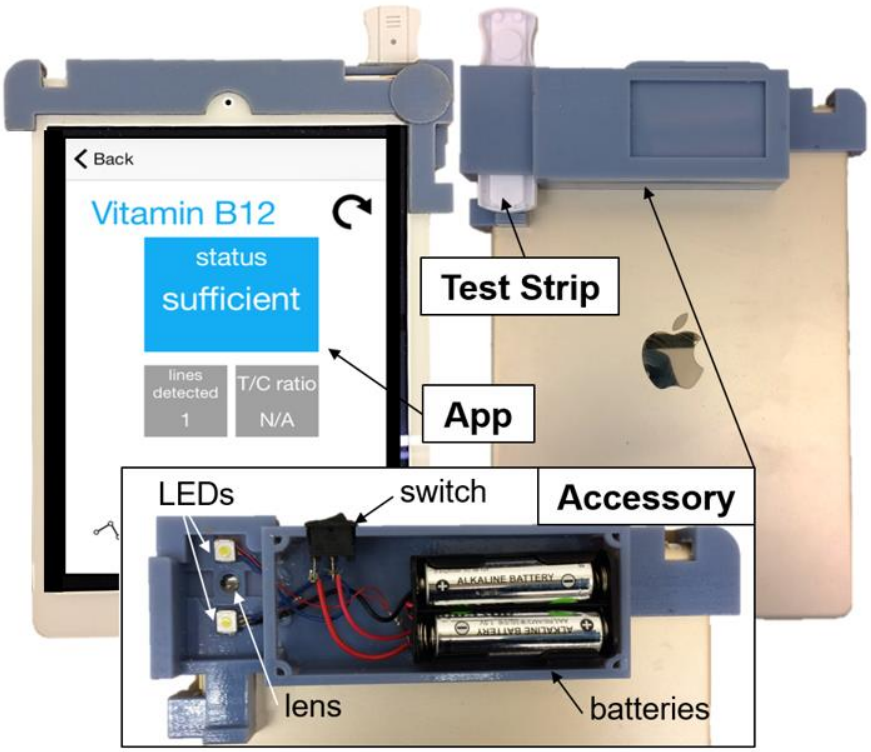

Figure A1.1: 1st generation NutriPhone accessory for iPads

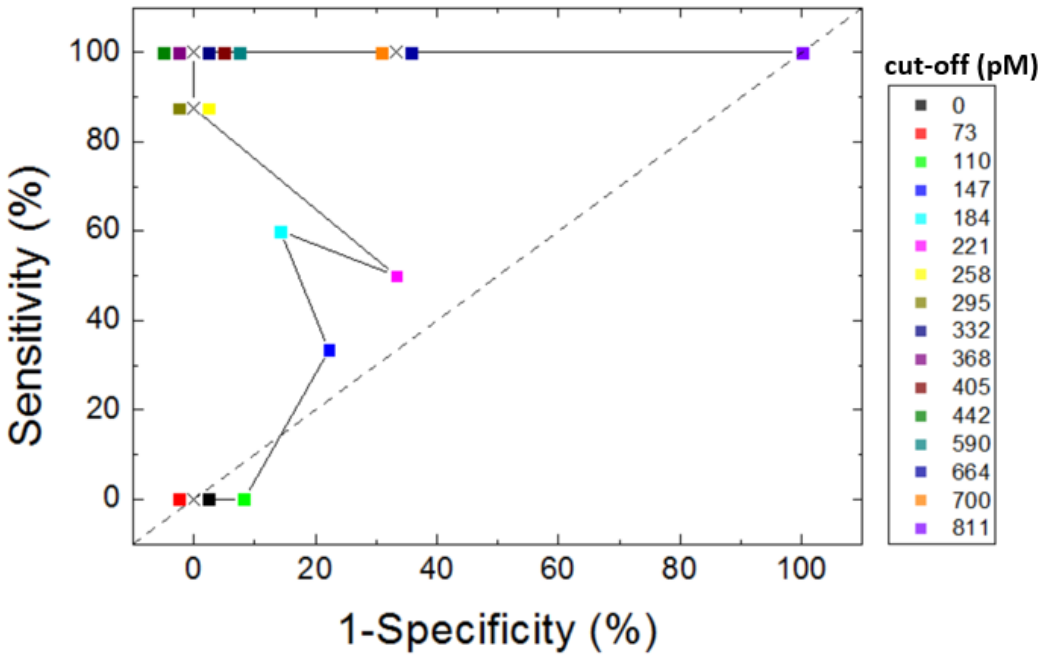

Figure A1.2: Receiver Operating Characteristic (ROC) curve for the NutriPhone human trials. The legend shows the B_{12} cut-off points, and the dotted line shows the reference line.

Appendix 2:

Supplementary information for Chapter 4

Table S.1 Test region red/green/blue/hue intensities at different CHIKV IgG/IgM concentrations

CHIKV IgG/IgM concentration	R intensity*	G intensity*	B intensity*	Hue intensity
0/600	159.32	210.35	250.36	206.36
150/450	169.29	197.84	242.06	216.45
300/300	184.79	200.85	237.46	221.70
450/150	200.41	197.51	231.28	245.15
600/0	204.44	183.71	225.19	269.97

*average values; in range 0-255

Table S.2 Test region red/green/blue/hue intensities for different test strip/regions in 4-plex testing

Test Strip/Region ID		R intensity*	G intensity*	B intensity*	Hue intensity
①	DENV	212.204	204.518	224.618	262.9433
	CHIV	216.733	201.066	223.519	281.8661
②	DENV	214.554	191.094	240.343	268.5813
	CHIV	Test region did not develop colors			
③	DENV	Test region did not develop colors			
	CHIV	213.846	160.614	223.378	290.8878
④	DENV	172.494	223.006	252.575	202.1543
	CHIV	158.632	218.455	249.947	200.6923
⑤	DENV	164.7	216.083	251.02	204.2843
	CHIV	Test region did not develop colors			
⑥	DENV	Test region did not develop colors			
	CHIV	135.397	200.066	245.636	204.8025
⑦	DENV	140.068	193.353	244.441	209.3685
	CHIV	209.939	175.355	230.87	277.378
⑧	DENV	203.236	177.782	227.576	270.6712
	CHIV	160.929	203.087	243.918	209.5203
⑩	DENV	211.813	186.983	241.995	267.0814
	CHIV	165.725	182.562	251.312	228.1966
⑪	DENV	170.395	185.021	241.316	227.6262
	CHIV	207.526	174.821	233.403	273.4966
⑫	DENV	180.676	182.326	240.405	238.3425
	CHIV	113.967	198.994	248.89	202.1887

*average values; in range 0-255

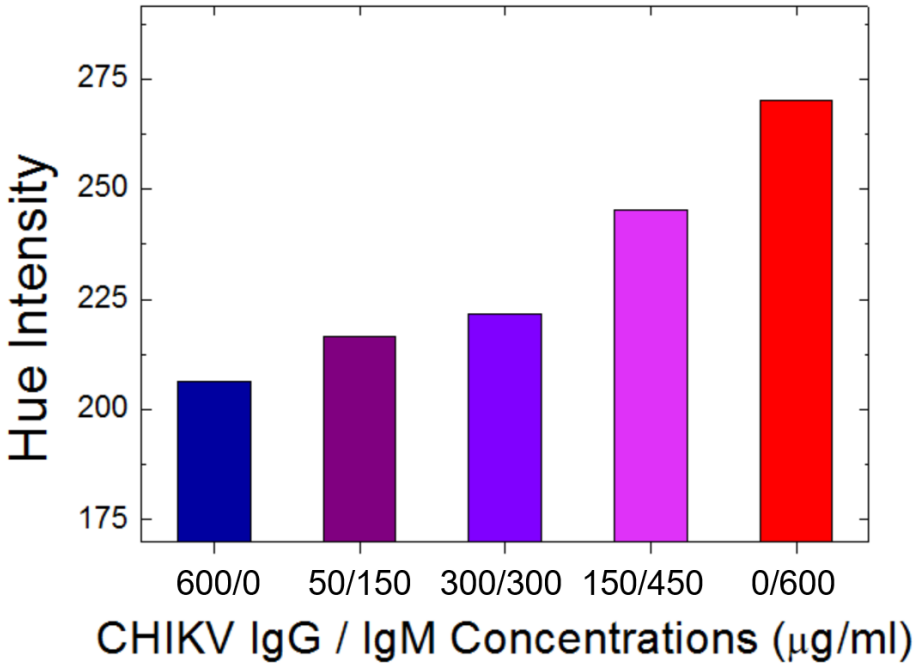

Figure S.1 Test region hue intensity at different CHIKV IgG/IgM concentrations. Hue values are presented in Table S.1

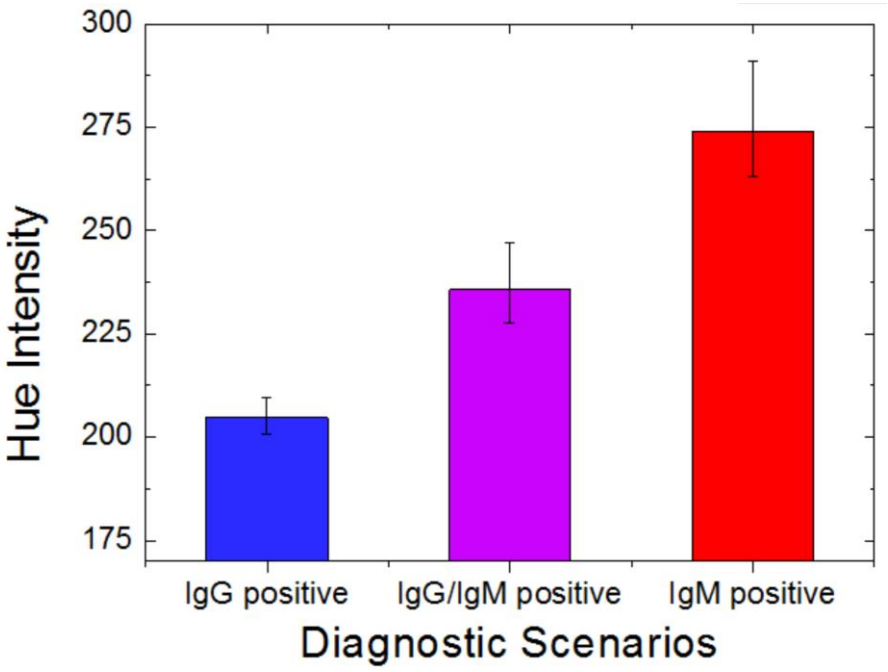

Figure S.2 Hue intensity and associated diagnostic scenarios from 4-plex testing of anti-CHIV and anti-DENV IgG/IgM